Material and Device Design for High Efficiency Polycrystalline Silicon Thin Film Solar Cells

多結晶 Si 薄膜の材料物性制御と高効率太陽電池の開発

Takuya MATSUI

January, 2002

Department of Physical Science
Graduate School of Engineering Science
Osaka University

Material and Device Design for High Efficiency Polycrystalline Silicon Thin Film Solar Cells

Takuya MATSUI

Department of Physical Science
Graduate School of Engineering Science
Osaka University

January, 2002

Abstract

A series of systematic studies has been made on material and device physics of polycrystalline silicon (poly-Si) thin film solar cells from both theoretical and experimental points of view. In order to perform an optimum design of p-i-n junction poly-Si thin film solar cells, a wide range of experimental issues has been explored from the material deposition and characterization to the device fabrication and the analysis of device operation.

The poly-Si thin films deposited directly onto glass substrate at low temperature are promising photovoltaic material in terms of low cost, however, this material typically show extremely small grain size of «1 μm. This work begins with the device modeling of poly-Si thin film solar cells to understand the role of grain boundary played in device operation with quantitative physical parameters. The dependence of photovoltaic performance on grain boundary properties has been investigated as a function of grain size, L_G, and surface

recombination velocity at grain boundary, S_{GB}. Simulation results have pointed out that photovoltaic performance is predominantly determined by two factors, i.e., the built-in electric field and the $L_G/2S_{GB}$. This result is followed by an important suggestion that the very thin photovoltaic layer below 3 μm is quite essential for poly-Si solar cells with a grain size of «1 μm in order to reduce recombination of both photo-generated and injection carriers at grain boundary.

In experimental studies, poly-Si thin films have been prepared by plasma enhanced chemical vapor deposition with a very high excitation frequency (100 MHz) for the development of p-i-n junction solar cells. Correlation between poly-Si microstructure and photovoltaic performance of poly-Si solar cells has been investigated as a function of deposition parameters such as deposition pressure, SiH_4 flow rate and SiH_4 concentration. It has been found that poly-Si microstructure including crystalline volume fraction, X_c, and crystallographic orientation is closely related to the atomic hydrogen flux during the film growth, which is evidenced from plasma diagnostics by in-situ monitoring of optical emission spectroscopy. It has been clearly shown that there is a universal relationship between poly-Si microstructure and photovoltaic performance. With an increase in X_c, open circuit voltage (V_{oc}) tends to decrease, whereas poly-Si with $X_c \geq 50\%$ and (220) preferential orientation is essential for high short circuit current density (J_{sc}). Consequently, the most appropriate condition for device-grade materials is concluded to be the poly-Si films with X_c~50% and (220) preferential orientation.

The structural dependence of carrier transport properties in thin poly-Si thin films has been investigated. The AC conductivity measurement has been proposed as a powerful tool for evaluating the carrier transport along poly-Si growth direction as well as for determining the electron and hole conductivities individually. It has been found that the Fermi energy level in poly-Si is quite sensitive against the film microstructure. From the results of temperature dependent AC-conductivity, poly-Si film with relatively low X_c~50% and (220) preferential orientation exhibits truly intrinsic character likewise intrinsic single crystalline Si, leading to the high performance solar cells. In contrast, poly-Si

layers with high X_c > 50% and (220) preferential orientation exhibit n-type character, which is likely to be associated with the oxygen-related donor at grain boundaries. Experimental and simulation results have suggested that poly-Si solar cells with high X_c result in lower V_{oc} due to n-type character and further electrical activation at grain boundary. In order to gain more insight into the carrier transport, Time-of-Flight experiments have been performed on a device-grade poly-Si film with X_c of ~50%. A significant difference has been found in particularly hole transport between for poly-Si and a-Si:H materials. It has been shown that the hole drift mobility of poly-Si films is estimated as 1.4 cm^2/Vs at room temperature, which is by more than two orders of magnitude higher than that of conventional a-Si:H films.

With a poly-Si layer thickness of around 3 μm, a light trapping technique is essential to reduce optical loss. A novel textured substrate consisting of ZnO/Ag/SnO_2/glass has been proposed for realizing effective light trapping in thin film poly-Si photovoltaic layer. Although the highly textured substrate shows excellent light trapping properties, it tends to deteriorate the poly-Si (220) preferential growth, yielding poor photovoltaic performance. The field-dependent carrier collection behaviors of solar cells have revealed that this structural deterioration attributed to the substrate texture gives rise to a reduction in carrier diffusion length in the poly-Si photovoltaic layer. In this experiment, the textured ZnO/Ag/SnO_2/glass substrate with RMS roughness of 38 nm is found to be most suitable for poly-Si solar cells, which effectively improves long wavelength responses. The highest conversion efficiency of 9.18% (J_{sc} = 25.1 mA/cm^2, V_{oc} = 0.523 V, fill factor = 0.7) has been achieved by employing this optimum textured substrate.

Acknowledgements

This work has been done at the Semiconductor Laboratory, Department of Physical Science, Graduate School of Engineering Science, Osaka University, Toyonaka, Osaka, under the direction of Professor Hiroaki Okamoto.

The author would like to express his deepest appreciation and gratitude to his supervisor, Professor Hiroaki Okamoto, for his kind advice, continuous supporting, valuable suggestion and encouragement throughout the course of this work as well as critical reading of this thesis.

The author is extremely grateful to Professor Masanori Okuyama and Professor Mikio Takai for their kind advice and critical reading of this thesis.

The author deeply grateful to Professor Takeshi Kobayashi, Professor Tetsuro kobayashi, Professor Shinji Urabe, Professor Sadahiko Yamamoto and Professor Kenji Gamo for their kind and useful guidance throughout course of this work.

The author sincerely acknowledges to Dr. Kiminori Hattori and Dr. Toshihiko Toyama for their instructive and heartfelt advises throughout the course of this study as well as also critical reading of this thesis. This work would not have been accomplished without their supports.

The author would like to express his sincere thanks to Professor Yoshihiro Hamakawa and Professor Hideyuki Takakura of Ritsumeikan University for their kind encouragement and useful suggestion throughout the course of this study as well as critical reading of this thesis.

The author would like to express his sincere gratitude to Mr. Chitose Sada for his kind encouragement and skillful technical assistance throughout the course of this work.

The author is much indebted to Dr. Minoru Noda, Mr. Kaoru Yamashita, Dr. Takeshi Kanashima and Dr. Dan Ricinschi for their continuous encouragement.

The author would like to express his deep thanks to Mr. Kazuo Sato and Mr. Makoto Fukawa of Asahi Glass Co., ltd. for providing SnO_2/glass substrates.

The author wishes to acknowledge to Dr. Bernd Rech, Mr. Tobias Repmann and Dr. Helmut Stiebig of Institute of Photovoltaics Forschungszentrum Jülich for their exciting and useful discussion when the author visited their laboratory.

The author wishes to express his gratitude to his co-workers in the Semiconductor Laboratory, Messrs. Shigeharu Taira, Masaharu Tsukiji, Riza Muhida, Hiroyuki Saika, Tomohiro Kawamura and Tomokazu Harano for their excellent collaborations and valuable discussions.

The author also wishes to express his gratitude to his co-workers of Ritsumeikan University, Messrs. Yuji Kumakura, Tsutomu Yamazaki, Masato Uchihara, Shinya Honda, Katsunori Tanida, Seiji Miura and Yusuke Nishimura for their excellent collaborations and valuable discussions.

The author is especially indebted to his colleagues in the Semiconductor Laboratory, Messrs. Kyotaro Nakamura, Osamu Maida, Masahiro Gotoh, Toshihiko Fujihara, Yasuharu Nakai, Atushi Asano, Shuya Abe and Ms. Masako Fujii for their help and encouragement.

The author wishes to thank to his friends, Dr. Takashi Minemoto and Messrs. Takahiro Senda, Junpei Haraguchi, Makoto Nakai, Shinya Shima, Masaya Itoh, Kouhei Okamoto, Hideki Takahasi, Takahiro Hikita and Mitsusada Fujita.

Finally, the author wishes to thank his parents for their endless and warm supports.

Contents

Chapter I Introduction ····· **1**
1.1 Historical background ····· 1
1.2 Purpose of this work ····· 5
References ····· 8

Chapter II Device modeling of poly-Si thin film solar cells ····· **10**
2.1 Introduction ····· 10
2.2 Simulation model for poly-Si thin film solar cells ····· 12
2.2.1 Basic calculation method for device simulation ····· 11
2.2.2 Two dimensional grain boundary model ····· 13
2.3 Effect of grain boundary on photovoltaic performance ····· 16
2.3.1 Grain size and surface recombination velocity at grain boundary ·· 16
2.3.2 Optimum i-layer thickness ····· 18
2.4 Summary ····· 20
References ····· 22

Chapter III Correlation between microstructure and photovoltaic performance of poly-Si thin films ····· **23**
3.1 Introduction ····· 23
3.2 Fabrication and characterization techniques of poly-Si solar cells ····· 25
3.2.1 Deposition technique for intrinsic poly-Si thin films ····· 25
3.2.2 Device structure and fabrication process ····· 28
3.2.3 Characterization techniques for poly-Si thin film and its solar cell ····· 29

3.3 Structural properties and photovoltaic performance of poly-Si thin film solar cells ····30
3.3.1 Deposition pressure dependence ····30
3.3.2 SiH_4 flow rate and SiH_4 concentration dependence ····39
3.3.3 Universal relationship between poly-Si microstructure and photovoltaic performance ····45
3.4 Summary ····47
References ····48

Chapter IV Characterization of electronic transport properties in poly-Si photovoltaic layer ····50
4.1 Introduction ····50
4.2 AC conductivity experiment on poly-Si thin films ····52
4.2.1 Small signal equivalent circuit ····52
4.2.2 Electron and hole conductivities in poly-Si layer ····54
4.2.3 Influence of film conductivity on photovoltaic performance ····59
4.3 Time-of-Flight experiment on poly-Si thin films ····63
4.3.1 Experimental setup ····63
4.3.2 Electron and hole transport in poly-Si thin films ····66
4.4 Summary ····74
References ····75

Chapter V Light trapping technique and rear side interface properties of poly-Si thin film solar cells ····77
5.1 Introduction ····77
5.2 Preparation of textured substrate for light trapping ····78
5.2.1 $ZnO/Ag/SnO_2$ textured back reflector ····78
5.2.2 Light trapping effect ····81
5.3 Influence of substrate texture on microstructure and

photovoltaic performance of poly-Si solar cells ·····83
5.3.1 Light trapping gain in short circuit current ·····83
5.3.2 Carrier transport in poly-Si layer near the textured substrate ·····85
5.4 Optimization of poly-Si i-layer thickness ·····90
5.5 Summary ·····95
References ·····96

Chapter VI Conclusions ·····97

Vita ·····101

Published notes ·····102

Chapter I

Introduction

1.1 Historical Background

Facing the increasing energy demands and undesirable environmental effects caused by the mass consumption of fossil fuels, development of renewable and sustainable energy resources is important subject assigned to modern science and technology. Within a variety of sustainable energy conversion technologies in progress, photovoltaic conversion of solar energy, which guarantees pollution-free and abundantly available everywhere in the world, appears to be one of the most promising ways of meeting the future energy demands. However, there is a big barrier impeding the expansion of the large-scale power source application in the photovoltaic system, i.e., high price of solar module [1]. In this respect, photovoltaic panels should be cheep and comprised of non-toxic materials, while these materials should allow handling and processing such that manufacturing at low cost is feasible for practical use.

Currently, wafer-based single crystalline or multi-crystalline silicon (c-Si, mc-Si) solar cells play a dominant role in the photovoltaic market. These materials have advantage of high efficiency potential [2], material abundance, ability of research sharing with the microelectronics market. About 300-μm-thick silicon wafers are produced by special silicon purification, expensive ingot

growth and dicing process, which takes about half of the cost of the complete finished solar cells. Therefore the wafer-based approach limits the potential for further cost reduction. A less expensive alternative is the thin film solar cells supported on a foreign substrate, such as silicon, cadmium-telluride (CdTe) and copper-indium-diselenide ($CuInSe_2$) thin film (1-10 μm) photovoltaic materials on glass or stainless steels. Except for silicon, other compound semiconductor materials must necessarily be in thin film form for the proper photovoltaic operation by virtue of their electrical and optical properties. However, it is not sufficient for the photovoltaic material to have only the desired electrical and optical properties, it is also necessary that it must be readily available in abundant supply of raw material in the world. Silicon thin films and their associated technologies are more fortunately placed in this respect, which offer an extremely attractive approach toward the future mass production of highly efficient and cost effective solar cells. Silicon can be deposited from the vapor or liquid phase. Concerning the processing temperature, the deposition technique for silicon thin films can be roughly divided into two categories, i.e., high temperature process at >700°C and low temperature process at <700°C. The high temperature deposition process can commonly produce the large grain polycrystalline silicon thin films by such as chemical vapor deposition (CVD: 700-1200°C) [3], liquid phase epitaxy (LPE:~1000°C) [4] and zone melt recrystallization (ZMR:~1200°C) [5] techniques. However, these processes require the temperature resistible substrate, *e.g.*, c-Si native wafer. Moreover, it needs a lift-off technique to transfer the deposited film from the native wafer to a foreign supporting substrate [5,6], and it also needs a post-hydrogenation step to passivate the grain boundary [5]. In contrast, low temperature process, including the plasma enhanced CVD (PECVD), hot wire CVD (HWCVD) [7] and reactive sputtering techniques [8], allows the direct silicon deposition on glass substrate and it makes sense for the possibility of large-area fabrication.

Low-temperature silicon deposition technique can modify the film microstructure from an almost perfectly disordered amorphous state, via a microcrystalline state, to a polycrystalline state. The research on these non-

crystalline and heterogeneous materials has proceeded over the past 30 years as one of the most active fields in solid state physics. In 1965, Stering and Swann first published the deposition of amorphous silicon using silane (SiH_4) in PECVD process [9]. In 1968, Vepřek and Marečel reported the first deposition of microcrystalline silicon on glass substrate using a hydrogen plasma chemical transport method [10]. In 1975, Spear and LeComber demonstrated that the hydrogen incorporated in amorphous silicon network plays an important role in lowering density of electronic states localized in forbidden gap, making it possible to dope both for n- and p-type [11]. In the next year, Carlson and Wronski reported a first hydrogenated amorphous silicon (a-Si:H) p-i-n junction solar cell with a conversion efficiency of 2.4% [12]. Since their report, a-Si:H based solar cells produced by PECVD process have progressed to play a major role in the R&D field in the thin film solar cells, and up to now their technologies have achieved an industrial level [13]. Microcrystalline silicon (μc-Si) or microcrystalline silicon carbide (μc-SiC) [14], which is commonly regarded to possess spherical small silicon crystallites embedded in amorphous matrix, has been successfully used as window ohmic contact layers of a-Si:H based solar cells due to their high optical transparency and efficient doping properties [15]. However, the a-Si:H solar cells have always been associated with low spectral response in the infrared regime of solar radiation spectrum due to a wider band gap (1.7-1.8 eV) than crystalline silicon (1.1 eV), hence the achievable efficiency is limited by its optical properties. Another serious disadvantage in the a-Si:H based solar cells is the light induced degradation in conversion efficiency being well-known as Staebler-Wronski effect [16] which has not been solved completely yet. This decrease in efficiency exceeds 30% under practical conditions encountered in the out door operation.

Quite recently, a breakthrough for the more stable silicon based thin film solar cells has arisen with a use of an alternative material, i.e., poly-Si thin film proposed by J. Meier *et al.* in 1994 [17]. They firstly applied PECVD produced intrinsic poly-Si films to p-i-n solar cell and demonstrated the conversion efficiency of 4.4%. After their report, poly-Si thin films have gathered much

attention as a new type photovoltaic material. The poly-Si films can be obtained using SiH_4 and H_2 gas mixture in an appropriate PECVD deposition condition at extremely low temperature (100-550°C), and this material typically exhibits columnar structure with grain diameter of sub-micron or less [18]. This structural feature of poly-Si is the most striking difference from that of μc-Si. Some definitions and typical feature of silicon thin films prepared by low-temperature PECVD process are summarized in Table 1.1. The columnar-structured poly-Si films are to be preferable with respect to the collection of photo-generated carriers because the solar cells are basically operated being perpendicular to the film plane (substrate). Furthermore, compared with a-Si:H, poly-Si is advantageous in terms of wide range spectral sensitivity for almost entire air mass 1.5 (AM 1.5) photons. In addition, poly-Si film shows high long-term stability against the prolonged light exposure [17]. Although the poly-Si thin film is very attractive material for applying solar cell photovoltaic layer, there remain many rooms for researching material properties and its photovoltaic operation mechanism being contrasted with mature a-Si:H material science and device technologies. In particular, the material and device design concept for realizing high efficiency solar cell is far from been established. In view of these backgrounds, this work is motivated to focus on poly-Si thin films as one of the most promising candidates for the next-age photovoltaic material, and aims to develop the high efficiency poly-Si thin film solar cells.

Table 1.1. Definitions and feature of various low-temperature silicon thin films.

Symbol	Phase	Structure	Feature size	Stability against light
a-Si:H	single phase	amorphous, homogeneous	none	×
μc-Si	mixed-phase (amorphous+crystalline)	inhomogeneous, crystallites in amorphous matrix	< 100 Å	○
poly-Si		inhomogeneous, columnar grain	> 100 Å	○

1.2 Purpose of this work

As mentioned above, low-temperature silicon thin films show a wide variety of microstructure by the change of deposition conditions, from a polycrystalline state, via a microcrystalline state, to an amorphous state. Even within a polycrystalline state, many researchers have demonstrated that poly-Si thin films prepared under various deposition conditions show various microstructure from low crystalline volume fraction to almost complete crystalline with different grain sizes and different crystallographic orientations. These structural changes of poly-Si thin films should directly influence carrier transport behavior that must correlate with photovoltaic performance. So far, however, it has been never sufficient for the systematic studies on carrier transport and photovoltaic performance in conjunction with the structural studies. The purpose of this work is to find out some universal relationships among the structural properties, carrier transport and photovoltaic performance. Based on these important relationships, this work is exactly aimed to design both material and device for the high efficiency poly-Si thin film solar cells.

In order to obtain the desirable and high quality photovoltaic poly-Si thin films, it is necessary to examine a wide range of experimental issues from film deposition and material characterization to the device fabrication and optimum design of thin film solar cells. Device modeling of poly-Si solar cell is also important approach in order to make sure of the existing problems and to give some useful guidelines for adequate device designing. In this thesis, the author has paid his special attention on following four items as the most important technical key issues for realizing high efficiency poly-Si thin film solar cells.

1) Grain boundary
2) Film microstructure
3) Carrier transport
4) Light trapping

First of all, the main drawback of low-temperature deposition is that it leads to extremely small grain size (« 1 μm) in comparison with high-temperature poly-Si thin films or any other available polycrystalline photovoltaic materials [18]. Therefore, it is necessary to investigate the effect of both grain size and grain boundary conditions on photovoltaic performance. Secondary, during film deposition process, it is quite essential to find out what is the dominant factor in determination of the poly-Si microstructure including crystalline volume fraction, grain size, crystallographic orientation. Also needed for the improvement of poly-Si solar cells is an analysis of the relationship between microstructure and photovoltaic performance. Thirdly, carrier transport should significantly reflect the microstructure in poly-Si photovoltaic layer. In this respect, the relationship between electronic transport properties of poly-Si films and its photovoltaic performance should be clarified in detail. Finally, for poly-Si thin film solar cell with a thickness of around 3 μm, the light trapping technique is of prime importance because silicon crystallites cannot absorb solar photons completely with such thin film thickness.

In chapter II, device modeling of p-i-n junction poly-Si thin film solar cells is carried out in order to analyze the effect of grain size and surface recombination velocity at grain boundary on photovoltaic performance. The simulation results suggest some important factors related to the grain boundary that dominates the photovoltaic performance.

In chapter III, the role of poly-Si microstructure in the photovoltaic performance is discussed on the basis of a systematic investigation of intrinsic poly-Si thin films prepared by 100 MHz VHF-PECVD for p-i-n junction solar cell. Atomic hydrogen during the film growth plays an important role in controlling poly-Si microstructure, which is presented in detail. In the final part of this chapter, an important universal relationship between poly-Si microstructure and photovoltaic performance is described.

In chapter IV, a novel electrical characterization technique is proposed to measure electron and hole conductivities individually. This conductivity measurement is applied to poly-Si thin films with different microstructure.

Based on these results, the relationship between electrical properties of poly-Si films and photovoltaic performance is discussed. Furthermore, Time-of-Flight experiment is performed on device grade poly-Si thin films. The electron and hole drift mobilities in poly-Si thin films are compared with those in conventional a-Si:H thin films, and their different carrier transport behaviors are discussed.

In chapter V, a novel textured back reflector consisting of ZnO/Ag/SnO_2 layers is proposed for realizing effective light trapping in thin film poly-Si photovoltaic layer. The systematic investigation is carried out concerning the dependence of poly-Si microstructure and photovoltaic performance on substrate texture as a function of root mean square roughness of substrate surface. Some detail discussions are also given on the carrier transport behavior particularly near the junction interface between poly-Si photovoltaic layer and textured substrate. Finally, the performance of p-i-n junction poly-Si solar cell with the highest conversion efficiency achieved throughout this work is demonstrated with an optimum poly-Si layer thickness as well as an optimum textured substrate.

In the final chapter, some conclusions obtained through this work are summarized.

References

[1] Y. Hamakawa: Proc. 1st World Conference on Photovoltaic Energy Conversion (WCPEC), Hawaii, (1994) p.34.

[2] M. A. Green, J. Zhao and A. Wang: Proc. 2nd World Conference on Photovoltaic Energy Conversion (WCPEC), Vienna, (1998), p.1187.

[3] T. Fuyuki, H. Yoshida and H. Matsunami: Proc. 1st World Conference on Photovoltaic Energy Conversion (WCPEC), Hawaii, (1994) p.1383.

[4] J. Hotzel, K. Peter, G. Willeke, E. Bucher: Proc. of 2nd World Conference on Photovoltaic Energy Conversion (WCPEC), Vienna, (1998), p.1278.

[5] H. Morisawa, Y. Kawama, Y. Matsuno, S. Hamamoto, K. Imada, T. Ishihara, K. Kojima and T. Ogama: Proc. 11th International Photovoltaic Science and Engineering Conference (PVSEC), Sapporo, (1999) p.529.

[6] H. Tayanaka, K. Yamauchi and T. Matsushita: Proc. 11th International Photovoltaic Science and Engineering Conference (PVSEC), Sapporo, (1999) p.543.

[7] J. K. Rath, A.J.M.M. van Zutphen, H. Meiling and R.E.I. Schropp: Proc. 2nd World Conference on Photovoltaic Energy Conversion (WCPEC), Vienna, (1998), p.956.

[8] P. Muller, W.M. Holber, W. Henrion, E. Nebauer, V. Schlosser, B. Sell, I. Sieber and W. Fuhs: Solid State Phenomena **67-68** (1999) 119.

[9] H.F. Sterling and R.C.G. Swann: Solid-State Electron. **8** (1965)653.

[10] S. Vepřek and V. Marečel: Solid-State Electron. **11** (1968) 683.

[11] W.E. Spear and P.G. LeComber: Solid State Commnu. 17 (1975) 1193.

[12] D.E. Carlson and C.R. Wronski: Appl. Phys. Lett. **28** (1976) 671.

[13] M. Konagai: Proc. 12th International Photovoltaic Science and Engineering Conference (PVSEC), Jeju, (2001) p.65.

[14] Y. Hattori, D. Kruangam, K. Katoh, Y. Nitta, H. Okamoto and Y. Hamakawa: Proc. 3th International Photovoltaic Science and Engineering Conference (PVSEC), Tokyo, (1987) p.171

[15] S. Usui and M. Kikuchi: J. Non-Cryst. Solids **34** (1979) 1.

[16] D. L. Staebler and C.R. Wronski: Appl. Phys. Lett. **31** (1977) 292.

[17] J. Meier, R. Fluckiger, H. Keppner, and A. Shah: Proc. 1st World Conference on Photovoltaic Energy Conversion (WCPEC), Hawaii, (1994) p.409.

[18] N. Wyrsch, C. Droz, L. Feitknecht, M. Goerlitzer, U. Kroll, J. Meier, P. Torres, E. Vallat-Sauvain, A. Shah, M. Vanecek: Mat. Res. Soc. Symp. Proc. **609** (2001) A15 1.1.

Chapter II

Device modeling of poly-Si thin film solar cells

2.1 Introduction

In most case of polycrystalline based solar cells, the grain boundaries dominate the photovoltaic performance. The grain boundaries are the regions of appreciable disorder with both structural defects and segregated impurities in large densities. Thus they are generally regions of extensive carrier recombination. The reduction in photovoltaic output parameters by this carrier recombination strongly depends on grain size in the photovoltaic layer. In a general sense, the grain size should be as large as possible in order that carriers diffuse to the junction to be usefully collected and not diffuse to grain boundary to be recombined. Recently, much attention has gathered on polycrystalline silicon (poly-Si) thin films produced at an extremely low temperature (~200°C) as a novel low-cost and stable photovoltaic material. It has been reported that the typical poly-Si thin films show columnar grains with a grain size (diameter) of being much less than the film thickness [1-4]. This structural anisotropy is a unique feature so that the effects of the structural aspect ratio between the grain size and the film thickness on the photovoltaic performance are expected to be much crucial, in comparison with the case of other available polycrystalline

photovoltaic materials with isotropic large grains. Also expected to be crucial is that carriers in the low-temperature poly-Si are highly sensitive for the electrical activity of localized states lying on grain boundaries because of the small grain size. Therefore, before applying the poly-Si thin film to solar cells as the active layer in experiments, some theoretical considerations must be approved with a device modeling technique.

Computer simulation for the comprehensive studies on device operation of solar cells is an indispensable technique to extract the existing problems and to estimate the internal physical parameters of layers or devices that cannot be measured by usual experimental ways. In the case of low-temperature poly-Si thin film solar cells with grain size bellow 1 μm, however, little effort has been done to obtain an accurate assessment of the effect of grain boundary on photovoltaic performance [5,6]. In this thesis work, a two-dimensional (2-D) numerical simulation method is applied to p-i-n junction poly-Si thin film solar cells as a viable tool for the optimum design [7]. Furthermore the developed simulation also offer an opportunity to gain insight the role played by grain boundary in device operation with quantitative physical parameters.

This chapter begins with a brief description of some simulation techniques for modeling the poly-Si thin film solar cell comprising of grain boundaries orientated perpendicular to the junction plane. We will discuss the dependence of photovoltaic performance on grain boundary conditions as a function of grain size, L_G, and surface recombination velocity at grain boundary, S_{GB}, for minority carriers. It is found that photovoltaic performance is predominantly determined by two factors, i.e., the built-in electric field and the $L_G/2S_{GB}$. This result is followed by an important suggestion that the very thin photovoltaic layer below 3 μm is quite essential for small-grain-size poly-Si solar cells in order to reduce recombination of both photo-generated and injection carriers at grain boundaries.

2.2 Simulation model for poly-Si thin film solar cells

2.2.1 Basic calculation method for device simulation

The simulation program is based on the solution of the set of semiconductor equations and on the physical models which describe the material properties. The basic set of semiconductor equations represents a mathematical description of semiconductor device operation under non-equilibrium and steady-state conditions. At first, basic semiconductor equations including Poisson's equation in eq. (2.1) and the continuity equations for electrons in eq. (2.2), and for holes in eq. (2.3) are given as

$$\nabla \cdot (\varepsilon \nabla \psi) = -q(p - n + N_D - N_A), \tag{2.1}$$

$$\nabla \cdot \mathbf{J}_n = -q(G - R), \tag{2.2}$$

$$\nabla \cdot \mathbf{J}_p = q(G - R), \tag{2.3}$$

where ε denotes the material dielectric constant, ψ the electrostatic potential, n (p) the electron (hole) density, N_D (N_A) the ionized donor (acceptor) concentration, G the generation rate, R the recombination rate and $\mathbf{J}_n$ ($\mathbf{J}_p$) the current density of electron (hole). The electron (hole) density and the electron (hole) current density in eqs. (2.1)-(2.3) are written by

$$n = n_i \exp\left(\frac{q(\psi - \phi_n)}{kT}\right), \tag{2.4}$$

$$p = n_i \exp\left(\frac{q(\phi_p - \psi)}{kT}\right), \tag{2.5}$$

$$\mathbf{J}_n = -q\left(-\mu_n n \nabla \psi - D_n \nabla n\right), \tag{2.6}$$

$$\mathbf{J}_p = q\left(\mu_p n \nabla \psi - D_p \nabla p\right), \tag{2.7}$$

where n_i denotes the intrinsic carrier density, ϕ_n (ϕ_p) the quasi-fermi level for electron (hole), μ_n (μ_p) the mobility of electron (hole), q the elemental charge, k the Boltzmann constant, and T the absolute temperature. The non-liner terms in eqs. (2.1)-(2.3), such as a term of a second derivative of the Poisson's equation, were approximated by Taylor expansion series to eliminate the higher order components. These linerized equations are then digitized on the 2-D grid points (100 × 100), and a computer program consistently solves this set of equations together with the imposed boundary conditions using a finite derivative method. The recombination process via the single-level states located at the intrinsic Fermi level was assumed in accordance with the Shockley-Read-Hall (SRH) statistics.

2.2.2 Two dimensional grain boundary model

Figure 2.1 shows a schematic illustration of simulation model for p-i-n junction poly-Si solar cell. In this model, light is incident on the p-layer and a

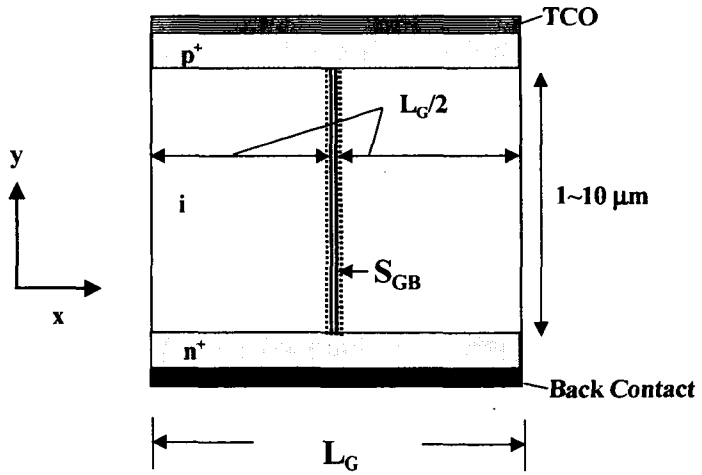

Fig. 2.1. Structure of simulation model.

Table 2.1 Major simulation parameters.

electron	lifetime	τ_n	0.5 (μs)
hole	lifetime	τ_p	0.1 (μs)
electron	mobility	μ_n	90 (cm^2/Vs)
hole	mobility	μ_p	25 (cm^2/Vs)
surface recombination velocity at grain boundary		S_{GB}	10-10^3 cm/s
grain size		L_G	0.01- 1μm
thickness of i-layer		d	1-10 μm

grain boundary in the i-layer is assumed to be perpendicular to the junction plane.

The typical simulation parameters employed in this study are shown in Table 2.1. Electron and hole mobilities were assumed to be moderate values of 90 and 25 cm^2/Vs, respectively, which are by about one order of magnitude lower than those of c-Si. With using these mobility values, it has been checked that the photovoltaic performance of highly efficient 'bulk' multi-crystalline solar cells with large and isotropic grown grains is well expressed by the simulation results [8]. To calculate the photo-current, the numerical data in the spectrum of the sun light under 100 mW/cm^2, AM1.5 and optical absorption coefficient of bulk c-Si were used for the simulation program. The grain boundary is characterized by two important parameters, i.e., the grain size, L_G (μm), and surface recombination velocity at grain boundary, S_{GB} (cm/s). The formula of S_{GB} for grain boundary is given by the following expression using carrier lifetime at grain boundary, τ_{GB},

$$\frac{1}{\tau_{GB}} = \frac{1}{\tau_G} + \frac{S_{GB}}{\Delta x} \quad , \tag{2.8}$$

where τ_G denotes the lifetime inside the grains, and Δx the grid point interval between grain boundary position and its contiguous point in the x direction. The preliminary tests have indicated that the lifetime of minority carriers inside grains should be 1/1000 of that in c-Si in order to reproduce recent experimental results in low temperature poly-Si thin film solar cells. The potential barrier effect associated with grain boundary was neglected in this simulation. As an example of calculation result, the counter plot of carrier recombination profile at short circuit condition is shown in Fig. 2.2, with L_G=1 μm and S_{GB}=10^3 cm/s under AM1.5 illumination. Also shown in Fig. 2.2 is the depth profiles of the recombination at different cross-sectional positions; one is that at the grain boundary and at the other position far by $L_G/4$. As can be seen in this figure, the recombination rate of the photo-generated carriers at the grain boundary is markedly higher than that inside the grains (x=0 or 1.0 μm). This recombination profile, which is never deduced experimentally, is one of the most representative results being useful for studying the effect of the grain boundary on device operation.

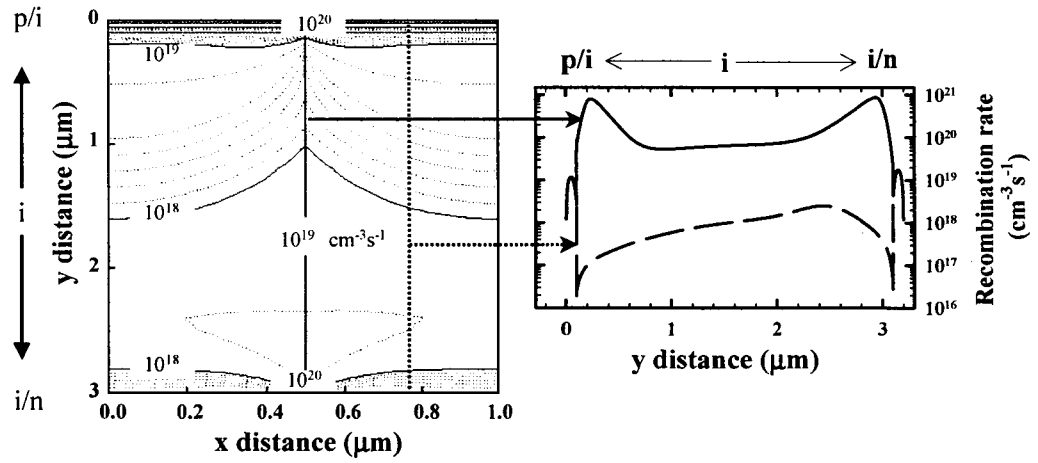

Fig. 2.2. Counter plot (left) and cross-sectional profile (right) of calculated carrier recombination rate.

2.3 Effect of grain boundary on photovoltaic performance

2.3.1 Grain size and surface recombination velocity at grain boundary

Figure 2.3 shows the calculated results of poly-Si photovoltaic performance, i.e., short circuit current density (J_{sc}), open circuit voltage (V_{oc}), fill factor (FF) and conversion efficiency (η), as a function of grain size in the range of 0.01-1 μm, with various surface recombination velocities at grain boundary (S_{GB}: 10, 10^2, 10^3 cm/s). In this calculation, the thickness of i-layer was set at 3 μm. As found in Fig 2.3, all the photovoltaic parameters decrease with a decrease in grain size or with an increase in S_{GB}. J_{sc} shows a rapid decrease at grain sizes below 0.1 μm when $S_{GB}=10^3$ cm/s, while it is almost unchanged at $S_{GB}=10$ cm/s and $S_{GB}=10^2$ cm/s for any grain sizes of the poly-Si i-layer. On the other hand, V_{oc} and FF are largely dependent on both the grain size and S_{GB} in contrast with J_{sc}. Even if grain size is relatively large, say > 0.1 μm, V_{oc} is still strongly dominated by S_{GB}.

A less pronounced dependence of J_{sc} on the grain size can be explained in terms of the high carrier drift velocity due to the presence of strong electric field through the i-layer at short circuit condition. However, the situation turns to be complicated at forward biased condition. The built-in electric field should decrease with an increase in applied forward voltage, photo-generated carriers then almost fully recombine at the grain boundaries if the grain size is quite small and S_{GB} is high. This leads to that photo-generated carrier collection strongly depends on the applied voltage, resulting in poor FF. Moreover, the carrier injection steadily increases with a decrease in grain size because carrier injection level is almost determined by the total carrier recombination throughout the photovoltaic i-layer, which leads to a significant reduction in V_{oc} and FF.

Meier *et al.*, reported that columnar structured poly-Si films prepared by PECVD at temperatures below 250°C have grains with a typical diameter of 0.02-μm, which was characterized by transmittance electron microscope (TEM) observation [9]. They applied these films to solar cell device and demonstrated

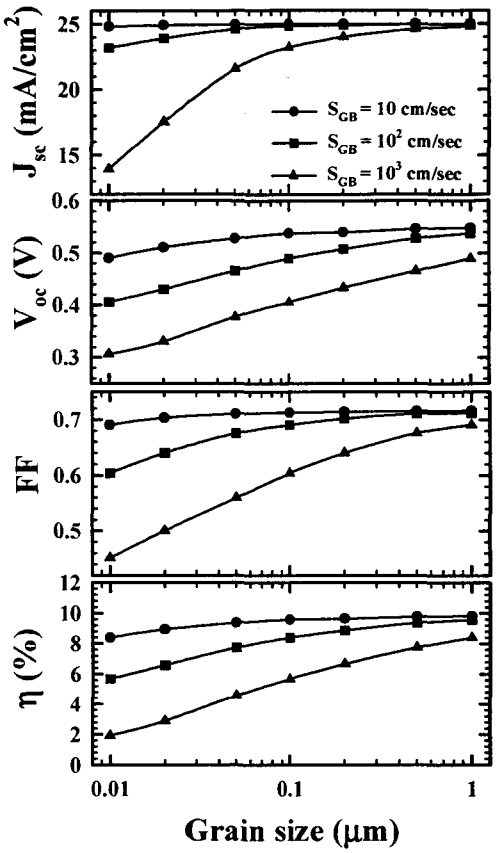

Fig. 2.3. Calculated results of photovoltaic performance as a function of grain size at different surface recombination velocities at grain boundary.

relatively high conversion efficiency exceeding 8%. A comparison of the photovoltaic performances obtained by their experiments, with those in our simulation results allows us to suppose that the grain boundaries of their poly-Si films should be well passivated with a very low surface recombination velocity at grain boundaries as low as 10 cm/s. This estimated surface recombination velocity is even less than that for passivated Si/SiO_2 interface which is commonly available for single crystalline silicon solar cells. Meanwhile, high temperature poly-Si solar cells need grain size at least »1 μm for achieving conversion efficiency of >8% [10], which implies that surface recombination

velocity at grain boundary is more than 10^3 cm/s in the high-temperature poly-Si, as learned in Fig. 2.3. An inactive grain boundary in low-temperature poly-Si thin films is likely achieved due to its specific microstructure such as crystalline-amorphous mixed-phase and hydrogen incorporation during film growth, which are not attained in high-temperature poly-Si [11]. The role of the microstructure will be described again in chapter III in conjunction with the results on our experimental studies.

2.3.2 Optimum i-layer thickness

Since the poly-Si films are materials exhibiting indirect optical transition, the required thickness of photovoltaic layer for obtaining sufficient photo-current reaches several tens microns. Concerning the p-i-n device structure, however, an increase in i-layer shall result in weak built-in electric field distribution through i-layer and then lower carrier drift velocity, which gives an adverse affect on the collection of photo-generated carriers as described above. Fill factor of the illuminated *J-V* characteristics thus strongly reflect the field-dependent carrier collection. Furthermore, thick i-layer gives rise to higher carrier recombination due to an increase in total amount of defects in the i-layer, which makes V_{oc} lower. As discussed above, the grain size and the surface recombination velocity at grain boundary strongly influence poly-Si photovoltaic performance so that an optimum i-layer thickness should be determined from the deep consideration of grain boundary effects.

Figure 2.4 shows calculated results of poly-Si photovoltaic performance as a function of $L_G/2S_{GB}$ at various i-layer thicknesses in the range of 1-10 μm. The $L_G/2S_{GB}$ would roughly correspond to the effective carrier lifetime until recombination at grain boundary [12,13]. This parameter allows us to compare the lifetime to recombine at grain boundary with the lifetime to recombine inside poly-Si grains, τ_G. Here, the τ_G for electrons and holes are set at about 10^{-7} sec. As found in Fig. 2.4, J_{sc} shows different dependence on $L_G/2S_{GB}$ for different i-layer thickness. The solar cells having thick i–layer, e.g., 10 μm, J_{sc} shows high

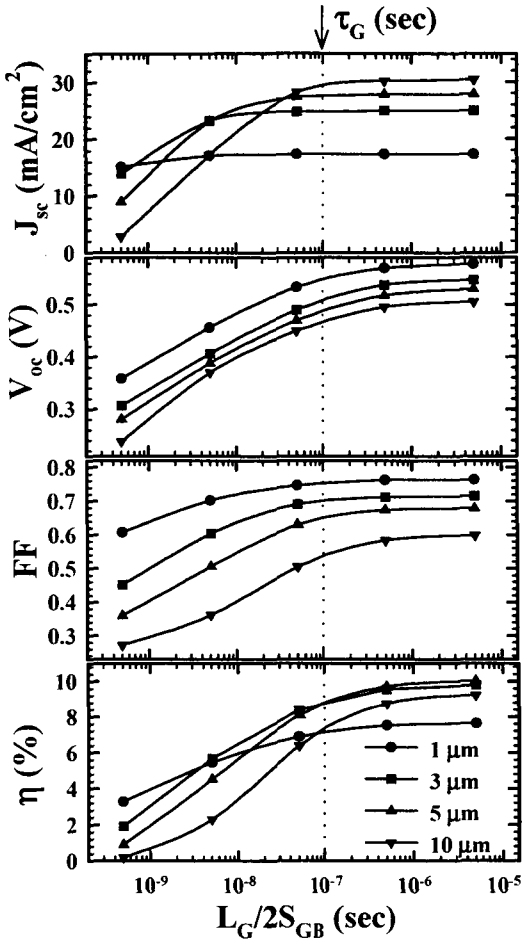

Fig. 2.4. Calculated results of photovoltaic performance as a function of $L_G/2S_{GB}$ at different i-layer thicknesses. Arrow indicates carrier lifetime value inside grains, τ_G. In this simulation, τ_G for electrons and holes are set at about 10^{-7} sec.

values of nearly 30 mA/cm^2 when $L_G/2S_{GB} \gg \tau_G$, while it shows dramatic decrease when $L_G/2S_{GB} \ll \tau_G$. On the other hand, for the solar cells with 1-μm thick i–layer, J_{sc} shows relatively low values of around 16 mA/cm^2 but it is almost unchanged against $L_G/2S_{GB}$. This indicates that effective carrier diffusion length of photo-generated carrier is determined by two competitive factors, i.e., $L_G/2S_{GB}$ and built-in electric field associated with i-layer thickness. In contrast, the

behavior of V_{oc} and FF against $L_G/2S_{GB}$ is different from that of J_{sc}. For any i-layer thickness, V_{oc} and FF monotonously increase with an increase in $L_G/2S_{GB}$ and tend to saturate when $L_G/2S_{GB}$ becomes close to τ_G. It is also found that relatively high V_{oc} and FF are expectable for thinner poly-Si solar cells if $L_G/2S_{GB}$ is equal to or more than τ_G. As the result of these different behaviors of J_{sc}, V_{oc} and FF against $L_G/2S_{GB}$, the conversion efficiency always shows higher values at the i-layer thickness of 3 μm within this calculation range of $L_G/2S_{GB}$.

As shown in Fig. 2.4, $L_G/2S_{GB}$ is found to be a crucial factor in determination of photovoltaic performance, indicating that effective passivation of grain boundary is quite essential if we use small grain poly-Si films as a photovoltaic layer. The simulation results also suggest that the thickness of poly-Si photovoltaic layer is required to be designed as thin as possible to reduce the grain boundary effects and to obtain high V_{oc} and FF. The light trapping techniques are then of practical importance to obtain high J_{sc} with thin photovoltaic layer.

2.4 Summary

Device modeling of p-i-n junction poly-Si thin film solar cells with different columnar grain sizes and surface recombination velocities at grain boundary, S_{GB}, has been investigated using two-dimensional device simulator. The dependence of J_{sc} on grain boundary conditions is relatively small if the built-in electric field through the photovoltaic i-layer is sufficient for carrier collection at short circuit condition. However, V_{oc} and FF considerably depend on both grain size and S_{GB} at grain boundary. The $L_G/2S_{GB}$ is found to be a crucial factor in determination of photovoltaic performance. The effective carrier diffusion length of photo-generated carrier is almost determined by $L_G/2S_{GB}$ as well as the built-in electric field through the photovoltaic layer. It is also found that relatively high V_{oc} and FF can be obtain when $L_G/2S_{GB}$ is comparable to the carrier lifetime inside the grains. Based on these simulation

results, it can be concluded that the very thin photovoltaic layer below 3 μm is quite essential for small-grain-size poly-Si solar cells in order to reduce recombination of both photo-generated and injection carriers at grain boundaries.

References

[1] K. Yamamoto, A. Nakajima, T. Suzuki, M. Yoshimi, H. Nishio, M. Izumiya: Proc. 1st World Conference on Photovoltaic Energy Conversion (WCPEC), Hawaii, (1994) p.1575.

[2] D. Fischer, S. Dubail, J.A. Anna Selvan, N. Pellaton Vaucher, R. Platz, Ch. Hof, U. Kroll, J. Meier, P. Torres, H. Keppner, N. Wyrsch, M. Goetz, A. Shah, K.D. Ufert: Proc. 25th IEEE Photovoltaic Specialist Conference (1996) p.1053.

[3] K. Yamamoto, M. Yoshimi, T. Suzuki, Y. Okamoto, Y. Tawada, A. Nakajima: Proc. 26th IEEE Photovoltaic Specialist Conference (1997) p.575.

[4] K. Saito, M. Sano, K. Matsuda, T. Kondo, T. Nishimoto, K. Ogawa and I. Kajita: Proc. 2nd World Conference on Photovoltaic Energy Conversion (WCPEC), Vienna, (1998) 351-354.

[5] S.A. Edmiston: J. Appl. Phys. **81** (1997) 2282.

[6] P.P. Altermatt and G. Heiser: Proc. 12th International Photovoltaic Science and Engineering Conference (PVSEC), Jeju, (2001) p.207.

[7] T. Matsui, T. Yamazaki, A. Nagatani, K. Kino, H. Takakura and Y. Hamakawa: Solar Energy Materials and Solar Cells **65** (2001) 87.

[8] H.Takakura, T. Matsui, M. Nakai, Y. Hamakawa: Proc. ISES'97 World Solar Congress, Taejon, Korea (1997) p.63.

[9] N. Wyrsch, C. Droz, L. Feitknecht, M. Goerlitzer, U. Kroll, J. Meier, P. Torres, E. Vallat-Sauvain, A. Shah, M. Vanecek: Mat. Res. Soc. Symp. Proc. **609** (2001) A15 1.1.

[10] R.B. Bergmann: J. Appl. Phys. **A69** (1999) 187.

[11] J. H. Werner: in Techn. Dig. 13th Sunshine Workshop on Thin Film Solar Cells, M. Konagai ed. (NEDO, Tokyo, 2000) p.41.

[12] H.C. Card and E. Yang: IEEE Trans. Electron Device **24** (1977) 397.

[13] A.K. Ghosh, C. Fishman and T. Feng: J. Appl. Phys. **51** (1980) 446.

Chapter III

Correlation between microstructure and photovoltaic performance of poly-Si thin film solar cells

3.1 Introduction

Thin film solar cells comprising an intrinsic polycrystalline silicon (poly-Si) photovoltaic layer have attracted much attention as one of the most promising candidates for a stable and highly efficient solar cell. The plasma-enhanced chemical vapor deposition (PECVD) technique with silane (SiH_4) highly diluted in hydrogen (H_2) is widely used for the fabrication of poly-Si films because of its low substrate temperature (~200°C) and mass productivity. Recently, some research groups have reported poly-Si solar cells prepared by PECVD at very high frequency (VHF) (~100 MHz) excitation [1–3]. Compared with the conventional rf (13.56 MHz) PECVD, VHF-PECVD has such advantages as high deposition rate without deterioration of crystallinity and photovoltaic performance [1]. Actually, using the VHF-PECVD technique, a high efficiency exceeding 8% has been achieved on a single-junction poly-Si solar cell produced at relatively high deposition rate (~4 Å/s) by the Institute of Photovoltaics (IPV) Jülich [2]. Their accomplishment is lead from the optimization of two

deposition parameters, i.e., SiH_4 concentration and VHF glow discharge power. On the other hand, Saito *et al.* suggested that SiH_4 flow rate is one of the important deposition parameters for attaining high photovoltaic performance particularly in the high deposition rate regime [3]. Moreover, high-pressure deposition in the SiH_4 depletion regime was recently reported by Fukawa *et al.* in order to increase deposition rate while maintaining good crystallinity of the poly-Si layer [4]. These preliminary studies on the poly-Si photovoltaic layer encourage us to develop highly efficient poly-Si solar cells with high deposition rate.

However, problems concerning material control of high-grade poly-Si solar cells in the VHF-PECVD process are far from being resolved. In particular, the control of poly-Si microstructure including crystalline volume fraction, the grain size and preferential orientation is regarded as one of the most crucial technical issues, that directly influence carrier transport properties in the poly-Si films. Therefore, the relationship between the deposition parameters and the poly-Si microstructure should be examined in detail. Also needed for the improvement of poly-Si solar cells is an analysis of the relationship between microstructure and photovoltaic performance.

In this chapter, the role of poly-Si microstructure played in the photovoltaic performance is discussed on the basis of a systematic investigation of intrinsic poly-Si thin films prepared by 100 MHz VHF-PECVD for p-i-n junction solar cell. A series of the solar cells has been fabricated with various i-layer deposition conditions, such as deposition pressure, SiH_4 gas flow rate and SiH_4 concentration. It is demonstrated that the structural properties of the poly-Si photovoltaic layers strongly depend on these deposition conditions. We will show the universal relationship between poly-Si microstructure and photovoltaic performance, especially open circuit voltage (V_{oc}) and short circuit current density (J_{sc}).

3.2 Fabrication and characterization techniques of poly-Si solar cells

3.2.1 Deposition technique (VHF-PECVD) for intrinsic poly-Si thin films

In a general sense, the deposition of poly- or microcrystalline (μc-Si) materials by means of PECVD process needs higher hydrogen dilution than that for the deposition of amorphous silicon. Hydrogen dilution plays a predominant role in determining film quality as well as the formation of crystalline silicon. Many researchers have devoted to elucidate the growth kinetics of poly-Si films and the role of hydrogen for the film growth, whereas it has been still in controversial. Due to the high hydrogen dilution in deposition process, only few concentrations of reaction source gas in plasma can contribute to film growth, which would result in quite low deposition rate. Furthermore, from the aspect of the optical absorption coefficient, required thickness for the poly-Si photovoltaic layer is relatively thicker than that in amorphous silicon solar cells. The low deposition rate is a serious drawback for the future mass production of poly-Si photovoltaic system. Recently, VHF-PECVD, i.e., PECVD with a plasma excitation frequency is modified from the conventional rf range (13.56 MHz) to VHF range (~100 MHz) has been proposed for enhancement of the deposition rate. Vepřek *et al.* have shown that an increase of excitation frequency leads to high concentration of electrons in plasma, which promotes to increase the ionization rate [5]. This increased ionization rate decreases plasma potential, V_p (see Fig. 3.1), which results in a decrease of mean ion energy, finally results in low energy and high ion flux on growing surface. At the same time, low-energy and high ion flux is now believed to enhance the surface mobility of radical species, so that the film properties remain device-quality even at a high deposition rate condition. Dutta *et al.* estimated the peak ion energy for silicon ions as a function of the excitation frequency [6] as shown in Fig. 3.2. The ion energy in plasma monotonically decreases with an increase in excitation frequency. The silicon-ion bombardment energies higher

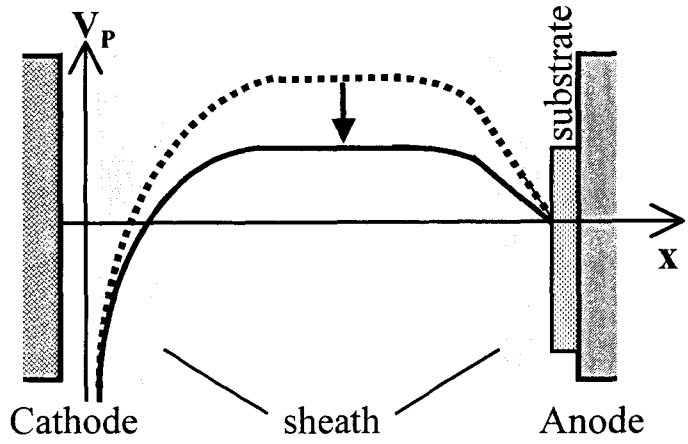

Fig. 3.1. Schematic representation of potential (V_p) distribution in glow discharge plasma. Solid and dotted lines represent V_p for VHF- and rf-excitation plasma, respectively.

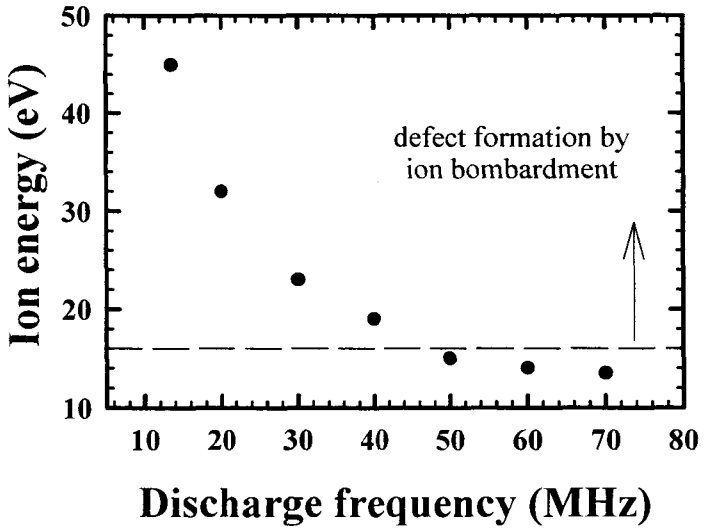

Fig. 3.2. Estimated peak Si-ion energies for SiH_4 plasma as a function of discharge frequency. (after Dutta *et al.* in ref. [6])

than 16 eV is believed to give rise to defect formation in the film [5]. As found in Fig 3.2, excitation frequency higher than 50 MHz successfully prevents the occurrence of Si ions with energies higher than 16 eV, which allows us to use

higher discharge power to maintain high deposition rate without any serious deterioration of the film quality.

In Fig. 3.3, a schematic diagram of the VHF-PECVD apparatus used in this experiment is shown. This apparatus consists of a single chamber for the deposition of poly-Si layer and a load lock for sample loading. The base pressure of the system is below 2×10^{-7} Torr maintained by turbo molecular pump (TMP). A 100 MHz VHF excitation source was used to produce glow discharge plasma in a capacitively coupled reactor with a cathode-anode gap of 2 cm. A mixture of SiH_4 and H_2 was used for the growth of the poly-Si layer. In this system, special attention has been paid to reduce the impurity contamination from the gas inlet line. The gas purifiers [7] for SiH_4 and H_2 lines are installed just before each mass flow controller (MFC). For plasma diagnostics, optical emission spectroscopy (OES) was employed, in which optical emission from a glow discharge chamber was guided via a quartz fiber into an optical multi-channel analyzer.

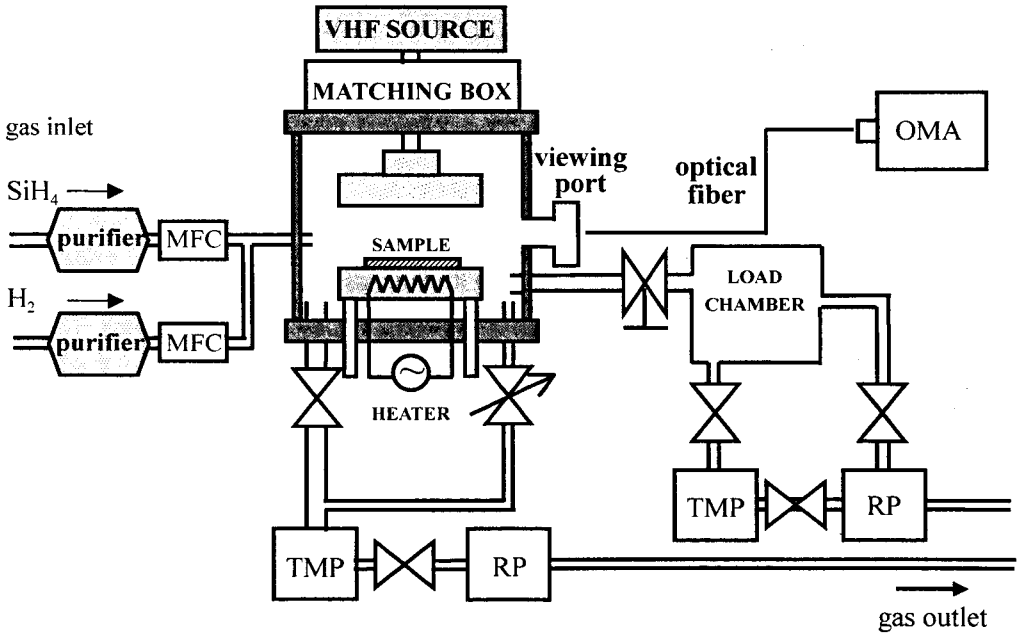

Fig. 3.3. Schematic diagram of VHF-PECVD system used in this experiment.

3.2.2 Device structure and fabrication process

The structure of poly-Si solar cell is illustrated in Fig. 3.4, which is composed of Ag-grid/transparent conductive oxide (TCO)/p-i-n/ZnO(1000 Å)/Ag(4000 Å)/ZnO(150 Å)/glass(Corning #7059). The first ZnO layer covered on glass is for maintaining film adhesion. A highly reflective ZnO/Ag double layer was used as a flat back contact. The microcrystalline silicon p-(350 Å) and n-(750 Å) layers, which are highly conductive and have activation energies less than 100 meV, were formed by the 13.56 MHz rf-PECVD system. Diborane (B_2H_6) and Phospine (PH_3) gases were used as dopant sources for p- and n- layer, respectively. The intrinsic poly-Si photovoltaic layer with a thickness of around 3 μm was deposited by VHF-PECVD. The deposition pressure was set at 0.08-1.0 Torr, the SiH_4 flow rate at 2.5-7.5 sccm, the SiH_4 flow rate over total gas flow rate, $[SiH_4]/([SiH_4]+[H_2])$, (defined here as the SiH_4 concentration) at 4.0-5.5%, the substrate temperature, T_s, at 180°C, and the VHF-power density at around 100 mW/cm^2. The typical deposition conditions for

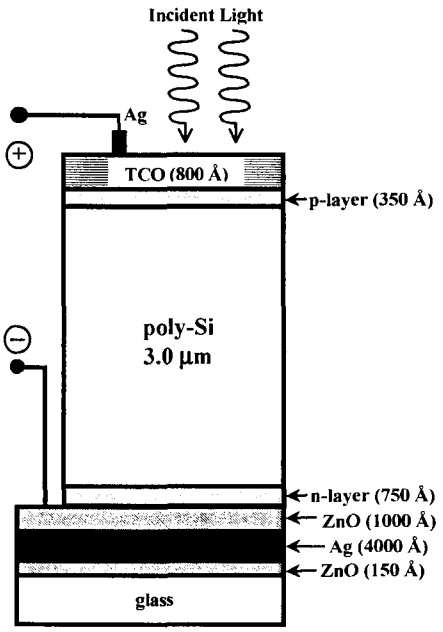

Fig. 3.4. Schematic illustration of solar cell structure.

each layer of p-i-n solar cells are summarized in Table 3.1. As the top TCO electrode, an indium tin oxide (ITO) or a ZnO film with a thickness of ~80 nm was formed on the p-layer with an Ag grid finger. The ITO and ZnO films were evaporated by the electron beam evaporation technique with sintered In_2O_3:SnO_2 (95:5 in weight %) and ZnO:Al_2O_3 (98:2 in weight %) targets, respectively. As the final step for complete device, an active area of the solar cell is patterned by a photolithography technique, and separated by wet etching process using a HF+HNO_3 enchant solvent, resulting in an active area of 0.23 cm^2.

Table 3.1. Deposition conditions for solar cells.

layer	gas flow rate (sccm)				P	T_s	freq.	power
	SiH_4	H_2	B_2H_6	PH_3	(Torr)	(°C)	(MHz)	(W/cm^2)
p	0.5	85	0.005	-	1.4	200	13.56	0.1
i	2.5-7.5	60-160	-	-	0.08-1.0	180	100	0.1
n	1.0	100	-	0.01	1.0	220	13.56	0.03

3.2.3 Characterization techniques of poly-Si thin film and its solar cell

Structural characterization of poly-Si films deposited on n-layer/ZnO/Ag/ZnO/glass was performed by Raman scattering spectroscopy using an Ar^+ ion 514.5 nm laser as the excitation source (Renishaw System-1000). X-ray diffraction (XRD) analysis in the θ-2θ scan geometry using the CuKα line (Rigaku RINT-2000) was also conducted. Current-voltage characteristics of the poly-Si solar cells were measured under air mass 1.5 (AM1.5), 100 mW/cm^2 illumination. Spectral response of solar cell was also measured with a conventional lock-in detection system.

3.3 Structural properties and photovoltaic performance of poly-Si thin film solar cells

3.3.1 Deposition pressure dependence

Raman spectra of the 3-μm-thick poly-Si photovoltaic layers deposited at different gas pressures ranging from 0.08 Torr to 1.0 Torr are shown in Fig. 3.5. The deposition rate of the poly-Si layer was almost constant at around 3 Å/s in this deposition pressure range. The Raman spectra mainly consist of two components, i.e., a broad band found at around 480 cm^{-1} being attributed to the amorphous silicon (a-Si) phase, and a sharp peak at around 520 cm^{-1} being

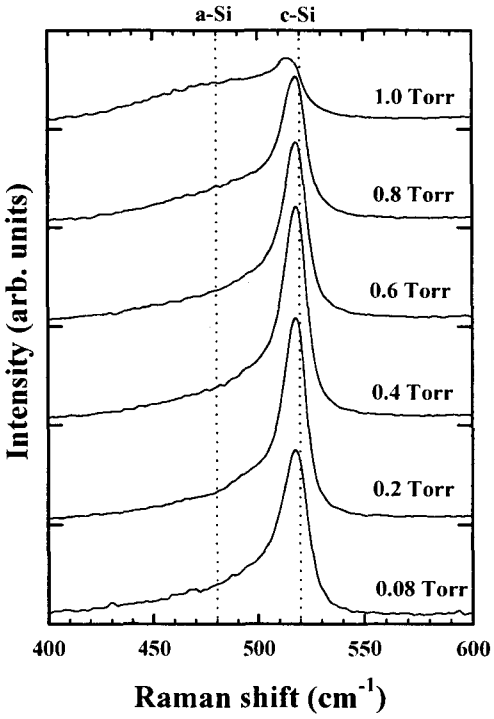

Fig. 3.5. Raman spectra of poly-Si layers on ZnO/Ag/ZnO/glass substrate deposited at different gas pressures. Subsequent deposition parameters are the same for all poly-Si layers, i.e., SiH_4 flow rate of 6.25 sccm and SiH_4 concentration of 4.5%.

attributed to the crystalline silicon (c-Si) phase. A less pronounced broad shoulder appearing at around 500 cm^{-1} is assigned to the presence of hexagonal structure induced by twin boundaries or stacking faults [8]. The 520 cm^{-1} peak is found to be dominant in the spectra of the poly-Si layers deposited below 0.8 Torr. Concerning the poly-Si film deposited at 1.0 Torr, the 480 cm^{-1} broad peak prevails, while the 520 cm^{-1} peak is very weak, implying that the crystalline volume fraction is quite low in the film. From the Raman spectra, crystalline volume fraction (X_c) is roughly estimated as

$$X_c = I_c/(I_a+I_c), \tag{3.1}$$

where I_c denotes the integrated intensity of the crystalline part and I_a, that of the amorphous part, both of which were evaluated from the spectrum by line fitting with a Lorentzian function. The definition of X_c in eq. (3.1) takes into account neither the difference in the Raman cross section [9] nor that in the optical absorption coefficient for the excitation light between amorphous Si and crystalline Si. Therefore, we must note that X_c discussed here represents a

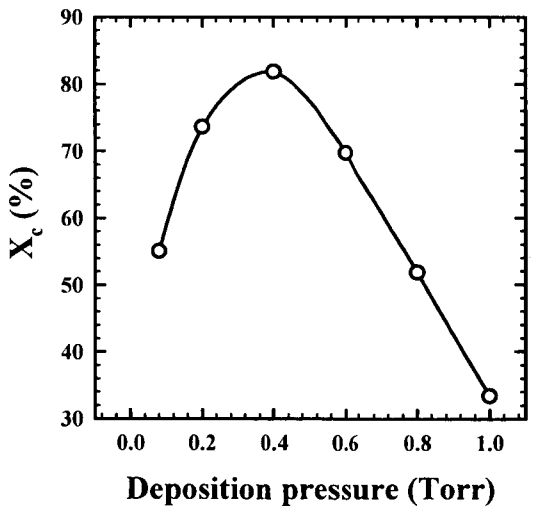

Fig. 3.6. Crystalline volume fraction of poly-Si layer (X_c) deduced from Raman spectra as a function of deposition pressure.

semi-quantitative value of the actual crystalline volume fraction of poly-Si films. In Fig. 3.6, X_c of the poly-Si layer obtained from Fig. 3.5 is plotted against the deposition pressure. With an increase in deposition pressure from 0.08 to 0.4 Torr, X_c increases and reaches the maximum of 83 %, then rapidly decreases above the deposition pressure of 0.4 Torr.

Figure 3.7 shows the XRD patterns of the poly-Si layers deposited at different deposition pressures, as also investigated by Raman scattering spectroscopy. The diffraction peaks are clearly observed at angles 2θ of 28.4°, 47.3° and 56.1°, which correspond to Si (111), (220) and (311), respectively. The other diffraction lines are originated from ZnO and Ag layers of the back

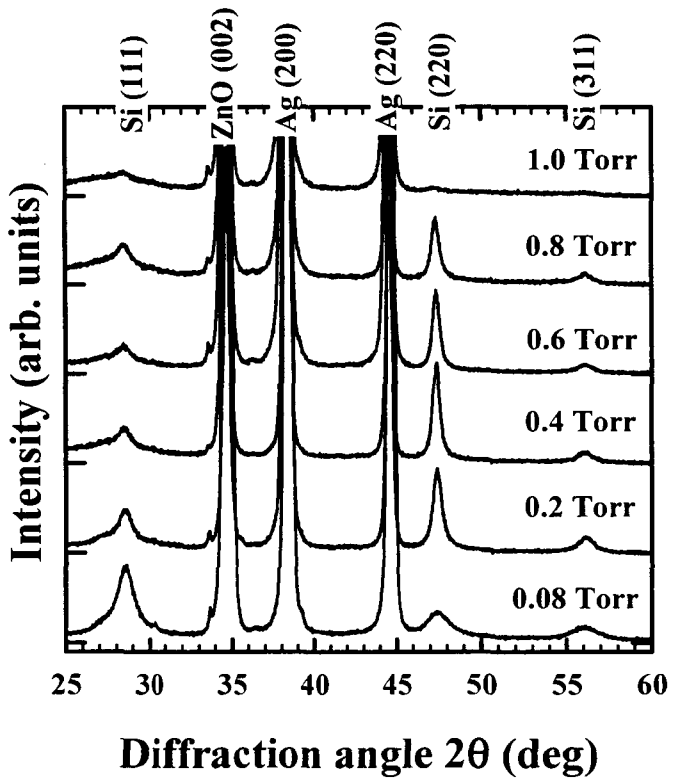

Fig. 3.7. XRD patterns of poly-Si layers on ZnO/Ag/ZnO/glass substrate at different deposition pressures.

reflector. All of the poly-Si layers basically exhibit the (220) preferential orientation except for the poly-Si layer deposited at 0.08 Torr and at 1.0 Torr. It is also found that the (220) diffraction peak intensity markedly changes with the deposition pressure in comparison to the (111) and (311) diffraction peak intensities. Figure 3.8 displays the deposition pressure dependence of the integrated intensities of the Si (220) diffraction line ($I_{(220)}$) together with its ratio to that of Si (111) and (311) (labeled $I_{(220)}/I_{(111)}$ and $I_{(220)}/I_{(311)}$, respectively).

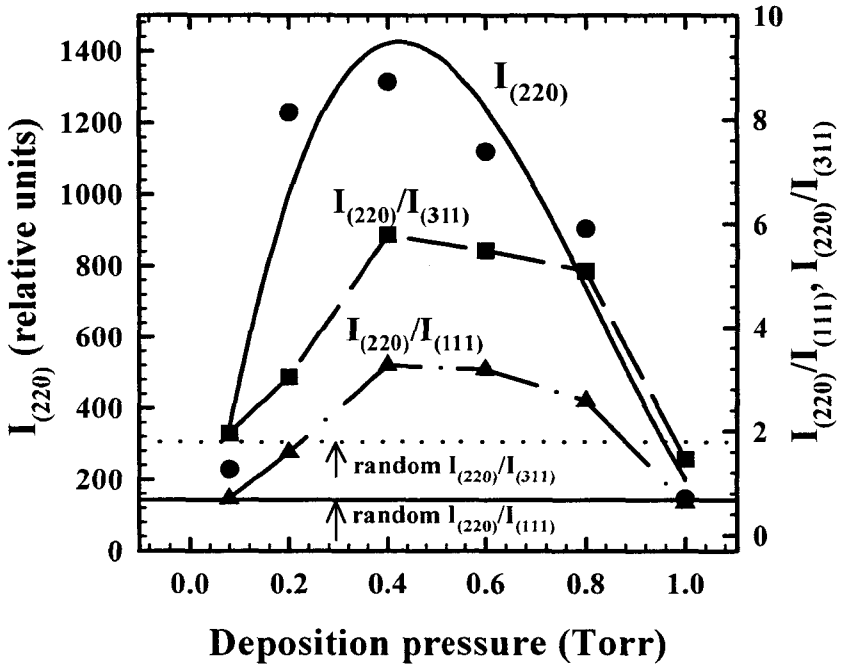

Fig. 3.8. Integrated X-ray intensities of Si (220) diffraction lines, $I_{(220)}$(●), together with its ratio to (111), $I_{(220)}/I_{(111)}$ (▲), and to (311), $I_{(220)}/I_{(311)}$ (■), as a function of deposition pressure. The lines are guides for the eyes. The straight lines seen at $I_{(220)}/I_{(111)}$=0.67 (solid line) and $I_{(220)}/I_{(311)}$=1.79 (dotted line) represent the theoretical values for those of the 3-μm-thick crystalline Si film with random crystallographic orientation.

In a series of these poly-Si layers, the change in $I_{(220)}$ correlates well with that in X_c deduced from the Raman spectra shown in Fig. 3.6. It is well known that the poly-Si films with (220) preferential orientation basically possess a columnar structure [10,11] and the grain size tends to increase along the growth direction [12]. On the other hand, the penetration depth of the excitation light used in Raman scattering measurement is less than 0.3 μm for the poly-Si films; thus the obtained X_c values should reflect the poly-Si microstructure just adjacent to the film surface. Accordingly, the agreement in tendency of the changes in $I_{(220)}$ and X_c against deposition pressure suggests that X_c of the poly-Si layer directly reflects the (220) grains size at poly-Si near surface. As is evident from XRD results as well as X_c, a decrease in deposition pressure in the range of 0.4-1.0 Torr basically enhances poly-Si crystallinity, especially in (220) grain size and crystalline volume fraction. With a further decrease in deposition pressure, however, a significant change in poly-Si microstructure takes place. When deposition pressure is decreased from 0.4 Torr to 0.08 Torr, $I_{(220)}$ and X_c decrease, while $I_{(111)}$ and $I_{(311)}$ increase. Both $I_{(220)}/I_{(111)}$ and $I_{(220)}/I_{(311)}$ ratios shown in Fig. 3.8, which give a clear indication of the degree of (220) preferential orientation of the poly-Si layer, exhibit low values at deposition pressures below 0.2 Torr in comparison with those of the poly-Si layers deposited at 0.4-0.8 Torr. This result implies that poly-Si crystallinity deteriorates due to the low-pressure plasma and the crystallographic orientation tends to become random.

In order to gain greater insight into the deposition pressure dependence of the poly-Si microstructure, OES measurement of the glow discharge plasma was carried out at different deposition pressures. We measured the intensities of SiH^* (λ = 412 nm), [SiH^*], and H_α (λ = 656 nm), [H_α], emission lines which are proportional to the generation rate of film precursor radicals and atomic hydrogen, respectively [13]. Figure 3.9 shows the OES intensities [SiH^*] and [H_α] as a function of deposition pressure. With decreasing deposition pressure, both [SiH^*] and [H_α] increase. [SiH^*] and [H_α] are basically determined by the product of gas density and energetic electron density, i.e., density of electrons having energies higher than the threshold energy for the dissociation of SiH_4

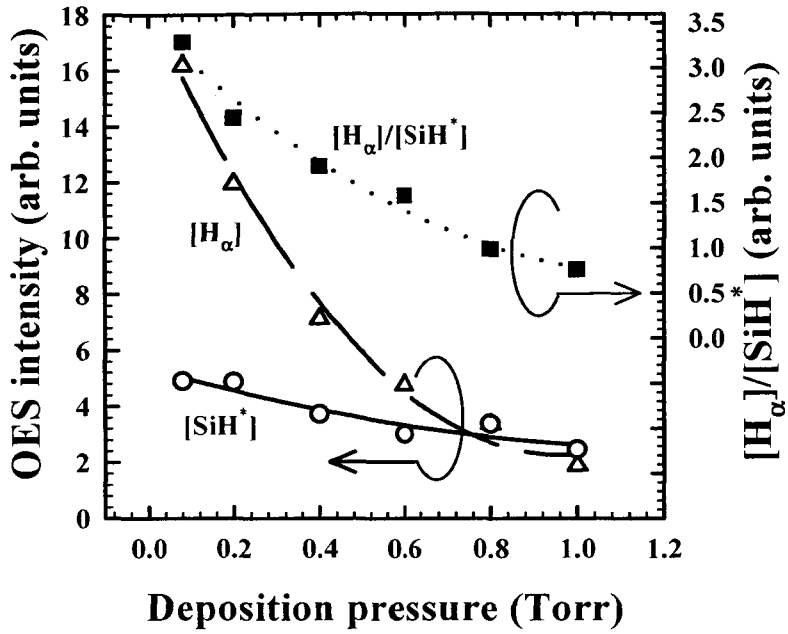

Fig. 3.9. OES intensities of SiH^* [○] and H_α [△] emission lines as a function of deposition pressure. The emission intensity ratio, $[H_\alpha]/[SiH^*]$ [■], is also plotted. The lines are guides for the eyes.

and H_2 molecules. In a lower gas density (pressure) regime, the energetic electron density increases due to the long electron mean free path in plasma. Thus, the OES result indicates that the dissociation of source gases, i.e., SiH_4 and H_2, is dominated by the energetic electron density rather than gas pressure as far as our present experimental conditions are concerned.

Furthermore, it is found that $[H_\alpha]/[SiH^*]$ is markedly changed by deposition pressure, presumably due to difference in the threshold electron energies for the dissociation of source gas molecules. The threshold electron energy for H_2 molecule is higher than that for SiH_4 molecule [14], resulting the monotonic decrease in $[H_\alpha]/[SiH^*]$ against deposition pressure, as shown in Fig. 3.9. Here, the contribution of atomic hydrogen created by SiH_4 dissociation to observed $[H_\alpha]$ should be negligible because H_2 partial pressure is much higher

than that of SiH_4 in this experiment. It is well known that $[H_\alpha]/[SiH^*]$ can be interpreted as the magnitude of atomic hydrogen flux per poly-Si mono-layer growth, which almost determines the crystallinity of poly-Si film [15]. Therefore, the decrease in both crystalline volume fraction and (220) grain size with an increase in deposition pressure is mainly due to the decrease in atomic hydrogen flux during film growth. In contrast, the deterioration of poly-Si crystallinity found at deposition pressures below 0.2 Torr might be ascribed to excess atomic hydrogen flux impinging onto the growing surface, which is unlikely to be effective for obtaining high crystalline volume fraction and (220) preferential orientation. Ion bombardment during growth of poly-Si film should be taken into account as another possible effect due to the high electron temperature in low-pressure plasma [16].

In Fig. 3.10, photovoltaic performance, V_{oc} and J_{sc}, of the poly-Si solar cells are plotted as a function of deposition pressure for the poly-Si layers. V_{oc} increases from 0.39 V to 0.52 V when the deposition pressure is increased from 0.08 Torr to 0.8 Torr, and saturates at >0.8 Torr. On the other hand, J_{sc} shows relatively high values of around 20 mA/cm^2 when the deposition pressure is in the range of 0.4-0.8 Torr. The change in J_{sc} can be explained by quantum efficiency (*QE*) spectrum. The corresponding external *QE* spectra of the solar cells are shown in Fig. 3.11. *QE* spectra of poly-Si layers deposited at 0.4-0.8 Torr show spectral peaks at around 620 nm with peak efficiencies of >80% and high response even at long wavelengths. At deposition pressures below 0.2 Torr, the *QE* peak shifts to a shorter wavelength with a decrease in peak efficiency, and the spectral responses at long wavelengths also decrease. The sudden decrease in *QE* when deposition pressure is decreased from 0.4 Torr to 0.08 Torr may be related to the significant change in poly-Si microstructure, i.e., transition from (220) preferential orientation to random orientation. The solar cell prepared at 1.0 Torr exhibits low *QE* for the long wavelength regime due to a quite low crystalline volume fraction of the poly-Si layer.

In order to understand the carrier transport behavior in the solar cells deposited at 0.4-0.8 Torr, which yields relatively high J_{sc}, the bias voltage

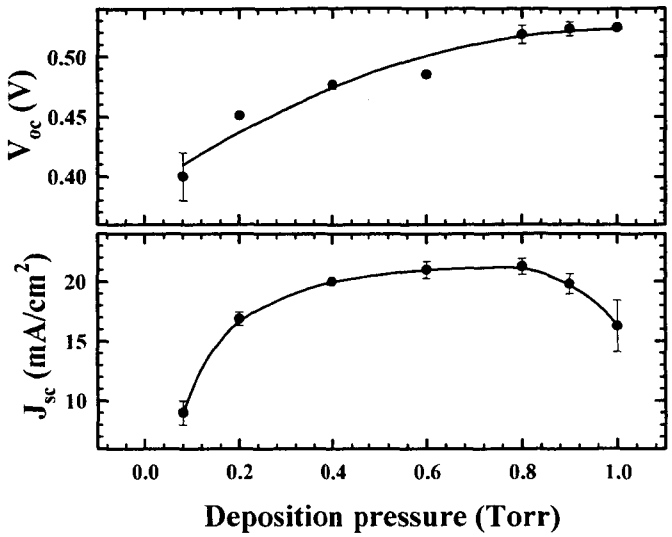

Fig. 3.10. V_{oc} (top) and J_{sc} (bottom) of poly-Si solar cells as a function of deposition pressure for poly-Si photovoltaic layers.

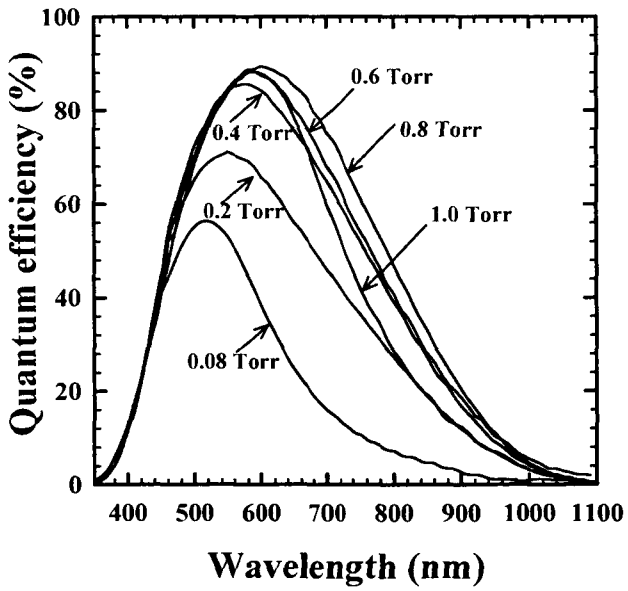

Fig. 3.11. External quantum efficiency spectra of poly-Si solar cells prepared at different deposition pressures.

dependence of the *QE* spectra is investigated. This analysis will provide some information concerning the field-dependent carrier transport and collection, which mainly reflects the magnitude of carrier recombination through the photovoltaic layer and at the interface [17]. Here, as usual, the *QE* spectra under applied reverse bias voltage of -1 V are demonstrated in the form *QE*(-1 V)/*QE*(0 V), i.e., normalized by corresponding spectra under bias voltage of 0 V. Figure 3.12 shows *QE*(-1 V)/*QE*(0 V) spectra of the solar cells deposited at 0.4 Torr, 0.6 Torr and 0.8 Torr. As can be seen in this figure, *QE*(-1 V)/*QE*(0 V) spectra for all of the poly-Si solar cells show the minimum at around 500 nm. The slight increase in *QE*(-1 V)/*QE*(0 V) in the shorter wavelength regime, i.e., 400-500 nm, may be caused by a surface recombination effect near ITO/p front contact side or the p/i junction interface. In the longer wavelength regime, *QE*(-1 V)/*QE*(0 V) steeply increases with each characteristic slope, then tends to

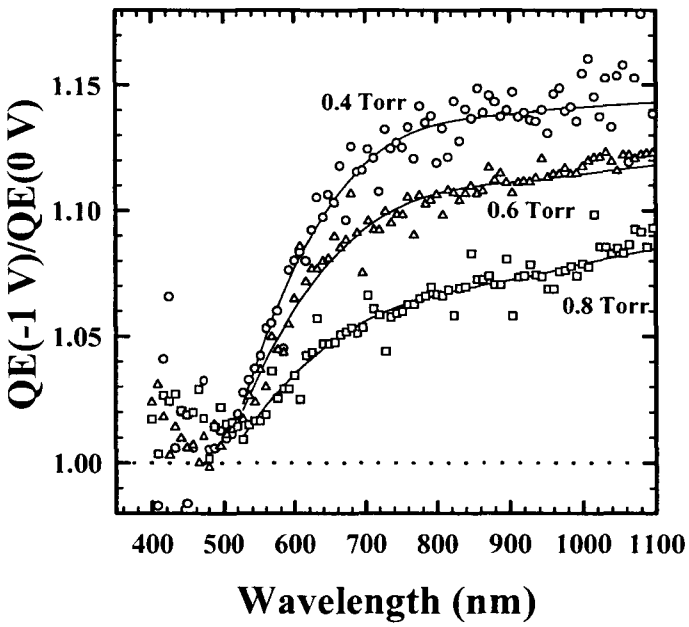

Fig. 3.12. Normalized quantum efficiency spectra, *QE*(-1 V)/*QE*(0 V), for the solar cells prepared at different deposition pressures [○ 0.4 Torr; △ 0.6 Torr; □ 0.8 Torr]. The lines are guides for the eyes.

saturate at around 650 nm where the penetration depth of the incident light is almost identical to the poly-Si layer thickness. Moreover, it is noted that *QE*(-1 V)/*QE*(0 V) increases remarkably in the long wavelength regime, with a decrease in the deposition pressure for the growth of poly-Si layers. Since the long wavelength response is largely dominated by the diffusion lengths of the photo-generated carriers, especially holes in this case, the increase in the *QE*(-1 V)/*QE*(0 V) is likely to be due to a decrease in the diffusion length. Namely, the recombination rate in the poly-Si layer might increase with a decrease in deposition pressure. A theoretical work revealed that J_{sc} is not influenced much in comparison with V_{oc}, by the recombination rate in the poly-Si photovoltaic layer due to the presence of a strong electric field in the short circuit condition [18]. In fact, as shown in Fig. 3.10, J_{sc} is almost unchanged with a decrease in deposition pressure from 0.8 Torr to 0.4 Torr, whereas V_{oc} shows a noticeable decrease. Therefore, it is reasonable to suppose that the decrease in V_{oc} is caused by the increase in the recombination rate presumably due to an increase in the defect density in the poly-Si layer, which is related to the change in poly-Si microstructure, because V_{oc} is largely influenced by defect density in the poly-Si layer.

3.3.2 SiH_4 flow rate and SiH_4 concentration dependence

Next, the dependence of poly-Si microstructure and photovoltaic performance on SiH_4 flow rate and SiH_4 concentration is explored. Figure 3.13 shows deposition rate of the poly-Si layers as a function of SiH_4 gas flow rate in the range of 2.5-7.5 sccm at various SiH_4 concentrations. Deposition pressure was held at 0.8 Torr. The deposition rate of the poly-Si layer, as shown in Fig. 3.13, steadily increases with increasing the SiH_4 flow rate at SiH_4 concentrations above 5.0%. In contrast, at SiH_4 concentrations below 4.5%, the deposition rate tends to saturate with an increase in SiH_4 flow rate, implying that the generation rate of SiH_x radicals, which is closely related to film growth, is likely to saturate. This is partially evidenced by plasma diagnostics in the in- situ monitoring of

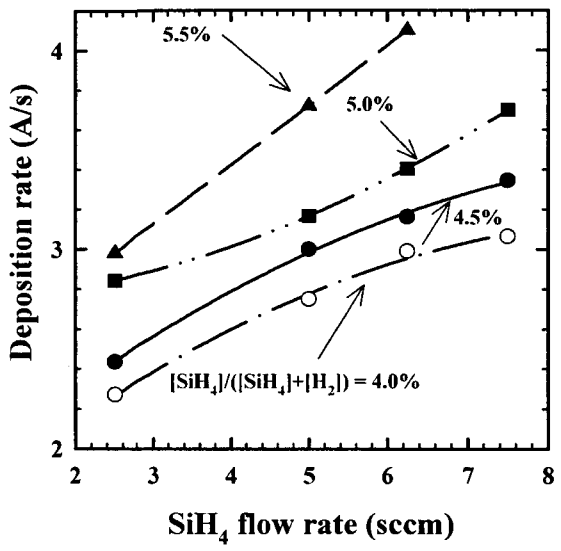

Fig. 3.13. Deposition rate of poly-Si layer at various SiH_4 flow rate and SiH_4 concentrations [○ 4.0%; ● 4.5%; ■ 5.0%; ▲ 5.5%].

OES. Figure 3.14 shows the emission intensities, i.e., [SiH^*] and [H_α], together with the emission intensity ratio, [H_α]/[SiH^*], at the SiH_4 concentration of 4.5% plotted against SiH_4 gas flow rate. The emission intensity, [SiH^*], increases with SiH_4 flow rate, then saturates in the flow rate regime higher than ~5 sccm. This trend of change in [SiH^*] against SiH_4 gas flow rate is in good agreement with that of the deposition rate. Therefore, it is confirmed that the deposition rate of the poly-Si layer is determined by the generation rate of SiH_x radicals which is proportional to [SiH^*] [19]. In the lower SiH_4 flow rate regime, [SiH^*] increases linearly with SiH_4 flow rate, indicating that the generation of SiH_x radical is dominated by SiH_4 gas supply (SiH_4 flow rate). In the higher SiH_4 flow rate regime at which [SiH^*] tends to saturate as found in Fig. 3.14, the deposition rate also tends to saturate, indicating that the dissociation of SiH_4 molecule is limited by the insufficient VHF-power supply. On the other hand, [H_α] seems to remain constant for any SiH_4 flow rate. However, with careful inspection of Fig. 3.14, [H_α] slightly

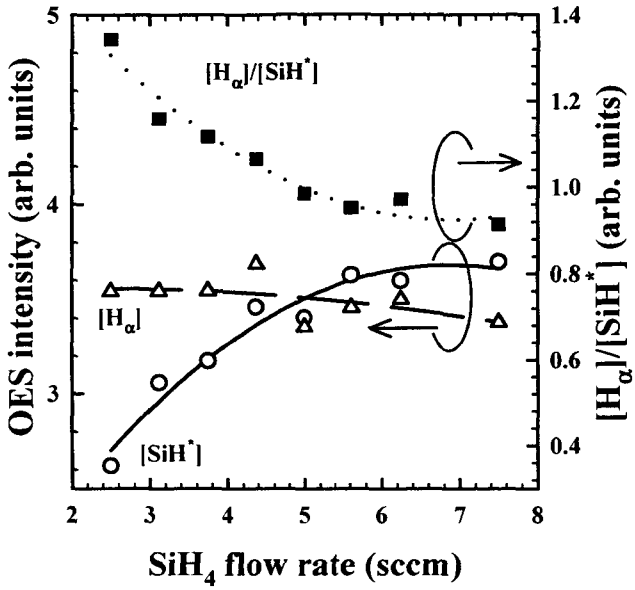

Fig. 3.14. OES intensities of SiH^* [○] and H_α [△] emission lines together with their ratio of $[H_\alpha]/[SiH^*]$ [■] plotted as a function of SiH_4 flow rate. SiH_4 concentration is fixed at 4.5%. The lines are guides for the eyes.

decreases at SiH_4 flow rates above 5 sccm where $[SiH^*]$ starts to saturate. Since both the deposition pressure and VHF power are kept constant in this experiment, the energetic electron density and the generation rate of atomic hydrogen in plasma should be almost unchanged. The decrease in $[H_\alpha]$ in the higher SiH_4 flow rate regime would then be explained in terms of an annihilation reaction of atomic hydrogen with excess undissociated SiH_4 molecule [16].

These different behaviors between generation rate of SiH_x radicals and atomic hydrogen against SiH_4 flow rate are likely to cause the structural change in the poly-Si layer. Figure 3.15 shows the crystalline volume fraction of the poly-Si layers, X_c, deduced from Raman scattering measurement, as a function of SiH_4 gas flow rate at various SiH_4 concentrations. For each poly-Si layer, X_c decreases with an increase in SiH_4 flow rate. This can be attributed to the monotonic decrease in atomic hydrogen flux during film growth, which is

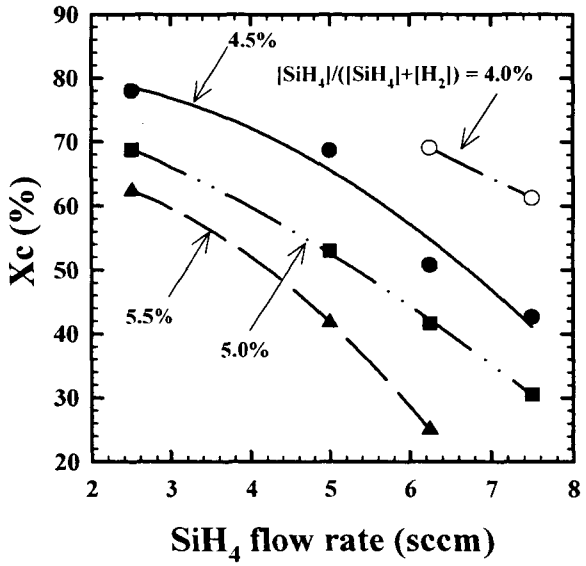

Fig. 3.15. Crystalline volume fraction of poly-Si layer (X_c) at various SiH_4 flow rate and SiH_4 concentrations [○ 4.0%; ● 4.5%; ■ 5.0%; ▲ 5.5%].

evidenced by the decrease in $[H_\alpha]/[SiH^*]$, as found in Fig. 3.14. Figure 3.16 shows the XRD patterns of the poly-Si films deposited at the SiH_4 concentration of 4.5% with various SiH_4 gas flow rates. As found in this figure, the (220) diffraction peak intensity alone decreases with increasing SiH_4 flow rate. The (220) diffraction peak is very weak at a SiH_4 flow rate of 7.5 sccm so that the poly-Si layer exhibits nearly random orientation. On the other hand, at a SiH_4 flow rate of 2.5 sccm, the poly-Si film shows strong (220) diffraction peak and almost perfect (220) preferential orientation. In this condition, the grain size, which is deduced from the line width of the (220) diffraction peak in accordance with Scherrer's formula, reaches about 300 Å. As a consequence, high crystalline volume fraction and large (220) grains are obtained at low SiH_4 flow rates and low deposition rates. In this regime (*e.g.*, SiH_4 flow rate of 2.5 sccm in Fig. 3.16), there should be sufficient atomic hydrogen for the growth of monolayer that could be responsible for the high crystallinity of the poly-Si

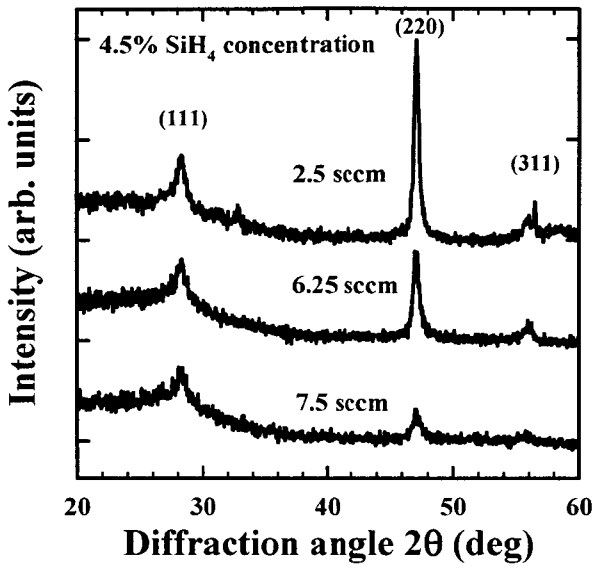

Fig. 3.16. XRD patterns of poly-Si layers on glass substrate deposited at SiH_4 concentration of 4.5% with different SiH_4 gas flow rates.

layer.

Figure 3.17 shows the photovoltaic performances, V_{oc} and J_{sc}, of the solar cells of which we discussed the SiH_4 flow rate and SiH_4 concentration dependence of the poly-Si layers. There is a clear correlation between photovoltaic performance of the poly-Si solar cells and the crystalline volume fraction in the poly-Si photovoltaic layer. In Fig. 3.17(a), V_{oc} tends to increase with an increase in the SiH_4 flow rate from 2.5 to 6.25 sccm. Additionally, V_{oc} shows a monotonic increase with increasing SiH_4 concentration for any SiH_4 flow rate. Since crystalline volume fraction significantly decreases with an increase in SiH_4 flow rate or SiH_4 concentration, the increase in V_{oc} would be related to the increase in the amorphous volume fraction in the poly-Si layer. Actually, some of the solar cells in Figs. 3.15 and 3.17(a), *e.g.*, those deposited at 6.25 sccm with the SiH_4 concentration of 5.5%, exhibit photovoltaic performances of amorphous Si solar cells, namely, high V_{oc} over 0.55 V with

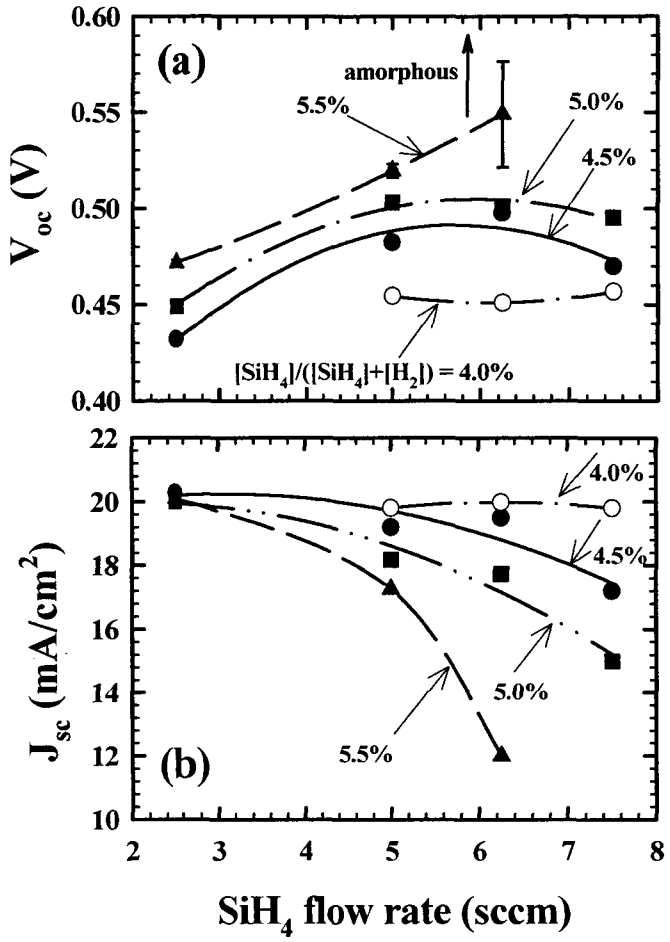

Fig. 3.17. V_{oc} (a) and J_{sc} (b) of poly-Si solar cells prepared at various SiH_4 flow rate and SiH_4 concentrations [○ 4.0%; ● 4.5%; ■ 5.0%; ▲ 5.5%].

quite low J_{sc}. Consequently, from the viewpoint of obtaining high V_{oc}, poly-Si with quite high crystalline volume fraction is unlikely to be effective for the poly-Si solar cells.

On the other hand, a high crystalline volume fraction is found to yield a high J_{sc}. Comparing Fig. 3.17(b) with Fig. 3.15, J_{sc} is around 20 mA/cm^2 for X_c > 50%. In contrast, J_{sc} steeply decreases with a decrease in X_c when X_c is below

50%. The relationship between J_{sc} and the structural properties of the poly-Si layer is also found in association with the grain size and preferential orientation. Judging from the results of the XRD patterns of the poly-Si layers and the corresponding photovoltaic performances, it can be considered that a high J_{sc} is obtained by using poly-Si photovoltaic layer with (220) preferentially oriented large grains. In other words, the columnar structure grown along the [110] direction is advantageous for photo-generated carrier collection.

3.3.3 Universal relationship between poly-Si microstructure and photovoltaic performance

As mentioned above, V_{oc} and J_{sc} show opposite dependence on crystalline volume fraction and (220) grain size. This could be identically found in the results of deposition pressure dependence except for the solar cell prepared below 0.2 Torr. The solar cell prepared at extremely low deposition pressure, i.e., 0.08-0.2 Torr, exhibits low J_{sc} even if the poly-Si layers has relatively high crystalline volume fraction. This can particularly be attribute to the change in the (220) preferential orientation, which may be related to the deterioration of crystallinity caused by excess atomic hydrogen flux during the film growth. At the deposition pressure of 0.4-0.6 Torr, poly-Si layers with high crystalline volume fraction and large (220) grain are obtained. These poly-Si layers yield relatively high J_{sc} of around 20 mA/cm^2, but yield a low V_{oc}, which is related to an increase in carrier recombination through the poly-Si photovoltaic layer.

In Fig. 3.18, V_{oc} and J_{sc} of the poly-Si solar cells are plotted as a function of crystalline volume fraction, X_c, deduced from Raman scattering measurement [20]. This relationship can be obtained from the experimental results of photovoltaic performance investigated in above three different deposition series for poly-Si layer, i.e., deposition pressure, SiH_4 flow rate and SiH_4 concentration. It is noted here that all films used in this figure basically exhibit (220) preferential orientation, and also noted here is that (220) grain size shows positive correlation with X_c value. In Fig. 3.18, a clear universality in the

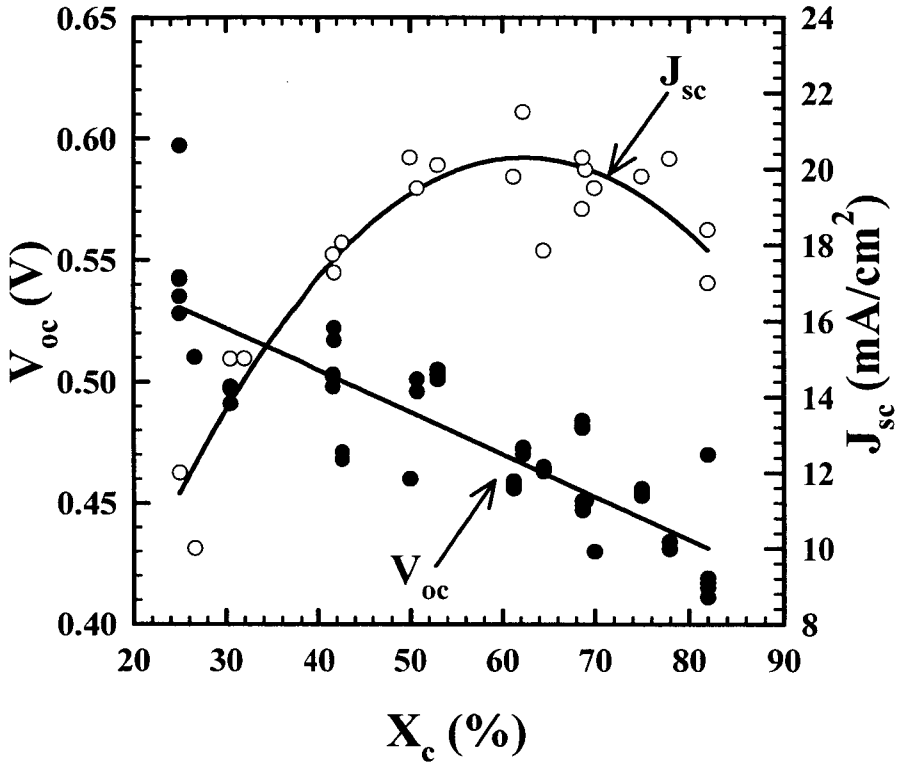

Fig. 3.18. V_{oc}(●) and J_{sc} (○) of poly-Si solar cells as a function of crystalline volume fraction (X_c) of poly-Si photovoltaic layer. X_c of poly-Si layer is controlled by changing deposition pressure, SiH_4 flow rate and SiH_4 concentration. All poly-Si films plotted here basically exhibit (220) preferential orientation.

relationship between X_c and V_{oc}, J_{sc} is emerged, i.e., V_{oc} shows monotonic decrease with X_c, while J_{sc} linearly increases and reaches the maximum at X_c of 50-60%. Due to the opposite tendency of these two photovoltaic paeameters against X_c, the maximum product of V_{oc} and J_{sc} is obtained at X_c as low as 50%, where the V_{oc} and J_{sc} are around 0.5 V and 20 mA/cm^2, respectively. The poly-Si film with X_c~50% also provide the highest conversion efficiency over 7% in

this experimental series. On of the most reliable deposition conditions for this poly-Si film is the SiH_4 flow rate of 6.25 sccm, the SiH_4 concentration of 4.5% and deposition pressure of 0.8 Torr. At this condition, the deposition rate of the poly-Si layer was as high as 3.8 Å/s. The design for light trapping structure in the poly-Si solar cell is necessary from the view point of obtaining further higher J_{sc}, which will be focused in chapter V.

3.4 Summary

A series of intrinsic poly-Si thin films for p-i-n junction solar cells has been examined at various deposition pressures, SiH_4 flow rates and SiH_4 concentrations by utilizing the 100-MHz VHF-PECVD system. Changes in the poly-Si microstructure have been explained in terms of the $[H_\alpha]/[SiH^*]$ ratio detected by the OES measurement. In the relatively high $[H_\alpha]/[SiH^*]$ regime, occurring at low deposition pressure (~0.4 Torr) or low SiH_4 flow rate (~2.5 sccm) condition, poly-Si with high X_c and strong (220) preferential orientation is obtained. Photovoltaic performance strongly depends on their microstructures. For obtaining high J_{sc}, $X_c \geq 50\%$ and (220) preferential orientation are needed. In contrast, an increase of X_c over 50% results in a noticeable reduction in V_{oc}, which is related to an increase in carrier recombination through the poly-Si photovoltaic layer. From the opposite tendency of V_{oc} and J_{sc} against X_c, we found the most suitable deposition conditions in this series, and X_c of the obtained poly-Si photovoltaic layer is as low as 50%. As a result, relatively high V_{oc} and J_{sc} of around 0.5 V and 20 mA/cm^2 have been achieved with 3-μm p-i-n junction solar cells and with a relatively high deposition rate of 3.8 Å/s for the poly-Si photovoltaic layer.

References

[1] J. Meier, R. Fluckiger, H. Keppner, and A. Shah: Proc. 1st World Conference on Photovoltaic Energy Conversion (WCPEC), Hawaii, (1994) p.409.

[2] O. Vetterl, R. Carius, L. Houben, C. Scholten, M. Luysberg, A. Lambertz, F. Finger and H. Wagner: Mat. Res. Soc. Symp. Proc. **609** (2000) A15.2.1.

[3] K. Saito, M. Sano, K. Matsuda, T. Kondo, T. Nishimoto, K. Ogawa and I. Kajita : Proc. 2nd World Conference on Photovoltaic Energy Conversion (WCPEC), Vienna, (1998), p.351.

[4] M. Fukawa, S. Suzuki, L. Guo, M. Kondo, A. Matsuda : Sol. Energy. Mat. & Sol. Cells **66** (2001) 217.

[5] S. Vepřek, F.A. Sarrott, S. Rambert and E. Taglauer: J. Vac. Sci. Techno. A **7** (1989) 2614.

[6] J. Dutta, U. Kroll, P. Chabloz, A. Shah, A.A. Howling, J.L. Dorier and Ch. Hollestein: J. Appl. Phys. **72** (1992) 3220.

[7] P. Torres, J. Meier, R. Fluckiger, U. Kroll, J.A.A. Selvan, H. Keppner, and A. Shah, S.D. Littlewood, I.E. Kelly, P. Giannoules: Appl. Phys. Lett. **52** (1988) 1675.

[8] L. Houben, M. Luysberg, P. Hapke, R. Carius, F. Finger and H. Wagner: Philos. Mag. A **77** (1998) 1447.

[9] E. Bustarret, M. A. Hachicha and M. Brunel: Appl. Phys. Lett. **52** (1988) 1675.

[10] K. Yamamoto: IEEE Electron. Dev. **46** (1999) 2041.

[11] N. Wyrsch, P. Torres, M. Goerlitzer, E. Vallat, U. Kroll, A. Shah and M. Vanecek: Solid State Phenomena **67-68** (1999) 91.

[12] J. Kočka, A. Fejfar, V. Vorlíček, H. Stuchlíková, J. Stuchlík: Mat. Res. Soc. Symp. Proc. **557** (1999) 490.

[13] A. Matsuda, T. Kaga, H. Tanaka, L. Malhotra and K. Tanaka: Jpn. J. Appl. Phys. **22** (1983) 115.

[14] F.J. Kamps and R.W. Griffith: J. Appl. Phys. **52** (1981) 1285.

[15] A. Matsuda: J. Non-Cryst. Solids **59&60** (1983) 767.

[16] M. Kondo, M. Fukawa, L. Guo and A. Matsuda: J. Non-Cryst. Solids **266-269** (2000) 84.

[17] H. Okamoto, H. Kida, S. Nonomura, K. Fukumoto and Y. Hamakawa: J. Appl. Phys. **54** (1983) 3236.

[18] T. Matsui, T. Yamazaki, A. Nagatani, K. Kino, H. Takakura and Y. Hamakawa: Sol. Energy Mat. & Sol. Cells **65** (2001) 87.

[19] A. Matsuda, T. Kaga, H. Tanaka, L. Molhotra and K. Tanaka: Jpn. J. Appl. Phys., **22** (1983) L115.

[20] T. Matsui, M. Tsukiji, H. Saika, T. Toyama, H. Okamoto: Proc. 12th International Photovoltaic Science and Engineering Conference (PVSEC), Jeju, (2001) p.355.

Chapter IV

Characterization of electronic transport properties in poly-Si photovoltaic layer

4.1 Introduction

It goes without saying that the electronic transport properties of photovoltaic materials, including band structure, carrier concentration, mobility, lifetime etc., play a significant role in determination of solar cell efficiency. The characterization of these transport parameters is of prime importance not only for the physical interest but also for giving a guiding principle for the further improvement in photovoltaic performance. The basic characterization techniques and theories of carrier transport in homogeneous single crystalline silicon have been already established in the early stage of semiconductor science and technology. As demonstrated in chapter III, poly-Si thin films produced by low temperature PECVD process show a variety of microstructure, which strongly depends on deposition conditions, from amorphous-like state to almost perfect crystalline state with different crystallographic orientations. Due to such inhomogeneous and complicated microstructure, the carrier transport properties of poly-Si thin film materials is difficult to be characterized and much less to be predicted from the known properties of the corresponding bulk

materials. Indeed, the experimental and theoretical analysis for carrier transport in poly-Si films are far from being perfomed sufficiently.

Anisotropic carrier transport occurs in various polycrystalline materials, reflecting the grain size, orientation and grain boundary. For the case of the columnar grains oriented perpendicularly to substrate, which are often observed in (220) preferentially orientated poly-Si thin films, the carrier transport can be separated into components along parallel and perpendicular (along growth direction) to substrate, as suggested by Fig. 4.1. In this case, the parallel conductivity should be strongly affected by the grain boundaries, whereas the perpendicular conductivity is affected very little. For PECVD produced poly-Si thin films, such experimental results have been reported by Kočka *et al.* [1]. In the practical p-i-n junction poly-Si thin film solar cells, carrier transport along perpendicular to substrate clearly dominates device operation, rather than that of parallel component. Therefore the carrier transport parameters of the poly-Si films should be characterized in the form of sandwich electrode geometry, as like solar cell structure.

In chapter III, we have evolved some important roles of poly-Si microstructure played in photovoltaic performance of poly-Si solar cells. However, questions still remain with respect to the structural dependence of carrier transport properties in poly-Si films. In this chapter, two characterization techniques are introduced for the evaluation of carrier transport parameters in poly-Si films with different microstructures. One is the AC-conductivity, which enables us to measure the conductivity of poly-Si thin films with sandwich electrode geometry. Another is the Time-of-Flight experiment on the p-i-n samples being identical with the solar cells, in which the electron and hole drift mobilities of poly-Si i-layer are deduced from the photo-current transients. From the AC-conductivity experiments, we show the usefulness of this technique for the individual evaluation of electron and hole transport. It is also found that the carrier density and Fermi energy level in poly-Si layer are quite sensitive to the film microstructure. Based on these results, the relationship between electrical properties of poly-Si films and its photovoltaic

performance is discussed. From the Time-of-Flight experiments, high hole drift mobility of poly-Si films is demonstrated through the comparative studies on carrier transport of poly-Si and hydrogenated amorphous silicon (a-Si:H) materials.

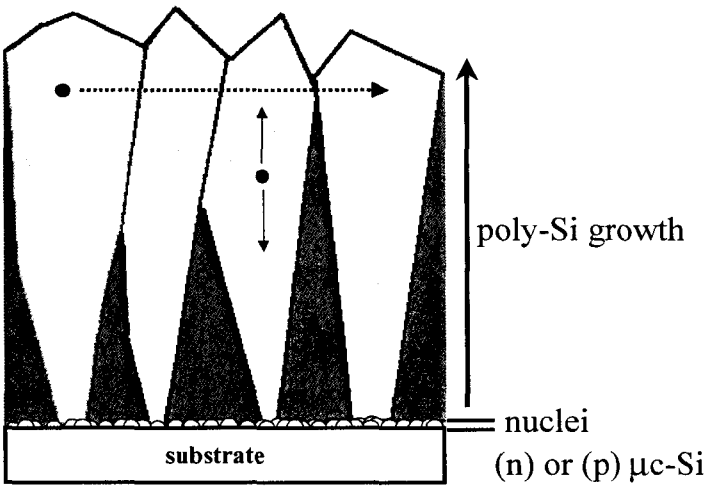

Fig. 4.1. Schematic model for carrier flow in poly-Si photovoltaic layer along different parallel and perpendicular directions. Columnar crystalline grains (bright field) surrounded by amorphous tissues (dark field) are illustrated. In this case, perpendicular transport is weakly affected by grain boundaries compared to parallel transport.

4.2 AC-conductivity experiment on poly-Si thin films

4.2.1 Small signal equivalent circuit

The simplest way to deduce the conductivity of materials is to measure the DC current-voltage characteristics. In the case of a metal/poly-Si/metal configuration, however, we do not have the simple linear Ohm's law type behavior, but a strongly nonlinear behavior. This is interpreted as due to the

presence of a depletion region acting as a contact barrier at metal/poly-Si interfaces. Figure 4.2(a) shows the schematic band profile of metal/poly-Si layers and its possible small signal equivalent circuit [1], in which the carrier injection effect is assumed to be negligible. The two $C||R$ components of ($C_{contact}$ || $R_{contact}$) and ($C_{geometry}$ || R_{film}) arise from the regions at contact and bulk, respectively. The $C_{contact}$ and $C_{geometry}$ are determined by the depletion width at contact and the thickness of poly-Si layer, respectively. $C_{contact}$ must be much larger than $C_{geometry}$ because the depletion width at contact is generally narrower than the sample thickness. On the other hand, $R_{contact}$ is much higher than R_{film} because of carrier depletion at contact region. In order to obtain the proper film conductivity of poly-Si layer, which of course corresponds to R_{film}, we adopted

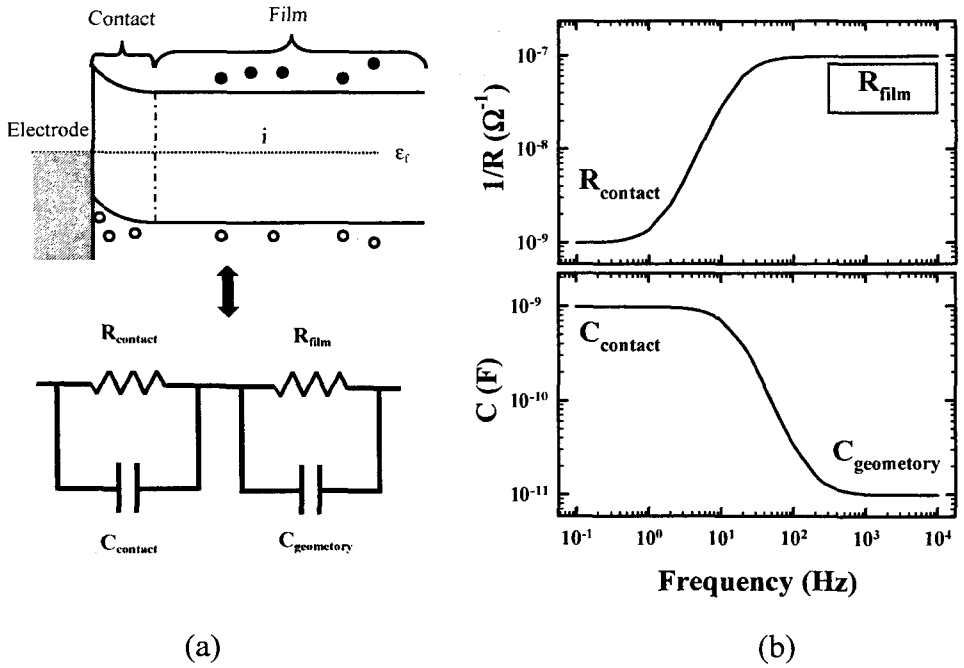

Fig. 4.2. (a) Schematic band profile of metal/poly-Si layer and its small signal equivalent circuit. (b) Simulation results of conductance $1/R$ and capacitance C of equivalent circuit as a function of AC frequency.

the AC- conductivity measurement to exclude the series $R_{contact}$ component [1]. The simulated result of this equivalent circuit is shown in Fig. 4.2(b), where $C_{contact}=10^{-9}$ F, $R_{contact}=10^{9}$ Ω, $C_{geometry}=10^{-11}$ F and $R_{film}=10^{7}$ Ω are assumed. As found in this figure, the $R_{contact}$ is dominant at low frequency regime, while the R_{film} corresponding to the true conductivity of poly-Si layer is dominant at high frequency regime, where the capacitance approaches the value of $C_{geometry}$[2].

4.2.2 Electron and hole conductivities in poly-Si layer

Figure 4.3 shows the two sample structures consisting of ZnO/*n-i-n*/SnO_2/glass and ZnO/*p-i-p*/SnO_2/glass for AC-conductivity measurement. In

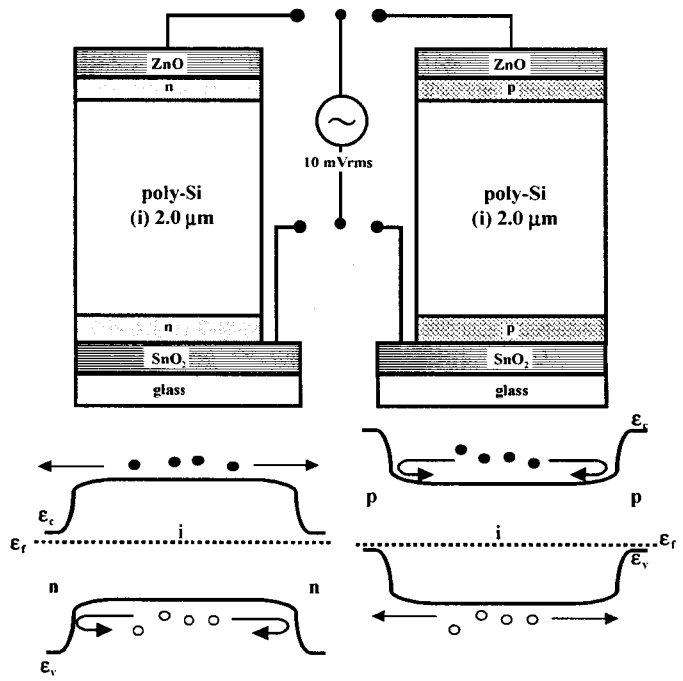

Fig. 4.3. Structure of *n-i-n* and *p-i-p* samples and their band profiles. The *n-i-n* structure suppresses hole flow, so that the electron flow is observed. Inversely, the *p-i-p* structure allows observation of hole flow.

this experiment, thickness of poly-Si i-layer was kept at 2 μm, while the film crystallinity was changed by deposition pressure in VHF-PECVD process as demonstrated in chapter III. Here, the flat ZnO and SnO_2 films were employed as front and rear side transparent electrodes, respectively. Materials and thickness of n- and p- layers are identical with those used for the solar cells. The corresponding ideal band profiles of these junction structures are also shown in Fig. 4.3. For the *n-i-n* structure, the n/i interfaces should act as barriers for the hole extraction, and then only electrons can contribute to the current flow if the applied voltage is much smaller than barrier height impeding hole extraction. On the contrary, the *p-i-p* sample can be expected to permit only holes for the current flow. The dark AC-conductivity was measured in the frequency range of 50 Hz - 1 MHz under applied AC voltage of 10 mV_{rms}. The photo conductivity was also measured under AM 1.5 100 mW/cm^2 illumination through the SnO_2/glass substrate side. In Fig. 4.4, typical frequency dependence of dark conductivity and effective permittivity, ε_{eff} of the *n-i-n* sample at various measurement temperatures are shown. The true conductivity of poly-Si layer for each temperature can be found at frequencies at which the ε_{eff} approaches a proper value of $\varepsilon_{eff}(Si)=(C_{geometory}d/\varepsilon_o S)=12$, where d is the sample thickness, ε_o is the vacuum dielectric constant and S is the sample area. The conductivity exhibits a power-low ($\propto f^2$) frequency dependence at the high frequency regime being independent of measurement temperature, which might be ascribed to the electrode resistance.

The temperature dependence of dark-conductivity measured for poly-Si i-layers with different crystalline volume fractions (X_c~50% and ~80%) in a temperature range of 100-400 K is shown in Fig. 4.5. Both of these poly-Si films exhibit (220) preferential crystallographic orientation. Figure 4.5 also demonstrates the dark-conductivity measured for the *n-i-n* and the *p-i-p* samples. A remarkable difference in the dark-conductivity behaviors of these two poly-Si i-layers is observed. Concerning the poly-Si film with X_c~50%, the activation energies of the dark-conductivity, ε_a, which is deduced from the Arrhenius plot at the higher temperature regime (300-400 K), are almost identical around 0.55 eV

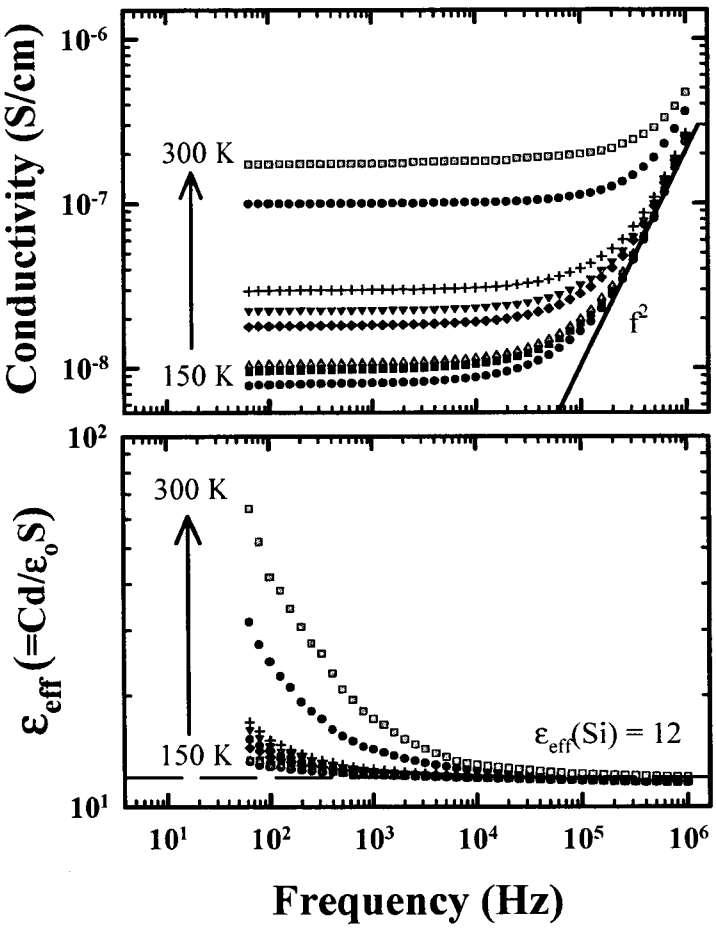

Fig. 4.4. Typical frequency dependence of dark conductivity and effective permittivity, ε_{eff} of the *n-i-n* sample at various measurement temperatures.

for both *n-i-n* and *p-i-p* samples. Since the activation energy of the dark conductivity is a good approximation of the energy separation between the Fermi level and band edge for the carrier transport, this result suggests that the Fermi level locates at the center of bad gap and this material is truly intrinsic. For the poly-Si with X_c~80%, on the other hand, a strong sample structure dependence of dark conductivity can be found, i.e., ε_a for *n-i-n* is much smaller than that for

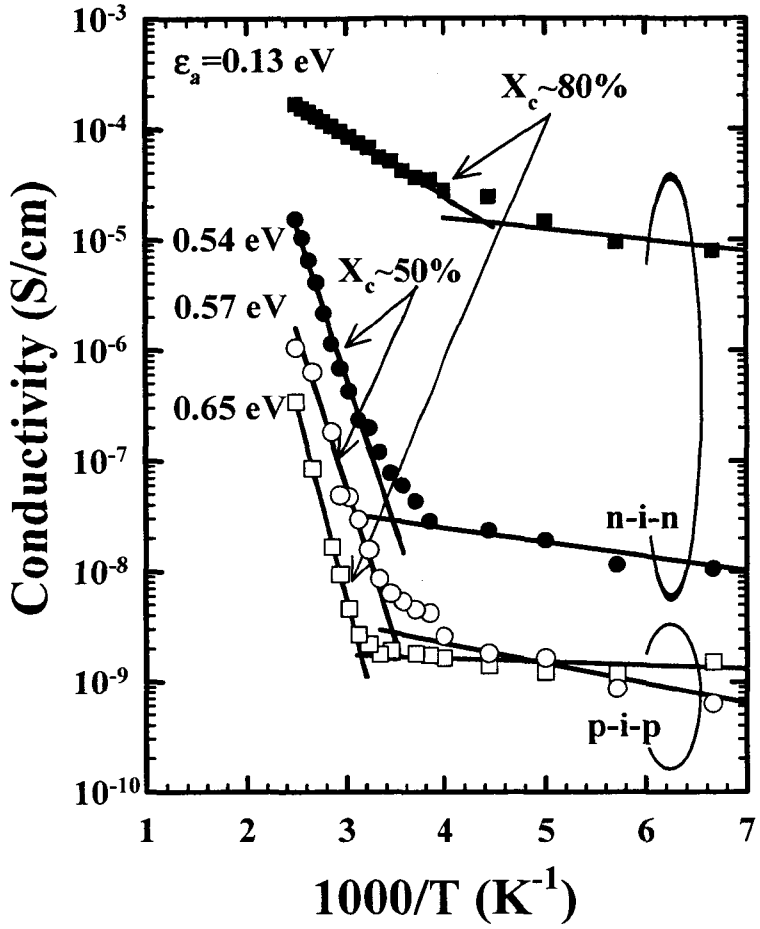

Fig. 4.5. Temperature dependence of dark-conductivity measured for poly-Si i-layers with different crystalline volume fractions of X_c~50% (circles) and ~80% (squares) with *n-i-n* (closed) and *p-i-p* (open) sample.

p-i-p, indicating that the Fermi level is close to conduction band edge, and this material is rather n-type.

This experiment is extended to the electrical characterization of poly-Si films with a wide variety of microstructure. Figure 4.6 shows the variation of the activation energy (ε_a) and photo-sensitivity (σ_{ph}/σ_d) for *n-i-n* and *p-i-p*

samples as a function of deposition pressure. In the top view graph, the crystalline volume fraction (X_c) and corresponding (220) orientation factor ($I_{(220)}/I_{(111)}$) of the poly-Si i-layers are also plotted. In Fig 4.6, a clear correlation between ε_a and σ_{ph}/σ_d is found. When the poly-Si film exhibits high crystalline volume fraction and strong (220) preferential orientation as deposited at 0.4 or

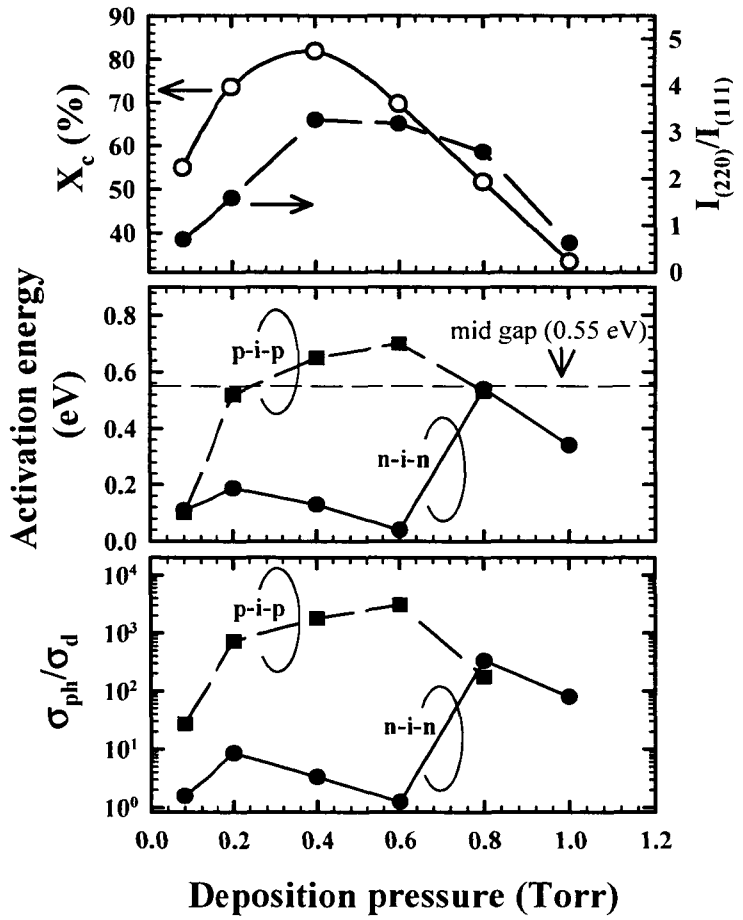

Fig. 4.6. Conductivity activation energies (ε_a) and photo-sensitivities (σ_{ph}/σ_d) as a function of deposition pressure for poly-Si growth, taken with *n-i-n* (●) and *p-i-p* (■) samples. Corresponding data of crystalline volume fraction, X_c, and crystallographic orientation factor, $I_{(220)}/I_{(111)}$, are also plotted in top view.

0.6 Torr, ε_a and σ_{ph}/σ_d show very low values for *n-i-n* samples, whereas both of them show very high values for *p-i-p* samples. The low ε_a for electron transport and high ε_a for hole transport indicate that these high X_c films exhibit n-type character, which is consistent with the fact that high σ_{ph}/σ_d is obtained only for *p-i-p* samples; photo-generated minority carrier in the 'n-type' layer plays a crucial role in determining σ_{ph}/σ_d. In contrast, ε_a and σ_{ph}/σ_d for both sample structures tend to decrease as the film becomes random orientation, implying that these films exhibit poor quality in terms of the short carrier lifetime. In this experimental series, the exact intrinsic poly-Si film with high photo-sensitivity is obtained only at 0.8 torr, where crystalline volume fraction of poly-Si film is as low as 50% with (220) preferential orientation.

4.2.3 Influence of film conductivity on photovoltaic performance

It has been reported that the origin of above-mentioned n-type character observed in highly crystallized poly-Si films is attributed either to intrinsic nature or to the electrically active oxygen-related complex [3,4]. In general, it is widely accepted that the oxygen-related donors concentrate at grain boundaries of poly-Si films [5] and also give rise to similar defect energy distribution as Si/SiO_2 interface [6]. The idea of extrinsic activation of grain boundaries in the poly-Si films is supported by the results of thickness dependence of photovoltaic performance.

Figure 4.7 shows the photovoltaic performance of poly-Si solar cells as a function of poly-Si i-layer thickness in the range of 1.0–5.6 μm, in which the different poly-Si layers is compared for X_c of 50% and 80%. The structure of the solar cells prepared in this experiment is Ag-grid/ZnO/p-i-n/ZnO/Ag/glass. For the i-layer thickness below 3 μm, J_{sc} linearly increases with increasing thickness. Additionally, no significant difference is found in the increasing rate of J_{sc} between X_c of 50% and 80%. However, J_{sc} rapidly starts to decrease at the thickness above 3 μm for the solar cell with X_c~80%, whereas it still gradually increases at the thickness above 5 μm for the solar cell with X_c~50%. On the

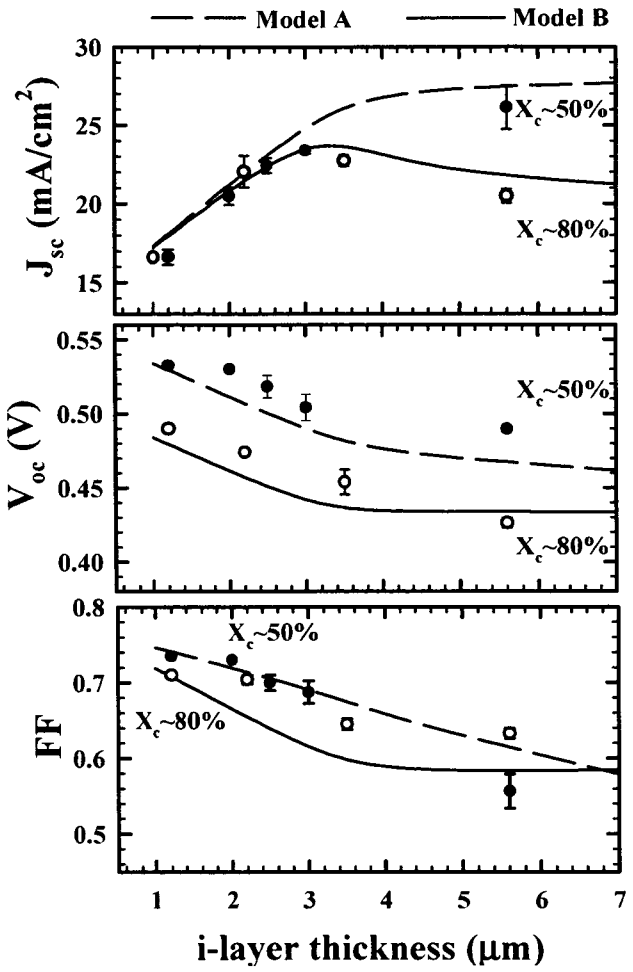

Fig. 4.7. Photovoltaic performance of poly-Si solar cells with different i-layer crystalline volume fractions [closed symbol: X_c~50%, open symbol: X_c~80%] as a function of i-layer thickness. Dashed lines are calculated results obtained by two-dimensional grain boundary model with grain size L_G of 0.01 μm, surface recombination velocity at grain boundary S_{GB} of 10 cm/s and effective donor concentration at grain boundary N_{GB} of 10^{13} cm^{-3} (Model A). The solid lines are also calculated results with L_G=0.01 μm, S_{GB}=20 cm/s and N_{GB}=10^{16} cm^{-3} (Model B) .

other hand, V_{oc} and FF significantly decrease with an increase in the i-layer thickness. Particularly, for any i-layer thicknesses, V_{oc} for X_c~80% is always lower than that for X_c~50%. These experimental results can be explained in terms of following two factors. First is based on the experimental data that films with X_c~50% exhibit intrinsic character (σ_d~10^{-7} S/cm), while films with X_c~80% exhibit n-type character (σ_d~10^{-4} S/cm). Secondly, poly-Si films with high crystalline volume fraction are supposed to contain defects with a high density. The lines shown in Fig. 4.7 are the simulation results, which are based on the two dimensional grain boundary model described in chapter II. Here, the solid lines (model A: intrinsic) indicate simulation results calculated with the grain size L_G=0.01 μm, surface recombination velocity at grain boundary S_{GB}=10 cm/s and the effective donor concentration at grain boundary N_{GB}=10^{13} cm^{-3}. For dotted line data (model B: n-type), L_G=0.01 μm, S_{GB}=20 cm/s and N_{GB}=10^{16} cm^{-3} are assumed. The parameters used in simulations for model A and B are assumed on the basis of the measured electron conductivities of poly-Si layers for X_c~50% and X_c~80%, respectively. The corresponding macroscopic dark conductivities of these modeled i-layers can be simply calculated using following expression

$$\sigma_d = q\mu_e \frac{N_{GB}\Delta x}{L_G} , \qquad (4.1)$$

where q denotes the elemental charge, μ_e the electron mobility and Δx the grain boundary width. In this simulation, μ_e=90 cm^2/Vs and Δx =0.1 nm are assumed. The electron concentration and dark conductivity are then calculated as n=10^{11} cm^{-3}, σ_d~10^{-7}S/cm for model A and n=10^{14} cm^{-3}, σ_d~10^{-4} S/cm for model B, respectively. As found in Fig. 4.7, simulation results of model A and B show reasonable agreement with the experimental data of X_c~50% and 80%, respectively. Further information can be derived by the investigation of the carrier recombination profile obtained by simulation. Figure 4.8 shows the calculated recombination rate of carriers along the grain boundary position for

both cases of model A and B at short circuit condition and at forward applied voltage 'V' of 0.43 V. In this simulation, the i-layer thickness is set at 5.0 μm. In short circuit condition (V=0 V), carrier recombination rate in model B is much higher than that of model A particularly adjacent to i/n interface. Since the hole mobility is assumed to be constant for both models, the considerable recombination loss of photo-generated carriers found in model B is ascribed to

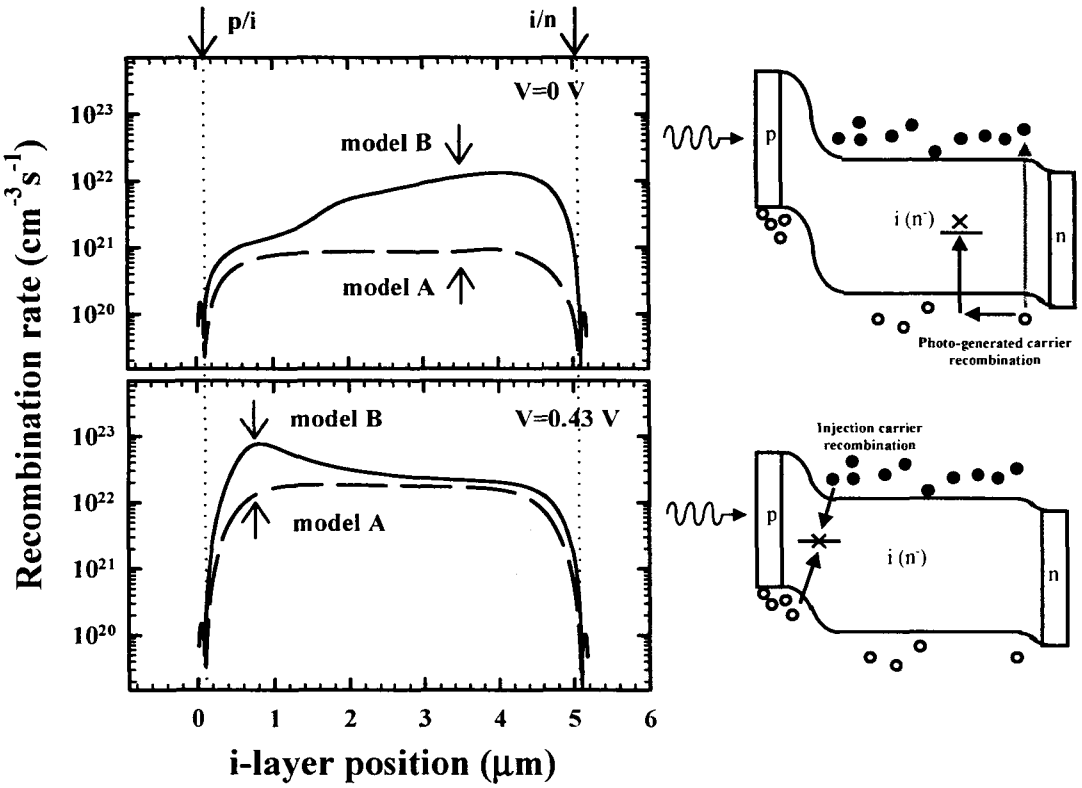

Fig. 4.8. Calculated carrier recombination rate profiles [dashed lines (Model A): L_G=0.01 μm, S_{GB}=10 cm/s, N_{GB}=10^{13} cm^{-3}, solid lines (Model B): L_G=0.01 μm, S_{GB}=20 cm/s and N_{GB}=10^{16} cm^{-3}] along the grain boundary position at short circuit condition V=0 V and forward biased condition V=0.43 V. For model B, a different position-dependent carrier recombination is observed between V=0 V and V~V_{oc}, as schematically shown in right diagram.

the higher S_{GB} as well as to lower built-in electric filed in the i-layer due to n-type character. This effect leads to the reduction of the effective carrier diffusion length, which would be responsible for the lower J_{sc} of poly-Si solar cell with high crystalline volume fraction. The situation is quite different at V=0.43 V at which forward applied voltage is nearly close to open circuit condition. Model B reveals that the intensive carrier recombination takes place near the p/i interface at V=0.43 V. Due to its n-type character, the built-in electric field should concentrate at p/i interface, where the carries are depleted. Therefore, carrier density at this depletion region is dramatically increased by forward bias application. Since the recombination rate depends on the product of majority carrier density and minority carrier density, holes are likely to recombine with 'majority' electrons at the depletion region via the defective grain boundaries. This effect would be responsible for that the V_{oc} for X_c~80% is always lower than that for X_c~50%.

4.3 Time-of-Flight experiment on poly-Si thin films

4.3.1 Experimental setup

The Time-of-Flight experiment for the study of carrier transport properties has been frequently performed on the low-carrier-mobility materials such as amorphous based materials and organic semiconductors or insulators [7-11]. However, only few experiments of this technique have been applied to low-temperature poly-Si thin film materials [12]. This is due to some difficulties in fulfilling Time-of-Flight conditions validity for the poly-Si materials.

As a principle of Time-of-Flight experiments, electron-hole pairs are injected at one-side surface of samples by light excitation with a short flash and short penetration depth, and then one signed carriers (electron or hole) are drifted across the sample thickness by an externally applied field. The drifting carriers generate a displacement current at the both sides of sample electrodes, which

induces a current in the external circuit. If the transit time of drifting carrier traveling from one side surface to another is detected, one can simply derive the carrier drift mobility (μ_d) by using following formula,

$$\mu_d = d/(t_T F) = d^2/(t_T V), \tag{4.2}$$

where d is the sample thickness, t_T the transit time of drift carrier, F the electric field, V the sum of the built-in potential and the externally applied voltage. The crucial point in using this relation is that homogeneous and uniform electric field throughout the sample has to be maintained at least the time scale from voltage application to finishing the transit-time measurement. In this respect, the material dielectric relaxation time (t_D) should be much longer than the carrier transition time, i.e., $t_D \gg t_T$. If this condition is not fulfilled, the equilibrium majority carriers are redistributed, resulting in inhomogeneous and non-uniform electric field inside the sample. Since the dielectric relaxation time depends on the material conductivity, $t_D = \varepsilon/\sigma$, where ε is the dielectric constant and σ is the dark conductivity, the highly conductive materials may encounter $t_D \gg t_T$ limitation. For practical measurement, $t_D > 1$ μs may be essential, and then σ of poly-Si samples should be lower than 10^{-6} S/cm. As described in the previous section, however, AC-conductivity measurement reveals that the poly-Si films with high crystalline volume fraction typically show strong n-type character and high dark conductivity over 10^{-4} S/cm at room temperature. Time-of-Flight experiment is no longer applicable to these highly conductive materials. On the other hand, poly-Si films with estimated crystalline volume fraction, $X_c \sim 50\%$, which are of great interest with respect to high quality materials for the solar cells, show relatively low dark conductivity below 10^{-7} S/cm and then they fortunately satisfy above-mentioned $t_D \gg t_T$ condition. Accordingly, the carrier transport in this device-grade poly-Si photovoltaic material was evaluated by Time-of-Flight experiment. The device grade a-Si:H film was also evaluated for verification test of measurement system as well as for comparison with poly-Si films.

For poly-Si films, the electron-drift-mobility measurement was performed

on a 1-mm^2 solar cell consisting of ZnO/p-i (5.6 μm)-n/flat-SnO_2/glass structure with excitation light through the p-layer side. The hole-drift-mobility

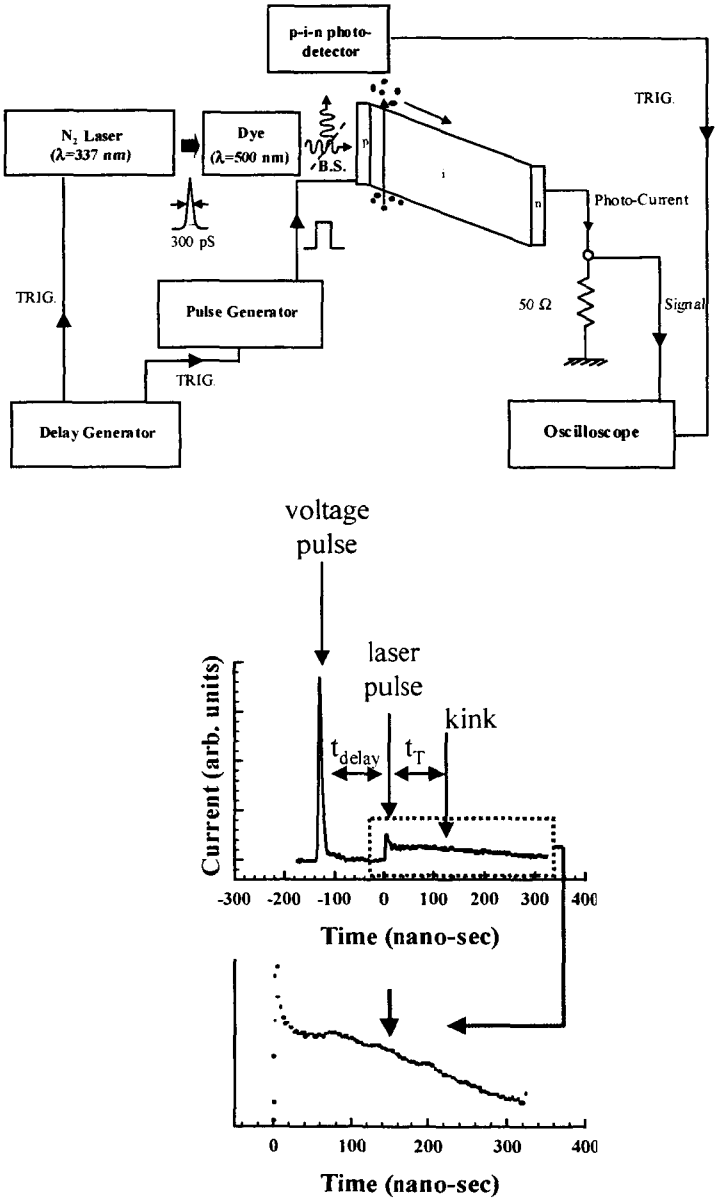

Fig. 4.9. Schematic block diagram of Time-of-Fright measurement system. Also shown is the typical electron current transient in linear scale.

measurement was also made on this sample with excitation light through the *n*-layer side. For a-Si:H films, the measurement conditions and sample structure are same as that for poly-Si sample but the different 3.5 μm and 1.8 μm thick a-Si:H i-layers were used for electron- and hole-drift-mobility measurement, respectively. Figure 4.9 illustrates the schematic diagram of Time-of-Flight measurement system. The typical current transient obtained by this measurement is also shown. A 300 ps flash light form N_2-dye pulse laser with a wavelength of 480 nm was used as an excitation light source. The incoming light was divided by a beam splitter into incident light on the sample and on a fast p-i-n photo-detector used for an optical trigger. The light pulse is timed to arrive at the sample surface a few handled nanoseconds after the reverse voltage pulse application, which is controlled by the delay generator. This delay time, t_{delay} is to keep waiting for the laser flash until the *CR* current decay approaches zero level. In addition, for maintaining uniformity of applied field until the transit-time measurement completes, t_{delay} was set at about 100 nanosecond, which is much less than dielectric relaxation time. The external signal current, which is induced by drifting photo-generated carriers inside the sample, is monitored through the current in 50 Ω loading resistor by the 500 MHz bandwidth digital oscilloscope. A large amount of the excess charge injection might disturb the homogeneous electric field inside the sample, therefore, the excitation light intensity is attenuated to reduce the injection charge (Q) being much less than the accumulated charge (CV) at the both electrodes induced by the externally applied reverse bias voltage.

4.3.2 Electron and hole transport in poly-Si films

The observation of a carrier transit time t_T is the first objective of this experiment. The electron (a) and hole (b) current transients of poly-Si sample measured at 300 K and at different applied voltage (4, 6, 8 V) are shown in Fig. 4.10. The t_T of the injected carriers can be determined from the kink appearing in the transient curves plotted in log-log scale. Since the both electron and hole

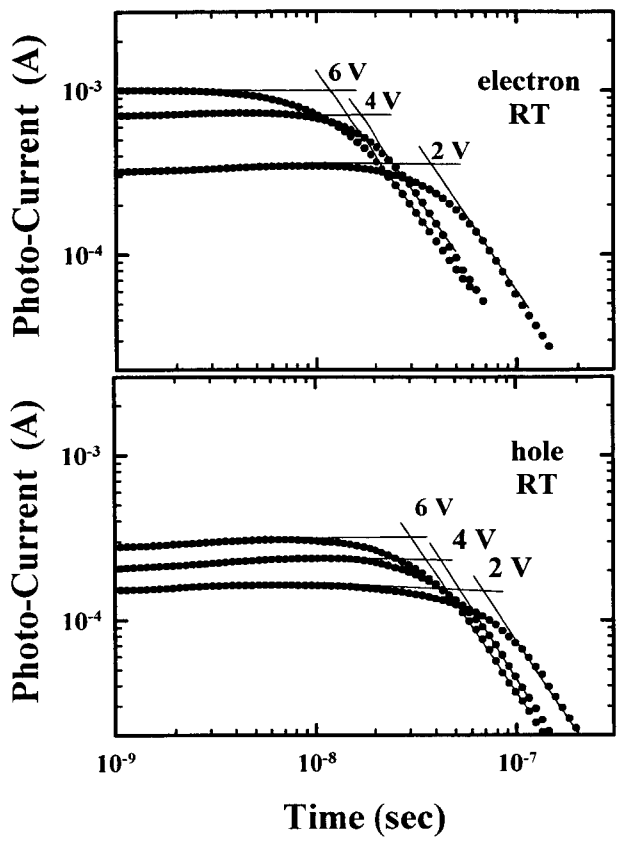

Fig. 4.10. Electron and hole current transients of 5.6 μm-thick poly-Si sample measured at room temperature for different applied voltage. Transit time is deduced from the crossing point of the fitted lines.

current transients are measured for the poly-Si sample with same thickness, the transit time of electrons is found to be slightly faster than that of holes if we compare electron transient with hole transient under the same applied voltage condition. As the applied voltage increases, for electron and hole transients, the initial current maximum steadily increases while the transit time t_T decreases. Corresponding electron and hole drift mobilities can be estimated in accordance with definition in eq. (4.2). In Fig. 4.11, d^2/t_T for electron and hole are plotted as a function of applied voltage in the range of 1.5-9.0 V. For both data, d^2/t_T is

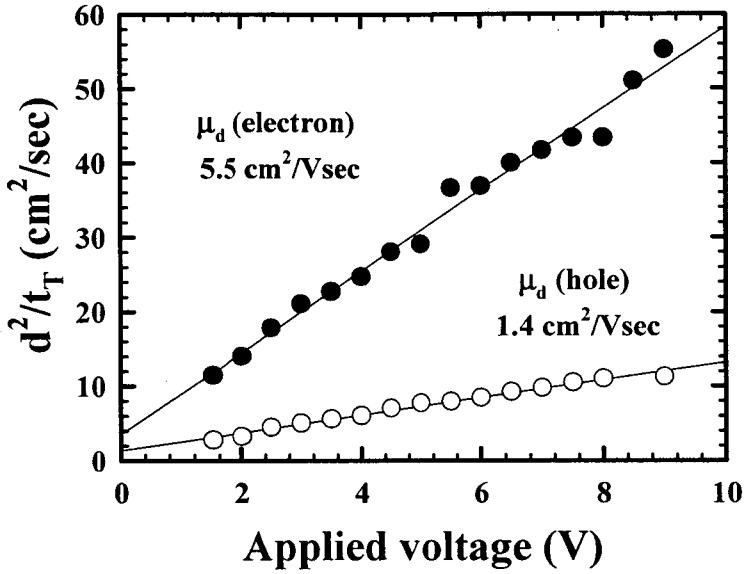

Fig. 4.11. d^2/t_T-V plots for estimation of electron (●) and hole(○) drift mobilities.

proportional to applied voltage. From the slope of these fitted straight lines, the electron and hole drift mobilities are estimated as μ_{de}=5.5 cm^2/Vs and μ_{dh}=1.4 cm^2/Vs, respectively.

The second interest of transport parameter is the carrier lifetime. Figure 4.12 shows the electron and hole collected charges Q for the poly-Si sample, which correspond to the integration of respective current transients, as a function of the applied electric filed (F). The circles plotted in Fig. 4.12 are experimental Q-F data obtained by Time-of-Flight experiment. It is found that collected electron and hole charges rapidly increase with an increase in applied field and approach the respective saturation levels at F~5×10^3 V/cm for electron and at F~1.5×10^4 V/cm for hole. The lines also shown in Fig 4.12 are the fitted curves using Hecht expression [13,14] given by

$$Q = Q_o \frac{\mu_d \tau_d F}{d}\left[1 - \exp\left(-\frac{d}{\mu_d \tau_d F}\right)\right], \qquad (4.3)$$

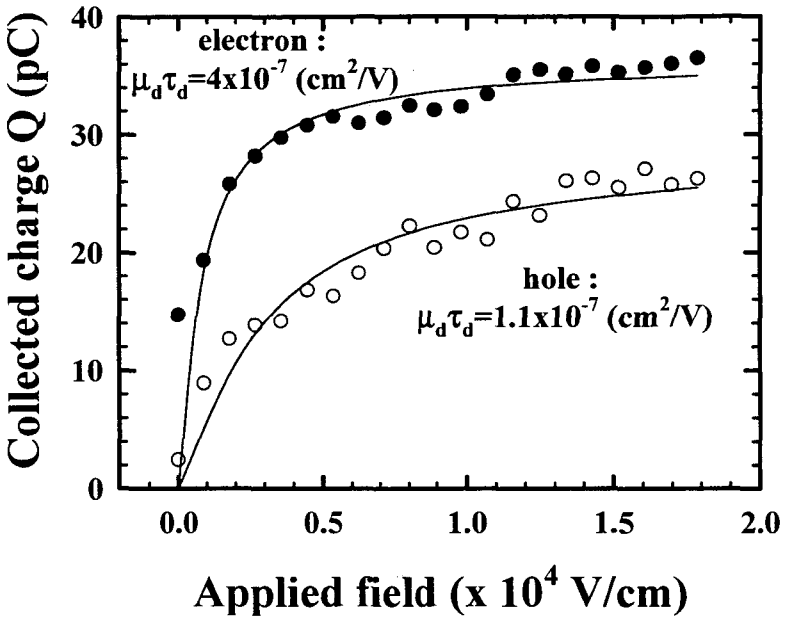

Fig. 4.12. Collected electron (●) and hole (○) charges measured for poly-Si sample as a function of applied electric field. Solid lines are fitted results for evaluation of mobility-lifetime product in accordance with eq. (4.3).

where Q_0 is the total charge generated by light pulse, and τ_d is the deep trapping lifetime of the drifting carrier inside the sample. From the fitting results, using eq. (4.3), the mobility-lifetime products for electrons and holes are estimated as 4×10^{-7} cm^2/V and 1.1×10^{-7} cm^2/V, respectively.

These important transport parameters of poly-Si sample measured at room temperature are listed in Table 4.1, together with those of a-Si:H samples measured under the same conditions used for poly-Si sample . The estimated electron and hole drift mobilities of a-Si:H samples are 0.83 cm^2/Vs and 8.5×10^{-3} cm^2/Vs, respectively. In a-Si:H samples, the hole drift mobility is much lower than the electron drift mobility. These values are almost consistent with those reported for conventional a-Si:H films [9,15-17]. No significant difference is found in electron drift mobility between for poly-Si and a-Si:H samples.

Table 4.1. List of transport parameters of poly-Si and a-Si:H samples obtained by Time-of-Flight experiments.

transport parameters	poly-Si	a-Si:H	a-Si:H [ref.]
elec. drift mobility:(cm^2/Vs)	5.5	0.83	1.0 [9]
hole drift mobility:(cm^2/Vs)	1.4	8.5×10^{-3}	1.0×10^{-3} [9]
elec. mobility-lifetime product:(cm^2/V)	4.0×10^{-7}	3.2×10^{-8}	1.8×10^{-7} [18]
hole mobility-lifetime product: (cm^2/V)	1.1×10^{-7}	5.3×10^{-9}	3.7×10^{-8} [18]

Surprisingly, however, hole drift mobility for poly-Si sample is by more than two orders of magnitude higher than that for a-Si:H sample. If we compare the mobility-lifetime product, both electron and hole $\mu_d\tau_d$ for poly-Si sample are by one or two orders of magnitude higher than those for a-Si:H samples.

Figure 4.13 shows the hole photocurrent transients measured at different temperature for poly-Si (a) and a-Si:H (b) samples. In poly-Si samples, firstly, the temperature dependence is found in current transient but it remains non-dispersive character and clear kink appears even at 200 K. In a-Si:H sample, on the other hand, it is evident that the current transients become progressively more dispersive and the transit times progressively longer at low temperature regime. At a temperature of 280 K, no clear kink is found in the current transient of a-Si:H, therefore, drift mobility is not measurable in this time scale. Figure 4.14 shows the temperature dependence of hole-drift mobilities for both samples deduced from above-mentioned current transients. Also shown in Fig.4.14 is the temperature dependence of electron drift mobility. All of the mobilities show thermally activated behaviors being independent of material and carrier type. In a-Si:H samples, the activation energies of 0.11 eV and 0.23 eV are deduced for the electron and hole drift mobilities, respectively, which are also consistent with those reported on conventional a-Si:H materials [9,15-17]. In poly-Si sample, on the other hand, temperature dependence of hole drift mobility is much smaller than that for a-Si:H sample, and estimated activation energy of

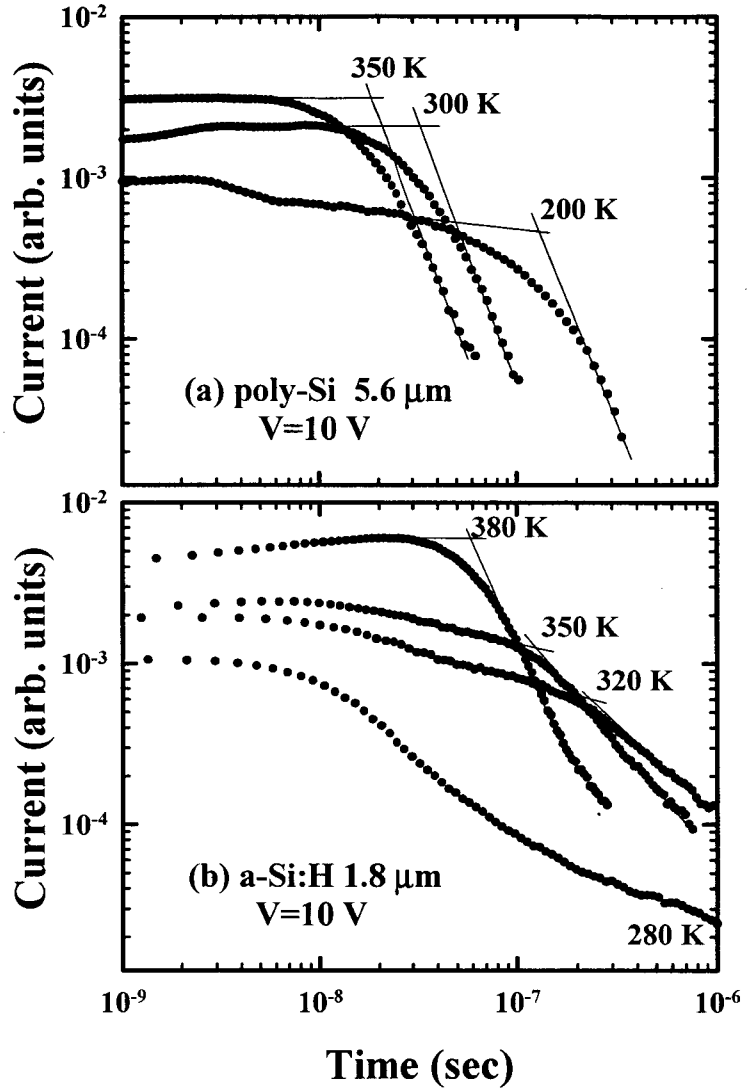

Fig. 4.13. Hole current transients for poly-Si (a) and a-Si:H (b) samples measured at different temperatures.

hole drift mobility is 0.11 eV which is almost identical with that of electron drift mobility.

The temperature dependent hole transport in a-Si:H material reveals strong dispersive character at temperature below 380 K, which is interpreted as

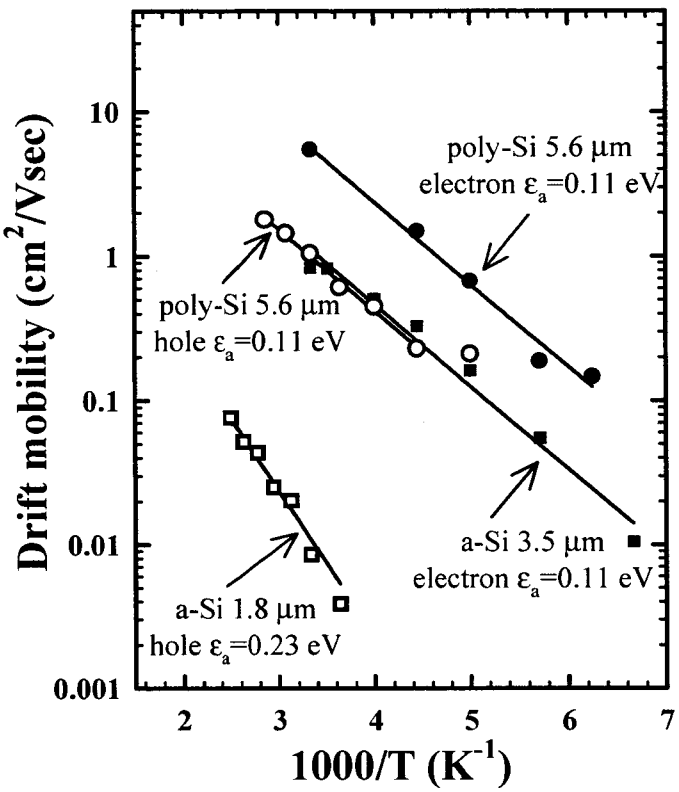

Fig. 4.14. Temperature dependence of electron (closed) and hole (open) drift mobilities for poly-Si (circle) and a-Si:H (square) samples.

multiple-trapping carrier transport [19,20]. The main feature of this model is that drifting carriers interact with an exponentially decreasing distribution of localized states extending into band gap, in which the carriers transit inside the material over many events of trapping and thermal re-emission. The carrier drift mobility is determined by both densities of free carriers and trapped carriers in the vicinity of band edge [20]. Hole drift mobility can be described as

$$\mu_d = \mu_f \frac{p_f}{p_f + p_t}, \tag{4.4}$$

where μ_f is the free hole mobility, i.e., mobility at the valence band edge state, and p_f and p_t are the densities of free holes at the extended state and trapped holes at the localized state, respectively. Since the trapped charge density p_t in eq. (4.4) is generally regarded as an exponential function of inverse temperature, the influence of p_t on drift mobility is then progressively significant at low temperature regime. Therefore, temperature dependence of hole drift mobility strongly reflects the localized states in the vicinity of valence band edge. Non-dispersive feature and low activation energy in poly-Si hole drift mobility would then imply the lower density of localized states. From a theoretical work, it has been reported that hydrogen composition in amorphous network determines the energy of valence band edge, whereas the energy of conduction band edge is independent of it. Based on this theory, it can be speculated that the hydrogen content in the films is tightly correlated with the hole transport properties in valence band [21]. Actually, the high hole drift mobility $\mu_h \sim 0.2$ cm^2/Vs was reported in a-Si:H materials prepared with a 'chemical annealing' treatment, in which the hydrogen content is lower than conventional a-Si:H [22]. As one of the possible reasons, the high hole drift mobility observed in poly-Si film may be attributed to the relatively low hydrogen content in poly-Si films.

Once again, the hole drift mobility for poly-Si film shows a significantly higher value than that for a-Si:H film, which may be responsible for the results of high performance in the p-i-n poly-Si solar cells. As shown in previous section, J_{sc} of poly-Si solar cells steadily increases with poly-Si thickness above 5 μm where built-in field decreases as low as 1 kV/cm. Since high J_{sc} is attributed to the enhancement in long wavelength response, which is confirmed by spectral response measurement, the effective hole diffusion length is longer than thickness of poly-Si photovoltaic layer (> 5 μm) even at relatively such low built-in field. This is also specific feature in poly-Si materials because the carrier collection behavior in a-Si:H solar cells is more field dependent. Therefore, it can be concluded that carrier transport in poly-Si material is dominated by crystalline phase and not by amorphous phase, nevertheless the film exhibits relatively low crystalline volume fraction.

4.4 Summary

AC-conductivity measurement technique is proposed as a powerful tool for evaluating the carrier transport along perpendicular direction as well as for determining the electron and hole conductivities individually. It has been found that the Fermi energy level in the poly-Si films is quite sensitive against to film microstructure. From the results of temperature dependent AC-conductivity, poly-Si layers with relatively low crystalline volume fraction, X_c~50% and (220) preferential orientation exhibit truly intrinsic character like intrinsic c-Si material, leading to the high performance solar cells. In contrast, poly-Si layers with high X_c~80% and (220) preferential orientation exhibit n-type character with an activation energy of less than 0.15 eV, which is likely to be associated with the oxygen-related donor at grain boundary. Experimental and simulation results suggest that poly-Si solar cells with high X_c result in lower V_{oc} due to n-type character and further electrical activation at grain boundaries. In order to gain more insight into the carrier transport, Time-of-Flight experiments are performed on a device-grade poly-Si film of X_c~50% with a complete p-i-n sample configuration. A significant difference is found in hole transport between poly-Si and a-Si:H materials. The temperature dependence of hole drift mobility has revealed that hole transport in poly-Si films shows non-dispersive transport even at 200 K, while that in a-Si:H films is quite dispersive below 380 K. The hole drift mobility for poly-Si films is estimated as 1.4 cm^2/Vs at room temperature, which is by more than two orders of magnitude higher than that for conventional a-Si:H films.

References

[1] J. Kočka, A. Fejfar, V. Vorlíček, H. Stuchlíková, J. Stuchlík: Mat. Res. Soc. Symp. Proc. **557** (1999) 490.

[2] J. Kočka, A. Fejfar, H. Stuchlíková, J. Stuchlík N. Wyrsch, P. Torres, J. Meier, A. Shah, A. Matsuda: Proc. of 2nd World Conference on Photovoltaic Energy Conversion (WCPEC), Vienna, (1998), p.785.

[3] P. Torres, J. Meier, R. Fluckiger, U. Kroll, J.A.A. Selvan, H. Keppner, and A. Shah, S.D. Littlewood, I.E. Kelly, P. Giannoules : Appl. Phys. Lett. **52** (1988) 1675.

[4] G. Dusher, J. Mullejans, J.H. Werner, M. Rühle: Mat. Sci. Forum **207-209** (1995) II-713

[5] Y. Nasuno, M. Kondo and A. Matsuda: Appl. Phys. Lette. **78** (2001) 2330

[6] J.H. Werner: Inst. Phys. Conf. Ser. **104** (1989) 63

[7] P.G. LeComber and W.E. Spear: Phys. Rev. Lette. **25** (1970) 509.

[8] D. Allan: Philos. Mag. B **38** (1978)

[9] T. Tiedje, J. M. Cebulka, D. L. Morel and B. Abeles: Phys. Rev. Lette. **46** (1981) 1425.

[10] P.B. Kirby and W. Paul: Phys. Rev. B29 (1984) 821.

[11] J. Shirafuji, M. Kuwagaki, T. Tato and Y. Insuishi: Jpn. J. Appl. Phys. **23** (1984) 1278.

[12] A. Fejfar, N. Beck, H. Stuchlíková, N. Wyrsch, P. Torres, J. Meier, A. Shah, J. Kocka,: J Non-Cryst. Solids. **227-230** (1998) 1006.

[13] K. H. Hecht, Z. Phys. **77**(1932) 235.

[14] D.S.Shen, S. Wagner, J. Appl. Phys. 79 (1996) 794.

[15] N. Beck, N. Wyrsch, E. Sauvain. A. Shah, Mater. Res. Soc. Sympo. Proc. 297 (1993) 479.

[16] R.A. Street, J. Zesch, M.J. Thompson: Appl. Phys. Lette. **43** (1983) 672.

[17] W.E. Spear, H.L. Steemers, P.G. LeComber, R.A. Gibson: Phil. Mag. B **50** (1984) L33.

[18] H. Antoniads, E.A. Schiff: Phys. Rev. B **44** (1991) 3627.

[19] T. Tiedje and A. Rose: Solild State Commun. **37** (1980) 49.

[20] T. Tiedje: "Semiconductor and Semimetals" Vol.**21**, ed. by J.I. Pankove (Academic Press, 1984) 207.

[21] D.P. Divincenzo, J. Bernholc and M.H. Brodsky: Phys. Rev. B **28** (1983) 3246.

[22] D. Das, H. Shirai, J. Hanna and I. Shimizu: Jpn. J. Appl. Phys. **30** (1991) L239.

Chapter V

Light trapping technique and rear side interface properties of poly-Si thin film solar cells

5.1 Introduction

Since poly-Si is an indirect band gap material and has low optical absorption coefficient in the visible-infrared region, the light trapping in thin film poly-Si layer by using textured substrate is one of the most important technical issues for achievement of high short circuit current. The key requirement for textured substrate is to realize the sufficient light trapping to enhance the path length of the incident light in thin film poly-Si photovoltaic layer, and reduce the weak-absorbable light getting out again from the surface of solar cell. However, one needs to take into account the influence of substrate texture not only on the light trapping but also on poly-Si microstructure, because the substrate surface morphology largely dominates the preferential growth of poly-Si photovoltaic layer [1,2]. So far, only few studies have been reported for the optimum design of substrate texture to realize further improvement of the photovoltaic performance of poly-Si solar cells [1-5].

For amorphous silicon solar cells, textured SnO_2 has been widely used as a

front transparent conductive oxide (TCO) layer due to its controllability of surface morphology as well as good light trapping performance [6]. We expect that the textured SnO_2 could be utilized for the light trapping even in the substrate-type poly-Si solar cells as a novel back reflector with a structure of $ZnO/Ag/SnO_2$ triple layers.

A series of the poly-Si solar cells has been fabricated on differently textured $ZnO/Ag/SnO_2$/glass substrates, in order to find the optimum textured substrate and realize the effective light trapping in the poly-Si solar cells. In this chapter, a systematic investigation has been carried out concerning the dependence of poly-Si microstructure and photovoltaic performance on substrate texture as a function of root mean square roughness of substrate surface. It has been demonstrated that the substrate texture directly affects the poly-Si preferential growth on it. Some detail discussions will be also given on the carrier transport behavior particularly near the junction interface between poly-Si photovoltaic layer and textured substrate. Finally, the performance of p-i-n junction poly-Si solar cell with the highest conversion efficiency achieved throughout this work is demonstrated with an optimum poly-Si layer thickness as well as an optimum textured substrate.

5.2 Preparation of textured substrate for light trapping

5.2.1 $ZnO/Ag/SnO_2$ textured back reflector

A series of four substrates with different surface texture was prepared and then used as the back reflector of poly-Si solar cells. For these substrates, a highly reflective ZnO(1000 Å)/Ag(2000 Å) double layer was formed on differently textured SnO_2(7000-10000 Å)/glass substrates (Asahi Glass Company). For comparison, ZnO/Ag/glass was also prepared as a flat substrate. A cross-sectional image of a typical $ZnO/Ag/SnO_2$/glass substrate is displayed in Fig. 5.1, which was taken by scanning electron microscope (SEM). The

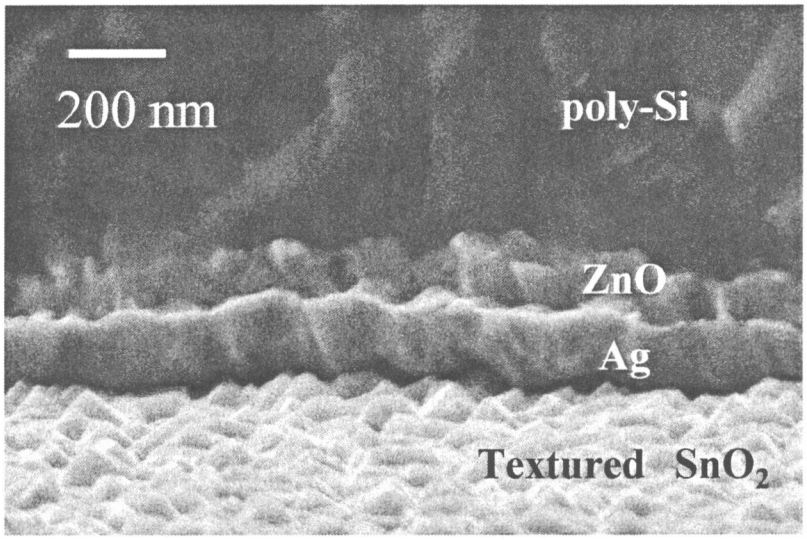

Fig. 5.1. Cross-sectional SEM image of typical ZnO/Ag/SnO_2/glass textured substrate for solar cell.

formation of ZnO/Ag textured layers, which directly reflect the SnO_2 surface with a native pyramid-like shape, can be observed.

Figure 5.2 displays the surface morphologies of five kind of substrates ((a)-(e)) used in this experiment, which were characterized by atomic force microscope (AFM) measurement. These AFM pictures clearly show that the surface morphology of ZnO/Ag/SnO_2/glass substrate are systematically controlled by changing the roughness of textured SnO_2 layer. Figure 5.3 represents the roughness height distributions of the back reflectors deduced from AFM data in Fig. 5.2, in which (a) corresponds to the surface of flat ZnO/Ag/glass substrate and (b)-(e) correspond to the surface of textured ZnO/Ag/SnO_2/glass substrates. The roughness height distribution of each substrate is well fitted by Gaussian function with the different mean heights and standard deviations. The substrate surface roughness is characterized by the root mean square (RMS) roughness, σ. The RMS roughness of these substrates are estimated as (a) 26 nm, (b) 34 nm, (c) 38 nm, (d) 46 nm and (e) 55 nm, respectively.

Flat: ZnO/Ag/glass

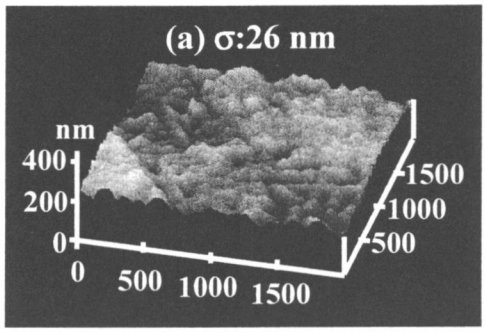

Texture : ZnO/Ag/SnO_2/glass

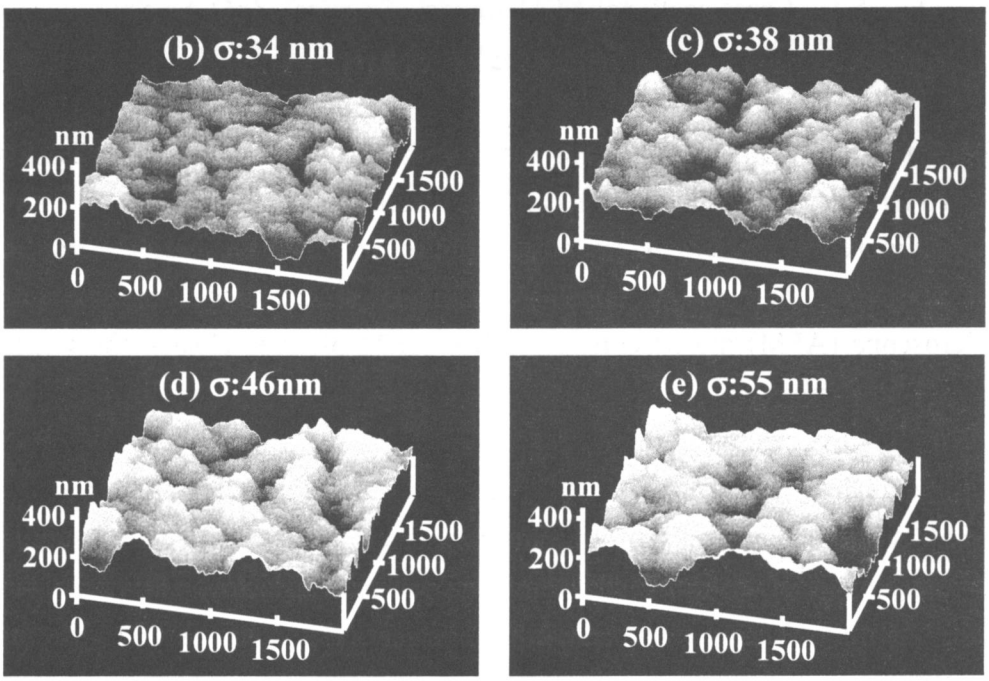

Fig. 5.2. AFM surface images of flat ZnO/Ag/glass (a) and textured ZnO/Ag/SnO_2/glass (b)-(e) substrates. The root mean square (RMS) roughness of each substrate is also indicated.

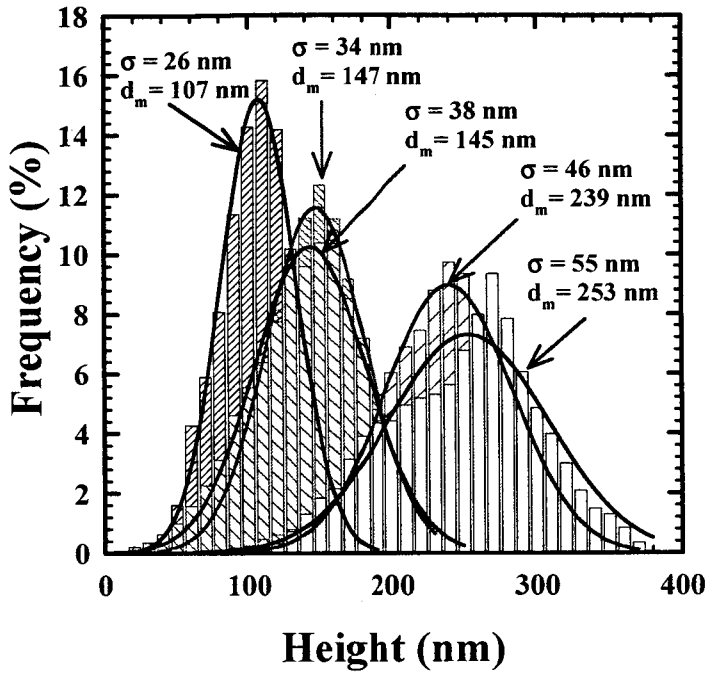

Fig. 5.3. Height distributions of flat ZnO/Ag/glass (a) and textured ZnO/Ag/SnO_2/glass (b)-(e) substrates measured by AFM. Solid lines are fitted result to Gaussian function. The root mean square (RMS) roughness, σ, and peak center, d_m, of each distribution are also indicated.

5.2.2 Light trapping effect

First of all, the light scattering properties of the series of back reflectors are evaluated. Figure 5.4 shows the typical reflectance spectra of the 3 μm-thick solar cells formed on flat ZnO/Ag/glass and differently textured ZnO/Ag/SnO_2/glass substrates. The solar cells of which poly-Si photovoltaic layer exhibits (220) preferential crystallographic orientation and approximately 50% crystalline volume fraction, which yields relatively high photovoltaic performances, as demonstrated in chapter III. The reflectance of solar cells was measured by spectrophotometer using spherical integrator. In Fig. 5.4, the

minimum reflectance is found to be almost 0% at a wavelength (λ) of around 530 nm for all samples, which is attributed to an anti-reflective effect due to the 80-nm thick TCO top layer. The reflectance and interference amplitude at $\lambda > 650$ nm steadily decrease with an increase in σ. Concerning the solar cell with σ = 55 nm, reflection interference at long wavelength regime almost disappears, and reflectance at 800 nm reduces by more than 20% in comparison with that of flat back reflector. This result indicates that the infrared light at $\lambda > 650$ penetrated to back surface is significantly scattered by the textured back reflector and effectively absorbed in the poly-Si layer.

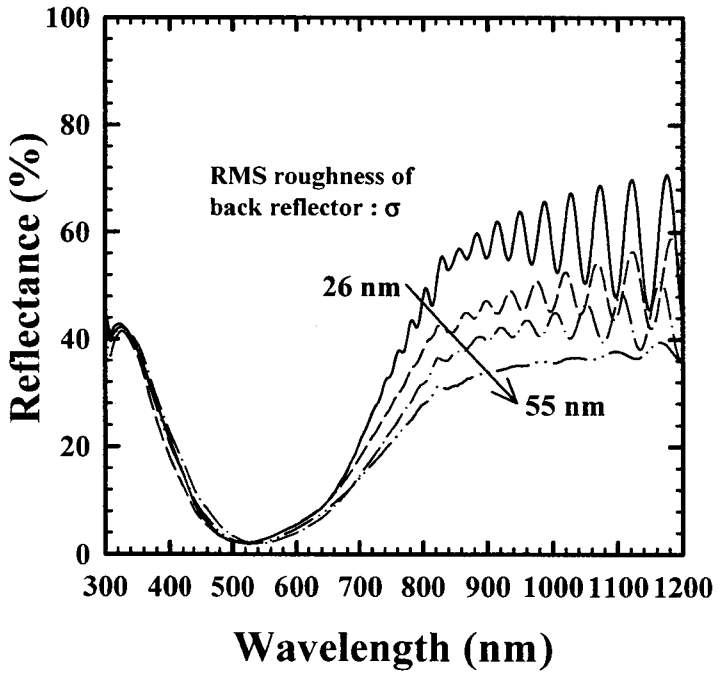

Fig. 5.4. Reflectance spectra of the 3 μm-thick solar cells formed on flat ZnO/Ag/glass (σ = 26 nm) and differently textured ZnO/Ag/SnO_2/glass (σ = 38, 46, 55 nm) substrates.

5.3 Influence of substrate texture on microstructure and photovoltaic performance of poly-Si solar cells

5.3.1 Light trapping grain in short circuit current

Figure 5.5 shows the spectral responses of poly-Si solar cells with typical three kind of substrates (σ = 26, 38, 55 nm). All quantum efficiency (*QE*) spectra show spectral peaks at around 600 nm with peak efficiencies of >80% and no significant difference in the short wavelength regime. Compared to the solar cell on flat ZnO/Ag/glass (σ = 26 nm), high *QE* at long wavelength regime can be observed for the solar cells formed on textured ZnO/Ag/SnO_2/glass substrates with the σ = 38 nm. A clear improvement in the long wavelength responses is also found in the inset of Fig. 5.5 in which the *QE* at λ =800 nm

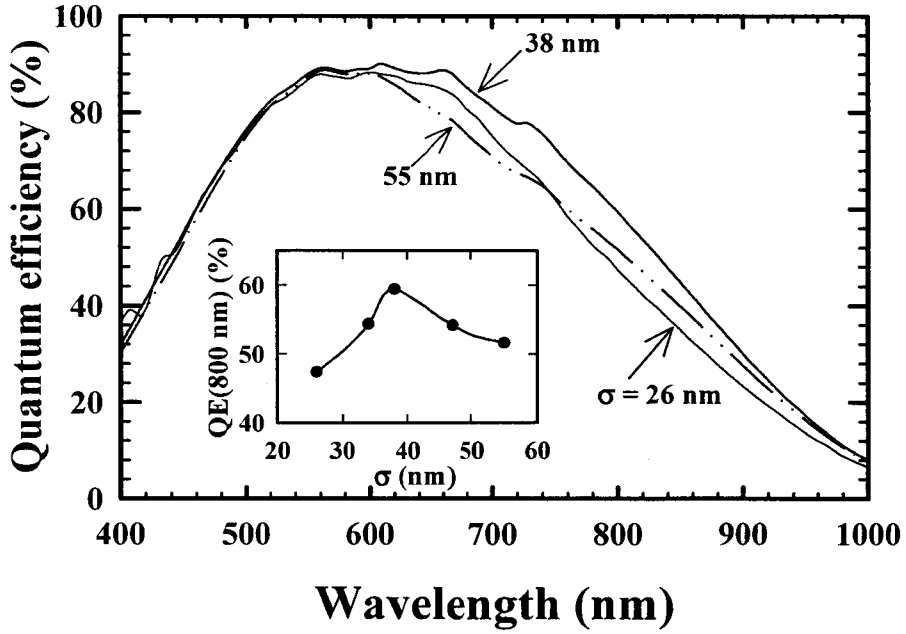

Fig. 5.5. External quantum efficiency (*QE*) spectra of the 3 μm-thick solar cells formed on flat ZnO/Ag/glass (σ = 26 nm) and differently textured ZnO/Ag/SnO_2/glass (σ = 38 and 55 nm) substrates. Inset shows *QE* at 800 nm plotted against σ.

shows an increase up to nearly 60% with increasing the σ from 26 to 38 nm. However, a further increase in σ causes a decrease in *QE* at $\lambda > 600$ nm.

Figure 5.6 shows the poly-Si photovoltaic performance, (a) short circuit current density J_{sc}, and (b) open circuit voltage V_{oc}, as a function of σ of substrate. With an increase in σ from 26 to 38 nm, J_{sc} increases by about 3 mA/cm^2 and reaches the maximum value of nearly 24 mA/cm^2, then rapidly decreases above

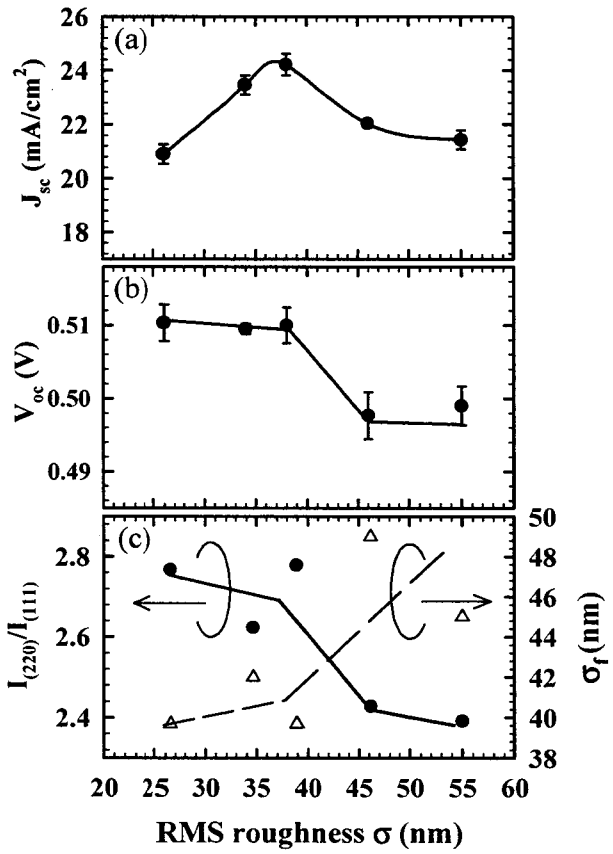

Fig. 5.6. J_{sc} (a) and V_{oc} (b) of poly-Si solar cells as a function of RMS roughness of substrate. The ratio of (220) and (111) integrated X-ray diffraction intensities $I_{(220)}/I_{(111)}$ (closed circle), together with RMS roughness of poly-Si front surface σ_f (open triangle), are also plotted (c). The lines are guides for the eyes.

the σ of 38 nm. Compared to the corresponding *QE* spectra (Fig. 5.5), it is found that the resulting J_{sc} values are mostly determined by the long wavelength responses. V_{oc} also shows a sharp decrease at σ > 38 nm where J_{sc} starts to decrease. At $\sigma \leq 38$ nm, V_{oc} is almost unchanged against σ and keeps relatively high values of around 0.51 V. We therefore find a most suitable substrate for poly-Si solar cell in this experimental series, i.e., ZnO/Ag/SnO_2/glass with σ of 38 nm.

In order to investigate the influence of substrate texture on poly-Si microstructure, XRD measurements were performed on the poly-Si films deposited on differently textured substrates. In the bottom view of Fig. 5.6, the ratio of (220) and (111) integrated diffraction intensities, $I_{(220)}/I_{(111)}$, which gives a clear indication of the degree of (220) preferential orientation of the poly-Si layer, is also plotted against the σ of substrate. Additionally, poly-Si front surface RMS roughness, σ_f, measured by AFM is also plotted. All poly-Si films basically exhibit (220) preferential orientation with $I_{(220)}/I_{(111)}$ values in the range of 2.4-2.8. It is found that a significant structural change in poly-Si layer takes place at σ >38 nm, i.e., the $I_{(220)}/I_{(111)}$ rapidly decreases and the poly-Si front surface roughness increases simultaneously. The decrease in $I_{(220)}/I_{(111)}$ is mainly due to the decrease in $I_{(220)}$. On the other hand, poly-Si surface morphology seems to be directly reflected by substrate texture at σ >38 nm. Since the both J_{sc} and V_{oc} show a noticeable decrease at σ >38 nm, these results are likely to suggest that the structural transition in the poly-Si layer attributed to the roughness of the substrate are responsible for the change in poly-Si photovoltaic performance.

5.3.2 Carrier transport in poly-Si layer near the textured substrate

Although the highly textured ZnO/Ag/SnO_2 back reflector shows the excellent light trapping properties, it tends to deteriorate the photovoltaic performance of poly-Si solar cells. This would be related to the change in poly-Si (220) preferential growth caused by roughness of substrate surface. It is well

known that the poly-Si films with (220) preferential orientation basically possess columnar structure [7,8]. Namely, the growth direction of ploy-Si film should be perpendicular to the local surface of the substrate. The decrease in $I_{(220)}/I_{(111)}$ shown in Fig. 5.6 implies that the growth direction of the poly-Si film tends to be perpendicular to the slant surface but not to substrate itself. Such diagonally oriented columnar growth may occur the collision with the growth of neighboring grain [1], which can be partially observed in a cross-sectional SEM image of poly-Si/textured substrate (σ =55 nm) interface shown in Fig. 5.7. This growth collision of poly-Si grains would create many grain boundaries and related defects particularly near the textured substrate surface. This hypothesis

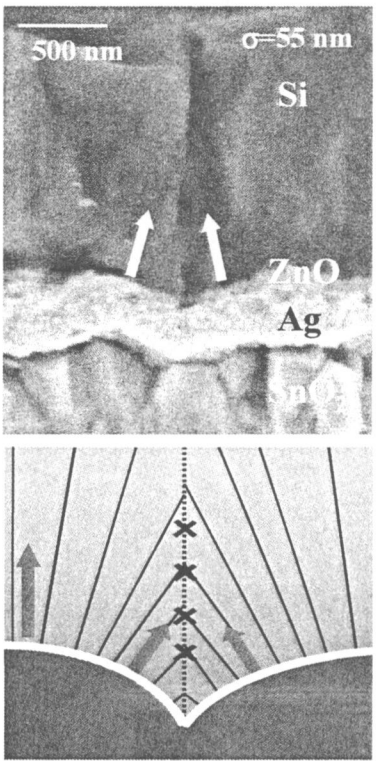

Fig. 5.7. Cross-sectional SEM image (top) and schematic illustration of growth collision (bottom) of poly-Si layer near textured substrate (σ =55 nm). Arrows indicate growth directions of poly-Si grains.

is supported by the studies of the filed-dependent carrier collection that gives some information about the carrier recombination through the photovoltaic layer [9]. In order to detect the magnitude of carrier recombination near the rear side junction of solar cell, poly-Si solar cells directly formed on textured SnO_2/glass substrate were prepared. With this sample structure, the spectral response can be measured by rear side illumination through the glass substrate as well as by usual front side illumination through the top TCO layer. In this experiment, a flat SnO_2/glass substrate (σ = 20 nm) and two differently textured SnO_2/glass substrates (σ = 57, 84 nm) were used to investigate the texture effect. A scheme of this idea is illustrated in Fig 5.8. In order to examine the field-dependent carrier collection behavior, the *QE* spectra under applied reverse bias voltage of -1 V are demonstrated in the form *QE*(-1 V)/*QE*(0 V), i.e., normalized by corresponding spectra under short circuit condition, as also demonstrated in chapter III. Figure 5.9 shows the *QE*(-1 V)/*QE*(0 V) spectra of the solar cells formed on the three SnO_2/glass substrates with different σ. This figure also provides a comparison of *QE*(-1 V)/*QE*(0 V) spectra for p-side (front) illumination and those for n-side (rear) illumination. In p-side illumination case, *QE*(-1 V)/*QE*(0 V) increases especially at long wavelength regime with an increase in the σ of SnO_2/glass substrate, implying the reduction in carrier diffusion length. The effect of substrate texture on spectral response reveals more clearly by illuminating through n-side of the solar cell. In n-side illumination case, *QE*(-1 V)/*QE*(0 V) markedly increases especially at short wavelength regime with an increase in the σ of SnO_2/glass substrate. Since the short wavelength light (λ~500 nm) can penetrate only 0.5 μm or less, the detected *QE*(-1 V)/*QE*(0 V) should reflect the hole transport in poly-Si layer just adjacent to the SnO_2 surface. These results are strong evidence for that the highly textured substrate gives rise to deterioration in carrier transport (hole in this case) and increase in carrier recombination at rear junction side. Consequently, it is reasonable to assign the carrier recombination at rear junction side to the grain boundaries formed by growth collision of poly-Si grains attributed to surface morphologies of textured substrate. An alternative possible

explanation is the enhancement in surface recombination related to the increase in the effective area of substrate surface. However, the SnO_2/glass used in this experiment is widely employed as TCO substrate for amorphous silicon solar cells (typically substrate with σ =57 nm), and there is no disadvantage in carrier transport by using this substrate in amorphous silicon solar cells. This interpretation may not stand good, so far as our experimental results are concerned.

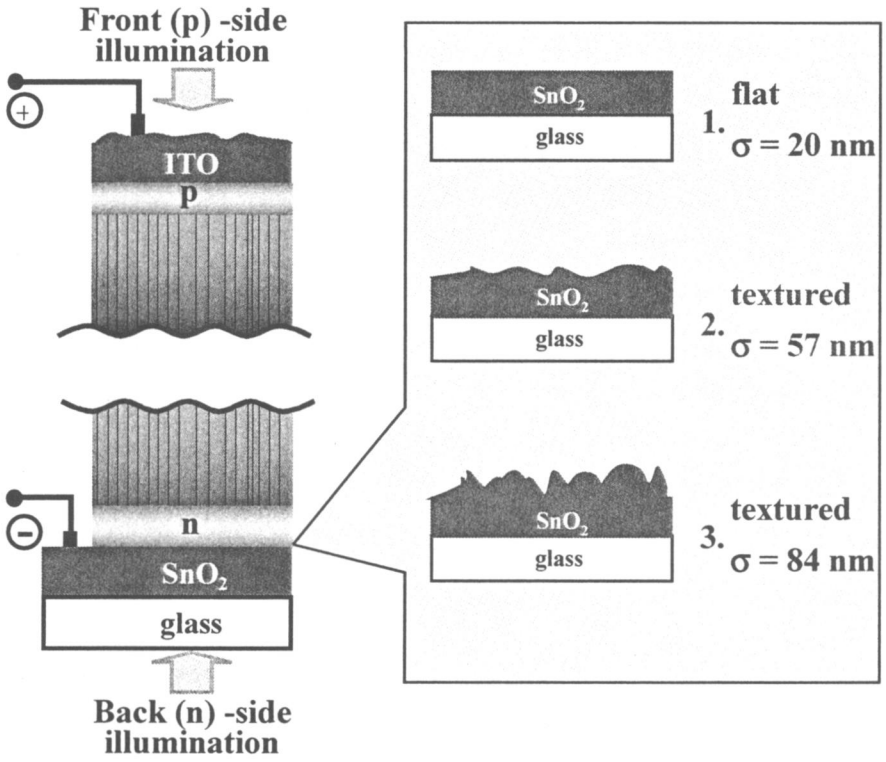

Fig. 5.8. Structure of poly-Si solar cell sandwiched by TCO layers for spectral response measurement with probe light illumination from front or rear side. Poly-Si solar cells on a flat SnO_2/glass (σ = 20 nm) and two kinds of differently textured SnO_2/glass (σ = 57, 84 nm) were prepared.

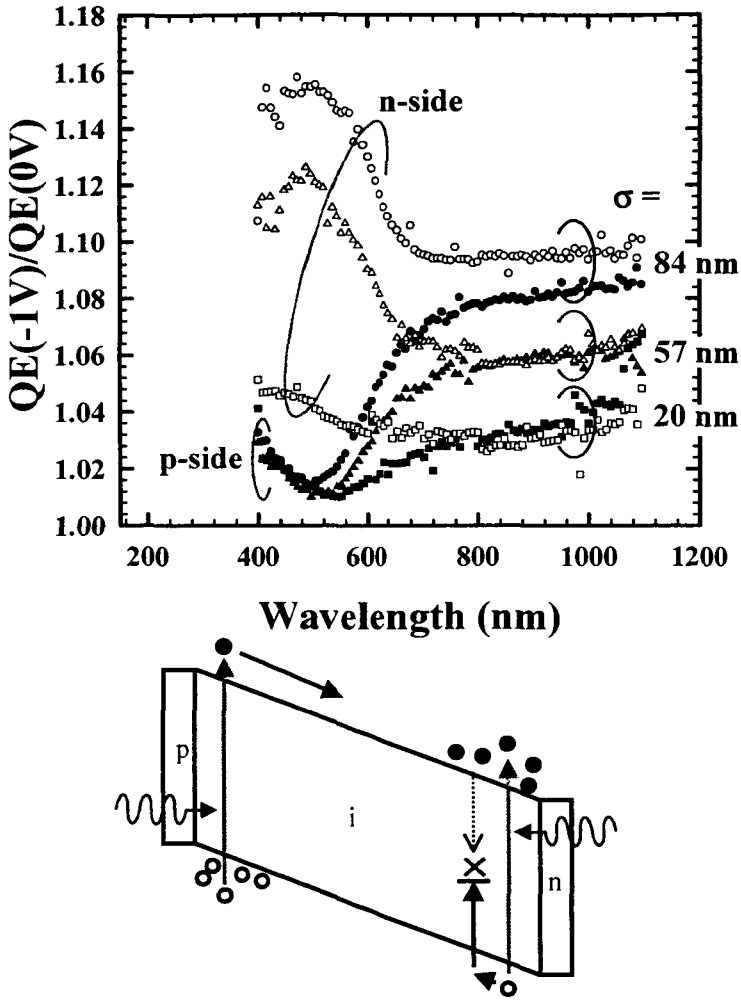

Fig. 5.9. Normalized quantum efficiency spectra, QE(-1 V)/QE(0 V), for the solar cells prepared on different substrates [squares: σ =20 nm, triangles: σ =57 nm, circles: σ =84 nm] (top). Close and open symbols indicate the QE(-1 V)/QE(0 V) with front and rear side illumination, respectively. Strong field-dependence of QE(-1 V)/QE(0 V) are observed at short wavelengths for σ > 57 nm and for n-side illumination, indicating that photo-generated holes considerably recombine near the n/i interface as schematically shown in bottom diagram.

5.4 Optimization of poly-Si i-layer thickness

As discussed in chapter II, the thickness of poly-Si photovoltaic layer is required to be designed as thin as possible to reduce the carrier recombination for obtaining higher V_{oc} and FF. In order to obtain highly efficient poly-Si p-i-n solar cells, therefore, achievement of high J_{sc} with thin i-layer is of prime importance by using effective light trapping technique. Based on a systematic investigation of light trapping effect by means of ZnO/Ag/SnO_2/glass textured substrate, the optimum substrate is found to show the RMS surface roughness of 38 nm. Employing this textured substrate, the optimum thickness of poly-Si i-layer is explored.

Figure 5.10 shows the poly-Si photovoltaic performance as a function of poly-Si i-layer thickness in the range of 1.2-5.6 μm. For comparison, the data of poly-Si solar cells with flat ZnO/Ag/glass substrate are also plotted in this figure. J_{sc} rapidly increases with an increase in i-layer thickness and tends to saturate at the thickness over 3 μm. Surprisingly, J_{sc} does not decrease in this thickness range and approaches about 27 mA/cm^2 at the thickness of 5.6 μm, where the J_{sc} values are almost identical for the solar cells with and without textured substrate. At thinner i-layer side, on the other hand, textured substrate effectively improves J_{sc}. Figure 5.11 provides a comparison of QE spectra for different i-layer thickness (d = 2.5, 5.6 μm) with textured substrate. The QE spectrum of 2.5-μm thick poly-Si solar cell is much lower than that of 5.6-μm solar cell at wavelength over 700 nm, which can be simply ascribed to optical absorption loss. Thus, this ZnO/Ag/SnO_2 textured substrate can not completely trap the infrared light into 2.5-μm thick i-layer. Further improvement of J_{sc} with thin film i-layer might be expected if the highly textured substrates which do not deteriorate the poly-Si preferential growth are developed. In contrast, V_{oc} and FF show similar dependence on i-layer thickness, being regardless of the substrate texture, they monotonically decrease with an increase in i-layer thickness. In consequence, conversion efficiency (η), which is determined by the compete balance of J_{sc} and V_{oc}, FF, reaches the maximum over 9% at the i-

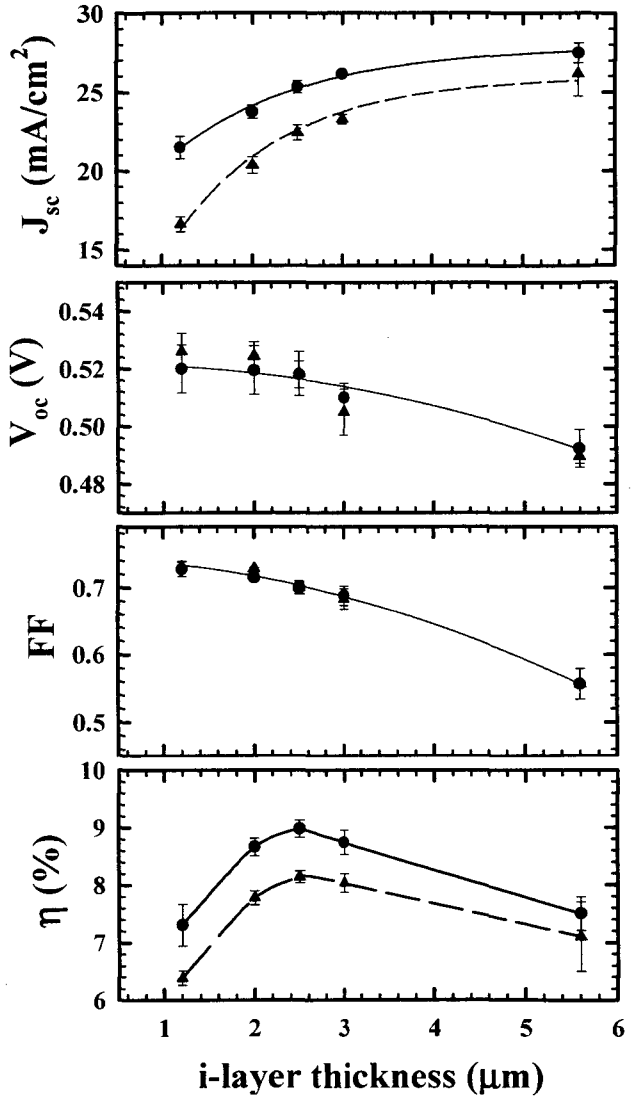

Fig. 5.10. Photovoltaic performance of the poly-Si solar cells on textured substrate (●: ZnO/Ag/SnO_2/glass, σ =38 nm) and flat substrate (▲: ZnO/Ag/glass, σ =26 nm) as a function of i-layer thickness. The lines are guides for the eyes.

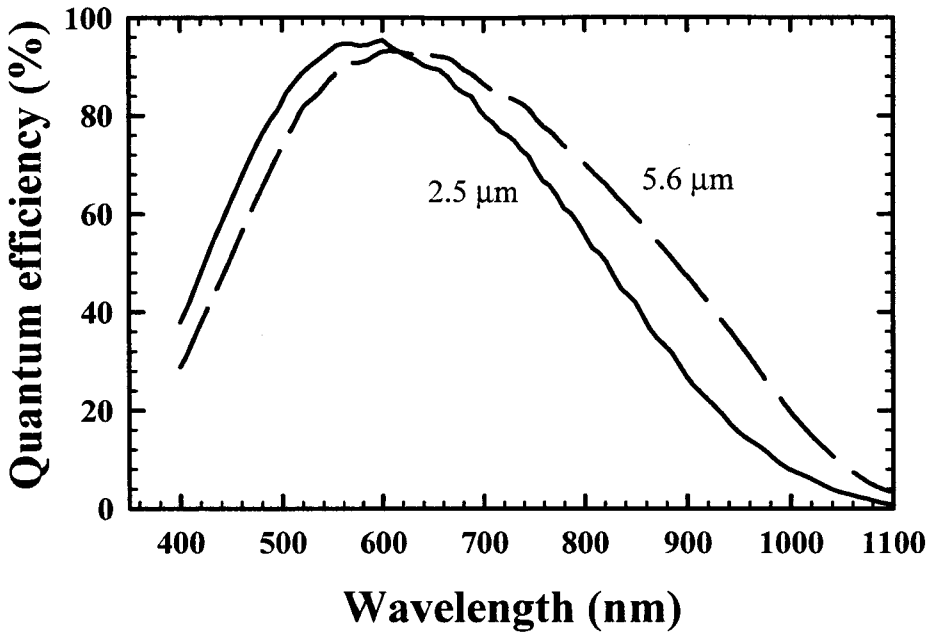

Fig. 5.11. External quantum efficiency spectra of poly-Si solar cells on textured substrate with different i-layer thicknesses (d=2.5 μm: solid line, d=5.6 μm: dotted line).

layer thickness of around 2.5 μm with textured substrate. Figure 5.12 demonstrates an illuminated *J-V* characteristics of poly-Si solar cell. This solar cell consists of Ag-grid/ZnO/p-i-n/ZnO/Ag/SnO_2/glass structure with i-layer thickness of 2.5 μm. The highest conversion efficiency of 9.18% (J_{sc} = 25.1 mA/cm^2, V_{oc} = 0.523 V, FF = 0.7) has been achieved. So far, an efficiency of 9.18% is the world highest record reported on poly-Si based thin film solar cells produced at high deposition rate over 3 Å/s and at low temperature as low as 180°C. The optimized poly-Si i-layer deposition conditions are summarized in Table 5.1 together with the sample structure and fundamental structural and electrical properties of optimized poly-Si i-layer.

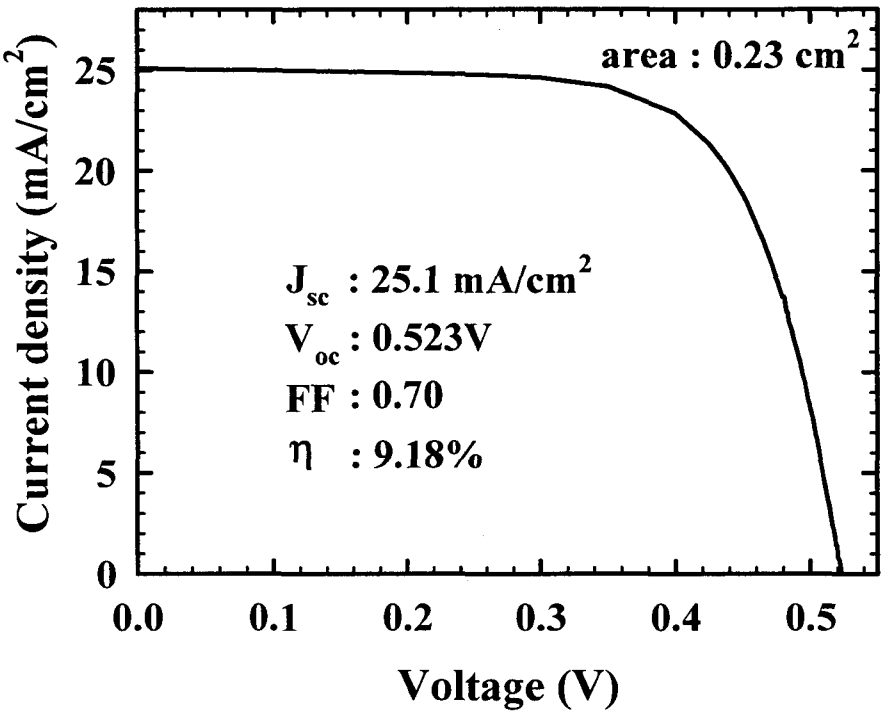

Fig. 5.12. Illuminated *J-V* characteristics of poly-Si solar cell in combination with an optimized conditions as described in Chapters III&V.

Table 5.1. List of optimized poly-Si i-layer deposition conditions, sample structure and fundamental structural and electrical properties of optimized i-layer.

Deposition conditions	
Substrate temperature	180°C
SiH_4 flow rate	5.8 sccm
$[SiH_4]/([SiH_4]+[H_2])$	4.5%
Deposition pressure	0.8 Torr
VHF-power density	100 mW/cm^2
Frequency	100 MHz
Deposition rate	3.8 Å/s
Sample structure	
i-layer thickness	2.5 μm
Structure	Ag-grid/ZnO/p-i-n/ZnO/Ag/SnO_2
Area	0.23 cm^2
Fundamental properties	
Crystalline volume fraction	~50% (Raman Ar^+ 514.5 nm)
Crystallographic orientation	(110) preferential
Dark conductivity	~10^{-7} S/cm (AC, at 300 K)
Photo conductivity	~3×10^{-4} S/cm (AC, at 300 K)
Conductivity activation energy	~0.55 eV

5.5 Summary

A series of the poly-Si solar cells has been fabricated on differently textured ZnO/Ag/SnO_2/glass substrates and investigated the influence of substrate surface morphology on poly-Si microstructure and photovoltaic performances. Although the highly textured back reflectors show excellent light trapping properties, it tends to deteriorate the poly-Si (220) preferential growth, yielding poor photovoltaic performances. The field-dependent carrier collection behaviors of solar cells reveal that this structural change attributed to the substrate texture gives rise to the change in transport properties in the poly-Si photovoltaic layer. When the RMS roughness of substrate increases over 38 nm, a pronounced reduction in carrier diffusion length is observed, which is main cause for low J_{sc} and V_{oc}. In this experiment, the textured ZnO/Ag/SnO_2/glass substrate with RMS roughness of 38 nm is found to be the most suitable for the poly-Si solar cells, which effectively improves long wavelength responses and leads a conversion efficiency up to 9.18% (J_{sc} = 25.1 mA/cm^2, V_{oc} = 0.523 V, *FF* = 0.7).

References

[1] Y. Nasuno, M. Kondo, A. Matsuda : Proc. 28th IEEE Photovoltaic Specialists Conference, Anchorage, 2000, p. 142.

[2] T. Matsui, M. Tsukiji, H. Saika, T. Toyama, H. Okamoto: J. Non-Cryst. Solids, in press.

[3] K. Yamamoto: IEEE Electron. Dev. **46** (1999) 2041.

[4] B. Rech and H. Wagnar :J. Appl. Phys. A **69**. (1999) 155

[5] K. Saito, M. Sano, A. Sakai, R. Hayashi and K. Ogawa: Proc. 12th International Photovoltaic Science and Engineering Conference (PVSEC), Jeju, (2001) p.429.

[6] H. Iida, N. Shiba, T. Mishuku, H. Karasawa, A. Itoh, M. Yamanaka, Y. Hayashi : IEEE Electron Dev. Lett. **EDL-4** (1983) 157.

[7] T. Matsui, M. Tsukiji, H. Saika, T. Toyama, H. Okamoto: Proc. 28th IEEE Photovoltaic Specialists Conference, Anchorage, 2000, p. 825.

[8] N. Wyrsch, P. Torres, M. Goerlitzer, E. Vallat, U. Kroll, A. Shah, M. Vanecek, in: J.H. Werner, H.P. Struck, H.W. Schock (Eds.), Polycrystalline Semiconductors V - Bulk Materials, Thin Films, and Devices, in series Solid State Phenomena, Scitech Publ., Uettikon am See, Switzerland, 1999,Vol. 67-68, p. 91.

[9] H. Okamoto, H. Kida, S. Nonomura, K. Fukumoto, and Y. Hamakawa : J. Appl. Phys. **54**, (1983) 3236.

Chapter VI

Conclusions

A series of systematic investigations has been carried out on p-i-n junction poly-Si thin film solar cells in order to establish the material and device design concept for realizing high efficiency solar cell. The main results and important findings acquired throughout this work are enumerated as follows:

1) Device modeling of p-i-n junction poly-Si thin film solar cells with different columnar grain sizes, L_G, and surface recombination velocities at grain boundary, S_{GB}, has been investigated using two-dimensional device simulator. It has been pointed out that photovoltaic performance is predominantly determined by two factors, i.e., the built-in electric field and the $L_G/2S_{GB}$. This result is followed by an important suggestion that the very thin photovoltaic layer below 3 μm is quite essential for poly-Si solar cells with a grain size of «1 μm in order to reduce recombination of both photo-generated and injection carriers at grain boundary.

2) A series of intrinsic poly-Si thin films has been deposited by 100 MHz VHF-PECVD using SiH_4 and H_2 gas mixture and the optical emission from glow discharge plasma has been investigated. Atomic hydrogen flux onto poly-Si growing surface in glow discharge plasma plays a predominant role in determination of poly-Si microstructure. At relative high $[H_\alpha]/[SiH^*]$ regime, which corresponds to magnitude of atomic hydrogen flux per growth of poly-Si monolayer, poly-Si with high crystalline volume fraction, X_c and strong (220) preferential orientation is obtained. However, excess $[H_\alpha]/[SiH^*]$ gives rise to deterioration in poly-Si (220) preferential growth.

3) A universal relationship between poly-Si microstructure and photovoltaic performances of p-i-n junction poly-Si solar cells has been found. For obtaining high J_{sc}, X_c>50% and (220) preferential orientation are needed. In contrast, increase of X_c over 50% results in a noticeable reduction in V_{oc}, which is related to an increase in carrier recombination through the poly-Si photovoltaic layer. From the opposite tendency of V_{oc} and J_{sc} against X_c, the most suitable deposition conditions is found in this series, and X_c of the obtained poly-Si photovoltaic layer is as low as 50%. In consequence, relatively high V_{oc} and J_{sc} of around 0.5 V and 20 mA/cm^2 are achieved with 3-μm p-i-n junction solar cell on flat substrate.

4) AC-conductivity measurement technique is proved successfully to evaluate the carrier transport along poly-Si growth direction as well as for determining the electron and hole conductivities individually. The Fermi energy level in poly-Si layer is quite sensitive against the film microstructure. Poly-Si layers with relatively low X_c~50% and (220) preferential orientation exhibit truly intrinsic character like intrinsic single crystalline Si materials, leading to the high performance solar cells. In contrast, poly-Si layers with high X_c>50% and (220)

preferential orientation exhibit n-type character, which is likely to be associated with the oxygen-related donor at grain boundary. Experimental and simulation results have suggested that poly-Si solar cells with high X_c result in short diffusion length due to its n-type character and further electrical activation at grain boundary, resulting in poor J_{sc} and V_{oc}.

5) Time-of-Flight experiments have been performed on a device-grade poly-Si film of X_c~50% and also on conventional a-Si:H film for comparison. A significant difference is found particularly in hole transport between poly-Si and a-Si:H materials. The temperature dependence of hole drift mobility has revealed that hole transport in poly-Si films shows non-dispersive transport even at 200 K, while that in a-Si:H films is quite dispersive below 380 K. The hole drift mobility for poly-Si films is estimated as 1.4 cm^2/Vs at room temperature, which is by more than two orders of magnitude higher than that for a-Si:H films.

6) Although the highly textured substrate shows excellent light trapping properties, it tends to deteriorate the poly-Si (220) preferential growth, yielding poor photovoltaic performances. The field-dependent carrier collection behaviors of solar cells have revealed that this structural change attributed to the substrate texture gives rise to the change in transport properties in the poly-Si photovoltaic layer. When the root mean square (RMS) roughness of substrate increases over 38 nm, pronounced reduction in carrier diffusion length is observed, which is a main cause for low J_{sc} and V_{oc}.

7) A novel textured substrate consisting of ZnO/Ag/SnO_2/glass has been proposed for realizing effective light trapping in thin film poly-Si photovoltaic layer. The textured ZnO/Ag/SnO_2/glass substrate with

RMS roughness of 38 nm is found to be the most suitable for poly-Si solar cells, which effectively improves long wavelength responses. The highest conversion efficiency of 9.18% (J_{sc} = 25.1 mA/cm^2, V_{oc} = 0.523 V, FF = 0.7) has been achieved by employing this optimum textured substrate. This efficiency is the world highest record among the poly-Si solar cells prepared at low temperature as low as 180°C and at relatively high deposition rate over 3 Å/s.

VITA

Takuya Matsui was born in Hannan Osaka, Japan in March 19, 1975. He graduated from Seifu Senior High School, Osaka in March 1993 and entered Ritsumeikan University, Kusatu, Shiga in April 1993. He graduated from Ritsumeikan University in March 1997 and entered the Graduate School in April 1997. He received his Master of Engineering degree in Electronic Engineering in March 1999 from Ritsumeikan University. In 1999, he entered the Graduate School of Osaka University, Toyonaka, Osaka.

Published Notes

1. Academic Journals

1-1 Takuya Matsui, Tsutomu Yamazaki, Akihiro Nagatani, Keiju Kino, Hideyuki Takakura and Yoshihiro Hamakawa, "2D-Numerical Analysis and Optimum Design of Thin Film Silicon Solar Cells", Solar Energy Materials and Solar Cells **65** (2001) 87.

1-2 Takashi Minemoto, Takuya Matsui, Hideyuki Takakura, Yoshihiro Hamakawa, Takayuki Negami, Yasuhiro Hashimoto, Takeshi Uenomiya, Masatoshi Kitagawa "Theoretical Analysis of the Effect of Conduction Band Offset of Window/CIS layers on Performance of CIS Solar Cells Using Device Simulation", Solar Energy Materials and Solar Cells **67** (2001) 83.

1-3 Takuya Matsui, Masaharu Tsukiji, Hiroyuki Saika, Toshihiko Toyama and Hiroaki Okamoto, "Correlation Between Microstructure and Photovoltaic Performance of Polycrystalline Silicon Thin Film Solar Cells", Jpn. J. Appl. Phys. **41** (2002) 20.

1-4 Takuya Matsui, Masaharu Tsukiji, Hiroyuki Saika, Toshihiko Toyama and Hiroaki Okamoto, "Influence of Substrate Texture on Microstructure and Photovoltaic Performances of Polycrystalline Silicon Solar Cells", J. Non-Cryst. Solids (in press).

2. International Conferences

2-1 Hideyuki Takakura, Takuya Matsui, Makoto Nakai, Yoshihiro Hamakawa, "An Optimum Design of High-Efficiency Low-Cost a-Si//poly-Si Tandem Type Solar Cells" Proceedings of ISES'97 World Solar Congress, Taejon, Korea (1997) pp.63-71.

2-2 Takuya Matsui, Tsutomu Yamazaki, Akihiro Nagatani, Keiju Kino, Hideyuki Takakura and Yoshihiro Hamakawa, "2D-Numerical Analysis and Optimum Design of Thin Film Silicon Solar Cells" Technical Digest of International PVSEC-11, Sapporo, Japan (1999) pp.711-712.

2-3 Shigeharu Taira, Masaharu Tsukiji, Takuya Matsui, Toshihiko Toyama and Hiroaki Okamoto, "Polycrystalline Si Thin-Film Solar Cell Formed on Highly-Crystallized-Seed layer", Technical Digest of International PVSEC-11, Sapporo, Japan (1999) pp189-190.

2-4 Takuya Matsui, Masaharu Tsukiji, Hiroyuki Saika, Toshihiko Toyama and Hiroaki Okamoto, "Thin Film Polycrystalline Silicon Solar Cells Prepared by PECVD Using Very High Excitation Frequency", Proceedings of 28th IEEE PVSC, Anchorage, Alaska, (2000) pp.825-828.

2-5 Takuya Matsui, Masaharu Tsukiji, Hiroyuki Saika, Toshihiko Toyama and Hiroaki Okamoto, "Influence of Microstructure and p/i Interface Properties on Photovoltaic Performances of Polycrystalline Silicon Thin Films", Technical Digest of International PVSEC-12, Cheju, Korea, (2001) pp.711-712.

2-6 Takuya Matsui, Masaharu Tsukiji, Hiroyuki Saika, Toshihiko Toyama and Hiroaki Okamoto, "Influence of Substrate Texture on Microstructure and Photovoltaic Performances of Polycrystalline Silicon Solar Cells", 19th International Conference on Amorphous and Microcrystalline Semiconductors, Nice, France, (2001).